RADC-TR-76-51
Final Technical Report
March 1976

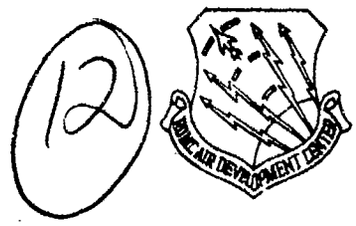

THEORETICAL STUDY OF NON-STANDARD IMAGING CONCEPTS

Optical Science Consultants

Sponsored by
Defense Advanced Research Projects Agency
ARPA Order 2646

Approved for public release;
distribution unlimited.

The views and conclusions contained in this document are those of the authors and should not be interpreted as necessarily representing the official policies, either expressed or implied, of the Defense Advanced Research Projects Agency or the U. S. Government.

Rome Air Development Center
Air Force Systems Command
Griffiss Air Force Base, New York 13441

This report has been reviewed by the RADC Information Office (OI) and is releasable to the National Technical Information Service (NTIS). At NTIS it will be releasable to the general public including foreign nations.

This report has been reviewed and is approved for publication.

APPROVED: Donald W. Hanson

DONALD W. HANSON
Project Engineer

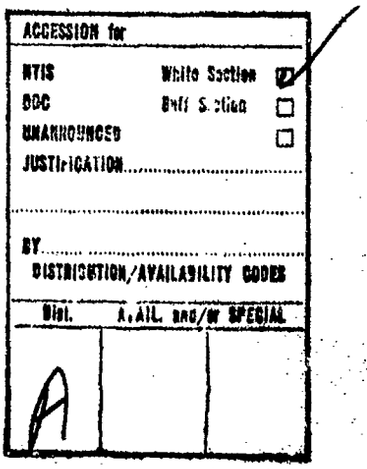

Do not return this copy. Retain or destroy.

THEORETICAL STUDY OF NON-STANDARD IMAGING CONCEPTS

Dr. David L. Fried

Contractor: Optical Science Consultants
Contract Number: F30602-74-C-0115
Effective Date of Contract: 23 January 1974
Contract Expiration Date: 1 November 1975
Amount of Contract: $57,500.00
Program Code Number: 4E20
Period of work covered: Feb 75 - Aug 75

Principal Investigator: Dr. David L. Fried
Phone: 714 524-3622

Project Engineer: Donald W. Hanson
Phone: 315 330-3145

This research was supported by the Defense Advanced Research Projects Agency of the Department of Defense and was monitored by Donald W. Hanson (OCSE), Griffiss AFB NY 13441.

UNCLASSIFIED

SECURITY CLASSIFICATION OF THIS PAGE (When Data Entered)

REPORT DOCUMENTATION PAGE	READ INSTRUCTIONS BEFORE COMPLETING FORM
1. REPORT NUMBER: RADC-TR-76-51	2. GOVT ACCESSION NO. / 3. RECIPIENT'S CATALOG NUMBER
4. TITLE (and Subtitle): THEORETICAL STUDY OF NON-STANDARD IMAGING CONCEPTS	5. TYPE OF REPORT & PERIOD COVERED: Final Technical Report, 15 Feb [illegible] - 15 Aug 75
	6. PERFORMING ORG. REPORT NUMBER: DR-048
7. AUTHOR(s): Dr. David L. Fried	8. CONTRACT OR GRANT NUMBER(s): F30602-74-C-0115, ARPA Order-2646
9. PERFORMING ORGANIZATION NAME AND ADDRESS: Optical Science Consultants, P O Box 388, Yorba Linda CA 92686	10. PROGRAM ELEMENT, PROJECT, TASK AREA & WORK UNIT NUMBERS: 62301E, 26460102, AF-2646
11. CONTROLLING OFFICE NAME AND ADDRESS: Defense Advanced Research Projects Agency, 1400 Wilson Blvd, Arlington VA 22209	12. REPORT DATE: Mar [illegible]76
	13. NUMBER OF PAGES: 173 (2186 P.)
14. MONITORING AGENCY NAME & ADDRESS (if different from Controlling Office): Rome Air Development Center (OCSE), Griffiss AFB NY 13441	15. SECURITY CLASS. (of this report): UNCLASSIFIED
	15a. DECLASSIFICATION/DOWNGRADING SCHEDULE: N/A

16. DISTRIBUTION STATEMENT (of this Report)

Approved for public release; distribution unlimited.

17. DISTRIBUTION STATEMENT (of the abstract entered in Block 20, if different from Report)

Same

18. SUPPLEMENTARY NOTES

RADC Project Engineer:
Donald W. Hanson (OCSE)

Copies available in DDC.

19. KEY WORDS (Continue on reverse side if necessary and identify by block number)

Atmospheric Optics
Imaging
Astronomy
Propagation Effects

20. ABSTRACT (Continue on reverse side if necessary and identify by block number)

This report is the final technical report on work performed on Contract F30602-74-C-0115, and covers the work performed during the period 15 Feb 75 to 15 Aug 75. This report is separated into two parts. Part I presents the analytic backup and computer code results of an effort to generate a fairly general computer code that would allow calculation of a variety of standard optical propagation effects. These effects are concerned with imaging resolution, heterodyne reception, laser transmitter antenna gain, (Cont'd)

DD FORM 1 JAN 73 1473 EDITION OF 1 NOV 65 IS OBSOLETE

UNCLASSIFIED

SECURITY CLASSIFICATION OF THIS PAGE (When Data Entered)

391 358

scintillation, predetection compensation, etc. The computer program is written in Extended BASIC and can be run on a 16K memory size NOVA-type computer. Sample calculations are presented. Part II of the report is concerned with the subject of isoplanatism and its measurement. It is demonstrated that the isoplanatic patch size will, in general, not be the same for predetection compensation and for ordinary short-exposure imagery. The concept of angle-of-arrival isoplanatism is introduced and a simple integral expression relating the distribution of C_N^2 to angle-of-arrival isoplanatism is developed. The procedure for inverting a set of measurements of the angle-of-arrival isoplanatism function to obtain the distribution of C_N^2, and from that calculating the predetection compensation isoplanatism function is studied. Details of the procedure and formulation of its noise sensitivity are presented. Using sample angle-of-arrival isoplanatism measurements made against the edge of the sun, the predetection compensation isoplanatism function is evaluated as well as its rms uncertainty. Because of problems with temporal stationarity in the data-taking process, the final results are of questionable accuracy, but appear to suggest that the useful isoplanatic patch size for predetection compensation is between 1 and 1.5 arc-seconds.

SUMMARY

The work reported here represents the final part of the work on Air Force Contract No. F30602-74-C-0115. Previous results developed under this contract have been reported in three contract technical reports which have been issued as RADC-TR-74-185, RADC-TR-74-276, and RADC-TR-75-182. All of this work has been concerned with analysis supporting the Compensated Imaging effort under the ARPA-sponsored Teal Blue Program.

This report covers work in two technical areas. The first of these has to do with the development of a computer program to facilitate the evaluation of any of the currently well-understood atmospheric turbulence effects. The program is written so as to allow evaluation of any of the effects under any specified set of propagation conditions. The second part of this report is concerned with evaluation of the isoplanatic dependence of predetection compensation imaging and its relationship to the isoplanatic dependence for angle-of-arrival measurements.

In Part I of this report, the theoretical results are presented in appropriate form to provide a basis for calculation of all of the quantities of interest, i.e., all the currently well-understood effects of atmospheric turbulence. A computer program written in BASIC is then presented, along with instructions for use of the program. Finally, sample results are developed by means of the program to provide examples of its use.

In Part II of this report, the subject of isoplanatism is first considered from the point of view of establishing that predetection compensation isoplanatism is distinct from other forms of isoplanatism dependence. This is done by developing an expression for short-exposure post-detection compensation isoplanatism and noting that this expression is entirely distinct from that previously developed for predetection compensation

Summary - Continued

isoplanatism. Physical arguments explaining this fundamental difference are pr. sented. After this, the concept of angle-of-arrival isoplanatism is introduced and it is remarked that because of the similarity between this expression and the expression for predetection compensation isoplanatism, it may be possible to convert measurements of angle-of-arrival isoplanatism into an estimate of predetection compensation isoplanatism. A formalism for carrying this out is set up and an expression governing the noise sensitivity is developed. Using sample data based on solar limb angle-of-arrival measurements (provided by Lockheed Palo Alto Research Laboratory), a representative set of calculations was carried out. The results imply a predetection compensation isoplanatic patch size of 1.0 to 1.5 arc seconds. However, the results showed considerable noise sensitivity, and the numerical results must be viewed as only tentative.

TABLE OF CONTENTS

Table of Contents (Continued)

Part I (Continued)

Table of Contents (Continued)

Part II (Continued)

LIST OF FIGURES

Part I.

Part II.

LIST OF TABLES

Part I.

List of Tables (Continued)

Part II.

PART I

A Computer Code
for
Calculation of Effects
of
Optical Propagation Through Turbulence

1. Introduction to Part I

Knowledge concerning the statistics of optical propagation in atmospheric turbulence has progressed in recent years to the point where calculation of many of the more significant effects of turbulence is a straightforward matter. In particular, we now know how to calculate the effects of turbulence on the performance of various optical devices (namely, receivers, transmitters, imagers, etc.) under conditions where strong (saturated) scintillation is not present. These results generally are available expressed in terms of integrals over the turbulence distribution along the propagation path. As a consequence, these results are not particularly useful to the average system analyst who, after all, is really interested in how the devices perform and not in propagation theory.

In order to make the results of propagation theory easily available to the system analyst, we have undertaken the preparation of a computer program for this purpose. The objective in the design of this program has been the preparation of a program which would require as inputs from the user only values of the propagation characteristic parameters (i.e., path length, wavelength, etc.) and information on the distribution of the strength of turbulence over the propagation path. The computer program has been written for interactive operation between the user and the program. The program will request from the operator the value of each of the parameters governing the propagation problem, and then will request user guidance as to which optical device effects it is to generate printed outputs for. In addition, the program will require a subroutine which it can utilize to calculate the optical strength of turbulence at various points along the propagation path.

In Part I of this document, we shall first review the propagation theory results which we have utilized in preparation of the program. We shall then present the program and its general structure. After that, we shall discuss the

nature of the turbulence subroutine and present guidelines for preparation of such a subroutine, as well as reviewing several sample subroutines. This will be followed by a reasonably concise description of how to use the program, presented in a form suitable for use by those not interested in understanding any of the inner details of the operation of the program. Finally, we shall present a variety of sample results generated by the program.

2. Propagation Theory

Virtually all the effects of optical propagation through turbulence on the performance of an optical device can be quantitatively expressed in terms of a function dependent on the device parameters and one or more of four quantities derived from propagation theory. These four parameters are r_0 , σ_ℓ^2 , d_0 , and H_0 . We shall refer to these as 1) the receiver coherence diameter, 2) the log-amplitude variance, 3) the scintillation averaging length, and 4) the isoplanatism effective path length, respectively.

2.1 Basic Parameter Evaluation

It will be convenient in this presentation to first describe the nominal significance of each of these parameters and present a formula for their evaluation. Then we shall present the formulations allowing optical device performance to be calculated from these parameters. In this presentation we shall avoid as much as possible any serious effort at derivation of results, and instead will simply present results and refer to other documents for the analysis.

2.1.1 Receiver Coherence Diameter

The quantity, r_0 , which we call the receiver coherence diameter is the basic measure of wavefront distortion. It has the dimensions of a length and represents the separation perpendicular to the (nominal) direction of propagation, for which the mean square magnitude of the difference of

complex phase* measured at two points a distance r apart has the value $6.88\,(r/r_0)^{5/3}$. If $\psi(\vec{r}\,')$ is the complex phase at $\vec{r}\,'$, then

$$\langle\,|\psi(\vec{r}\,') - \psi(\vec{r}\,'+\vec{r})|^2\,\rangle = 6.88\,(r/r_0)^{5/3} \quad , \tag{1}$$

where the angle brackets, $\langle\ \rangle$, denote an ensemble average. The physical significance of r_0 relative to the performance of an optical instrument can be sensed from the fact that over a circular region (aperture) of diameter r_0, the ensemble average of the area-averaged wavefront distortion will be one radian-squared.[1]

The value of r_0 expressed as an integral over the propagation path can be written as[2,3]

$$r_0 = \left\{0.423\,k^2 \int_{\text{Path}} ds\; C_N^2\; Q_1(s)\right\}^{-3/5} \tag{2}$$

where $k = 2\pi/\lambda$ is the optical wavenumber, C_N^2 is the refractive-index structure constant (which is a measure of the optical strength of turbulence), and $Q_1(s)$ is a function of s, which depends on whether the optical source is a point source or an infinite plane wave source. $Q_1(s)$ is defined by the equation

$$Q_1(s) = \begin{cases} 1 & \text{, for an infinite plane wave source} \\ (s/\mathcal{L})^{5/3} & \text{, for a point source} \end{cases} \quad , \tag{3}$$

where $\mathcal{L}$ is the propagation path length, s, the variable of integration in Eq. (2), runs along the propagation path, starting at the source, i.e., $s = 0$ at the source.

---

* The complex phase $\psi(\vec{r})$ is composed of two parts. The real part is the ordinary phase, $\phi(\vec{r})$, and the imaginary part is the negative of the log-amplitude, $\chi(\vec{r})$. We can write

$$\psi(\vec{r}) = \phi(\vec{r}) - i\,\chi(\vec{r}) \quad .$$

Some further insight into the physical significance of the receiver coherence diameter can be inferred by taking note of the fact that if an image is formed by an aberration-free lens of very large diameter, the resolution of the image will not be determined by the aperture diameter. Rather, it will be controlled by the wavefront distortion, with a resolution value determined by the receiver coherence diameter, r_0 . If we define the "resolution length" in a sense akin to the way an electrical engineer defines "rise time" of a system, i.e., as one-half the inverse of the bandwidth, only more conservatively take it as twice the "rise time," then it can be shown that atmospheric turbulence imposes a resolution limit for a very large diameter aberration-free aperture given in angular units by[4]

$$\theta_{min} = 4\,\pi^{1/2}/(k\,r_0) = 7.08982/(k\,r_0) \quad , \tag{4}$$

and in units of length at the source, assuming the source is a point source,

$$x_{min} = \ell\,\delta\theta = 7.08982\,\ell/(k\,r_0) \quad . \tag{5}$$

We can identify θ_{min} (and x_{min}) with the apparent full width, i.e., diameter of the image of a point source.

To recognize the full physical significance of Eq.'s (4) and (5), we note that in the absence of turbulence-induced wavefront distortion, the resolution values, θ_{min} and x_{min} would be given by Eq.'s (4) and (5) with r_0 replaced by the aperture diameter, D . As far as resolution is concerned, r_0 is the effective diameter of a very large diameter (i.e., $D \gg r_0$) lens.

2.1.2 Log-Amplitude Variance

Optical propagation through turbulence results in variations of the intensity of the wave. For many analytic purposes, it is convenient to consider the variations of $\ell(\vec{r})$, the logarithm of the amplitude of the wave at $\vec{r}$ (rather than the intensity variations at $\vec{r}$). One of the reasons for this is that the log-amplitude $\ell(\vec{r})$ appears to follow a normal distribution. This distribution is characterized by a mean $\overline{\ell}$ and a variance, σ_ℓ^2 , the log-amplitude variance. It has been shown[5] that (for point sources and infinite plane wave sources), as a consequence of conservation of energy,

$$\overline{\ell} = -\sigma_\ell^2 \quad . \tag{6}$$

Obviously, then, the log-amplitude variations are characterized by a single parameter, the log-amplitude variance.

The relationship between the normalized intensity variance, σ_I^2 , and the log-amplitude variance can be shown to be[5]

$$\sigma_I^2 = \exp(4\sigma_\ell^2) - 1 \quad , \tag{7}$$

where

$$\sigma_I^2 = \frac{\langle [I(\vec{r}) - \langle I(\vec{r})\rangle]^2 \rangle}{\langle I(\vec{r})\rangle^2} \quad . \tag{8}$$

Table 1 shows the relationship between the log-amplitude variance, σ_ℓ^2 , and the normalized intensity variance, σ_I^2 .

Table 1

Normalized Intensity Variance

σ_ℓ^2	0.01	0.03	0.05	0.07	0.1	0.2	0.3	0.5
σ_I^2	0.041	0.127	0.22	0.32	0.49	1.22	2.3	6.4

As can be seen, the normalized intensity variance increases very rapidly with increasing values of the log-amplitude variance. Because of the phenomena known as saturation of scintillation,[6] it does not appear to be possible for σ_ℓ^2 to take a value larger than 0.5 , and there is reason to question all theoretical predictions concerning intensity and log-amplitude fluctuations when the propagation conditions are such that the theory leads to a value of σ_ℓ^2 in excess of one-half.

So long as the propagation conditions do not lead to predictions of saturation of scintillation, we expect the log-amplitude variance to have a value given by the equation

$$\sigma_\ell^2 = 0.56\, k^{7/6} \int_{\text{Path}} ds\, C_N^2\, Q_s(s)\, (\ell - s)^{5/6} \quad , \tag{9}$$

where all of the quantities have the same meaning as in Eq.'s (2) and (12).

2.1.3 Scintillation Averaging Length

The variation of log-amplitude and of intensity is partially correlated for measurements at a pair of points with some finite separation. It is customary to speak of a correlation distance as that separation for which the correlation of the variations is some small fraction of the variance. Unfortunately, the correlation distance for log-amplitude or for intensity variations is difficult to give a precise meaning to for a general propagation problem.* A study[7] of the subject of aperture averaging of intensity fluctuations over any type of propagation path leads to the definition of a length which governs aperture averaging. We recognize the relevance of this quantity to the correlation distance for intensity variations, but avoid imputing any more to this quantity than has been demonstrated, calling it the

* For propagation over a path of length ℓ with homogeneous turbulence statistics, it is easy and useful to consider $\sqrt{\lambda \ell}$ as the correlation distance for log-amplitude variations. However, for a path with varying turbulence statistics, such a simple formulation is inappropriate.

scintillation averaging length. We denote the scintillation averaging length by d_0 . It has been shown that the value of the scintillation averaging length is given by the equation

$$d_0 = 2.399\, k^{-1/2} \left\{ \frac{\int_{Path} ds\, C_N^2\, Q_2(s)\, (\ell - s)^2}{\int_{Path} ds\, C_N^2\, Q_3(s)\, (\ell - s)^{5/3}} \right\}^{3/7} \tag{10}$$

The quantities in Eq. (10) have the same meaning as defined for Eq. (2). The functions $Q_2(s)$ and $Q_3(s)$ have values determined by whether the optical source is a point source or an infinite plane wave source. They are defined by the equations

$$Q_2(s) = \begin{cases} 1 & \text{, for an infinite plane wave source,} \\ (s/\ell)^{-1/3} & \text{, for a point source} \end{cases} \tag{11}$$

$$Q_3(s) = \begin{cases} 1 & \text{, for an infinite plane wave source} \\ (s/\ell)^{5/3} & \text{, for a point source.} \end{cases} \tag{12}$$

2.1.4 Isoplanatism Effective Path Length

For a number of applications, it is important to know the size of the field-of-view over which the wavefront distortion pattern over the aperture is nearly constant, i.e., independent of field angle. This subject is called "isoplanatism,"[8] and the field-of-view is referred to as the isoplanatic patch, or the isoplanatic region. It is reasonable to expect the size of the isoplanatic patch to be equal to the wavefront distortion coherence range (a quantity of the order of the receiver coherence diameter, r_0), divided by a quantity of the order of the path length. Detailed analysis[9]

shows that the angular size of the isoplanatic patch is conveniently defined in terms of the quantity

$$\vartheta_0 = \tfrac{1}{2}\, r_0 / H_0 \qquad (13)$$

where ϑ_0 is an angular quantity we may call the isoplanatic angle (i.e., the radius of the isoplanatic patch), and H_0 is a quantity with dimensions of length, which we call the isoplanatic effective path length. H_0 is of the order of magnitude of the propagation path length, or at least of the path length in the turbulence. Its value is given by the equation

$$H_0 = \left\{ \frac{\int_{\text{Path}} ds\, C_N^2\, Q_1(s)\, (\ell - s)^{5/3}}{\int_{\text{Path}} ds\, C_N^2\, Q_1(s)} \right\}^{3/5} . \qquad (14)$$

Here the quantities have the same meaning as in Eq. (2). We note that H_0 is independent of wavelength, but that since r_0 is proportional to wavelength to the 6/5-power, then so is ϑ_0 .

2.2 Optical Device Performance Evaluation

With the four basic quantities, r_0 , σ_χ^2 , d_0 , and H_0 now defined in terms of formulas suitable for computation, we are ready to turn our attention to the evaluation of the performance of various types of optical devices. We shall consider the following types of optical devices: 1) ordinary imaging optics, 2) laser transmitter, 3) optical heterodyne receiver, 4) predetection compensation imagery, and 5) incoherent detection ("photon bucket") receiver. In addition, to obtain a more complete handle on the nature of the wavefront distortion and scintillation, it is desirable to know something about 6) the spatial power spectrum of log-amplitude and phase variations. We shall take up each of these matters in the following subsections.

2.2.1 Ordinary Imaging Optics

In discussing the performance of ordinary imaging optics as limited by atmospheric turbulence, it is necessary to distinguish between long-exposure imaging and short-exposure imaging. The distinction pertains to the fact that in short-exposure imagery, wavefront tilt does not degrade the sharpness of the image. Rather, it merely displaces the image on the focal plane. In long-exposure imagery, this tilt is varied during the period of exposure and the image is consequently smeared. In long-exposure imagery, wavefront tilt is a meaningful portion of the wavefront distortion.

For convenience, we shall refer to long-exposure imagery as "slow operation," and to short-exposure imagery as "fast operation." For slow operation, we shall only ask about the resolution, but for fast operation we shall ask not only about the resolution, but also about the variability or "jitter" of the image of a point associated with the unknown random tile. We define resolution in the same sense as in Eq.'s (4) and (5), i.e., as the inverse of the one-dimensional imaging bandwidth to be associated with the turbulence-limited MTF of the imaging device. We define the jitter as twice the rms variation in the position of the image of a source.

It can be shown[10] that for slow operation, the atmospheric turbulence limited resolution of an aberration-free imaging device with entrance aperture diameter D is given by the expression for angular resolution,

$$\delta\theta_{slow} = \theta_{min} R_{slow}(D/r_o) \quad , \tag{15}$$

or for a point source, for which it is meaningful to speak of the resolution projected on the source plane as

$$\delta\ell_{slow} = x_{min} R_{slow}(D/r_o) \quad . \tag{16}$$

Here the function $R_s(D/r_0)$ is defined by the equation

$$R_{slow}(D/r_0) = \left\{ \frac{16}{\pi} \left(\frac{D}{r_0}\right)^2 \int_0^1 u\, du \left[\cos^{-1} u - u(1-u^2)^{1/2}\right] \right.$$

$$\left. \times \exp\left[- 3.44 \left(\frac{D}{r_0}\right)^{5/3} u^{5/3} \right] \right\}^{-1/2} \quad . \tag{17}$$

For fast operation, it has been shown that the corresponding expressions for resolution are

$$\delta\theta_{Fast} = \theta_{min}\, R_{Fast}\, (D/r_0) \quad , \tag{18}$$

and

$$\delta\ell_{Fast} = x_{min}\, R_{Fast}\, (D/r_0) \quad , \tag{19}$$

where

$$R_{Fast}(D/r_0) = \left\{ \frac{16}{\pi} \left(\frac{D}{r_0}\right)^2 \int_0^1 u\, du \left[\cos^{-1} u - u(1-u^2)^{1/2}\right] \right.$$

$$\left. \times \exp\left[- 3.44 \left(\frac{D}{r_0}\right)^{5/3} u^{5/3} (1-u^{1/3}) \right] \right\}^{-1/2} \quad . \tag{20}$$

A convenient procedure for estimating the jitter associated with fast operation is to note that the slow resolution, $\delta\theta_{slow}$ or $\delta\ell_{slow}$ should be (approximately) the quadrature sum of the fast resolution, $\delta\theta_{Fast}$ or $\delta\ell_{Fast}$ and the jitter. Since resolution was defined as the equivalent of twice the "rise-time," or as the full width of a spot image, i.e., (approximately) twice the rms spread of the image, then the jitter we will calculate from the inversion of this quadrature sum relationship will be (approximately) twice the rms uncertainty of the short-exposure image position. Expressed in terms of angular field-of-view subtense, or for the case of a point source in terms of the length subtended on the source plane, we have

$$\delta\theta_{Jitter} = [(\delta\theta_{Slow})^2 - (\delta\theta_{Fast})^2]^{1/2}$$

$$= \theta_{min} R_{Jitter}(D/r_0) \qquad (21)$$

and

$$\delta\ell_{Jitter} = [(\delta\ell_{Slow})^2 - (\delta\ell_{Fast})^2]^{1/2}$$

$$= x_{min} R_{Jitter}(D/r_0) \quad , \qquad (22)$$

respectively. Here we have used R_{Jitter} to denote

$$R_{Jitter}(D/r_0) = \{[R_{Slow}(D/r_0)]^2 - [R_{Fast}(D/r_0)]^2\}^{1/2} \quad . \qquad (23)$$

In Table 2, we show a set of numerical values of $R_{Slow}(D/r_0)$, $R_{Fast}(D/r_0)$, and $R_{Jitter}(D/r_0)$ for various values of D/r_0.

Table 2

$R(D/r_0)$ as a Function of D/r_0

D/r_0	0.1	0.215443	0.464159	1.0	2.15443	4.64159	10.0
$R_{Slow}(D/r_0)$	10.111	4.827	2.4625	1.4983	1.1765	1.0718	1.0312
$R_{Fast}(D/r_0)$	10.019	4.6726	2.2065	1.0886	0.62407	0.54627	0.69329
$R_{Jitter}(D/r_0)$	1.3658	1.211	1.0935	1.0295	0.99737	0.92218	0.76341

As can be seen from an examination of Table 2, the jitter is relatively constant, independent of aperture diameter, changing by less than a factor of two as diameter varies over two decades. The resolution for slow operation is a monotonically improving (i.e., decreasing) function of aperture diameter. However, for fast operation the resolution reaches an optimum (i.e., a minimum) for D/r_0 in the vicinity of five. The minimum is quite broad, as can be seen from the data.

2.2.2 Laser Transmitter

By making use of the demonstrated reciprocity[11] between transmitter and receiver performance, it is possible to directly equate the performance of a laser transmitter with that of an aberration-free imaging system. If the laser beam uniformly fills the transmitter aperture, then the results of the preceding section for resolution and jitter can be equated to the beam spread and jitter results for the laser transmitter. Before delving further into this, however, it is appropriate to say a bit about the meaning of the terms "fast" and "slow" operation in a laser transmitter.

The laser transmitter pointing must be controlled by some mechanism which will be able to sense the apparent position of the aimpoint. If the transmitter is hard-mounted, as in a fixed installation communications link, the sensor is the individual who originally installed or most recently adjusted the laser transmitter. In some applications, however, the laser pointing must be updated either to take out the effect of transmitter mount motion or of aimpoint motion. The servo that controls this will have some bandwidth selected on the basis of required performance. Most likely, it will require a beacon of some sort at the aimpoint, which the sensor that controls the pointing servo will detect. If the sensor utilizes the same aperture as the transmitter, the wavefront tilt it senses in viewing the beacon correspond exactly* to the angular deflection the transmitted laser beam will experience.[11] This means that if the pointing servo can respond sufficiently rapidly, the pointing can be adjusted to cancel that portion of the turbulence effect that would correspond to a tilt of the laser beam. We would classify such a device as a fast operating laser transmitter. In the absence of these two features (i.e., adequately high servo bandwidth and a sensor that shares the aperture with the transmitter), we would classify the device as a slow operating laser transmitter.

* For a laser on the ground illuminating a satellite in orbit, there is a point-ahead requirement of $2v/c$. This point-ahead angle can be so large that the wavefront tilt seen by the sensor will be only poorly correlated with the tilt that turbulence will impose on the laser beam.

It follows directly from the reciprocity of transmitter and receiver performance that for a slow operating laser transmitter, the full width of the laser beam expressed in angular units will be $\delta\theta_{slow}$, as defined in Eq. (15), and if the beam is focused at the aimpoint, then the laser spot full width at the aimpoint will be $\delta\ell_{slow}$, as defined in Eq. (16). [The instantaneous laser beam full width will be $\delta\theta_{fast}$, and for a focused laser beam at the aimpoint plane, the instantaneous full width of the spot will be $\delta\ell_{fast}$. The jitter of the instantaneous beam direction will cover a range (where range ≡ two times rms motion) of $\delta\theta_{Jitter}$. For a focused laser beam, the instantaneous spot at the aimpoint plane will wander over a range (range ≡ two times rms wander) of $\delta\ell_{Jitter}$.]

For a fast operation laser transmitter, the achieved laser beam full width expressed in terms of an effective angular subtense will be $\delta\theta_{fast}$, as defined in Eq. (18), and the laser transmitter servo loop will have to apply pointing corrections over an angular range (corresponding to twice the rms pointing correction jitter) of $\delta\theta_{Jitter}$, as defined in Eq. (21). If the laser beam is focused at the aimpoint, then it is convenient to speak of the spot width, which will be $\delta\ell_{fast}$, as defined in Eq. (19). The servo jitter required to take out the atmospheric turbulence tilt will have a range (twice rms excursion) expressed in terms of equivalent displacement of the laser spot on the plane of the aimpoint, of $\delta\ell_{Jitter}$, as defined in Eq. (22).

Central to the calculation of laser transmitter performance is the quantity r_0 . The value of r_0 to be used for laser transmitter performance is actually the same one that would be used in evaluation of an imaging device's performance for an imaging device co-located with the laser transmitter, and a laser transmitter aimpoint co-located with the source the imaging device would be viewing. Clearly, then, the value of r_0 for evaluation of the performance of a laser transmitter would be based on use of Eq. (2), with the propagation path integral running from $s = 0$ at the aimpoint

to $s = \ell$ at the transmitter aperture. The form of $Q_1(s)$, according to the options defined in Eq. (3), would be the point source form if the laser beam were focused at the aimpoint, and would be the infinite plane wave form if the laser beam were transmitted as a collimated beam. Thus we would "consider" that we were dealing with a point source propagation problem for a laser transmitter (which is actually the source) transmitting a focused beam, and an infinite plane wave source for a laser transmitter sending out a collimated beam. To apply the previous propagation results to the laser transmitter, we have to consider the aimpoint as the (virtual) source, and the transmitter as simply the optical device interacting with the ("radiation" from the virtual) source.

2.2.3 Optical Heterodyne Receiver

The performance of an optical heterodyne receiver is measured almost entirely in terms of the signal power and signal power to noise power ratio of its output. Atmospheric turbulence will affect those values. In addition, turbulence will change the apparent angle of arrival of the signal wavefront, and if the heterodyne receiver alignment servo is fast enough, i.e., if we are dealing with a fast operation optical heterodyne receiver rather than with a slow operation unit, this tilt will cause the alignment unit to dither over some angular range. To characterize the performance of a slow operation optical heterodyne receiver, we shall wish to know how the average signal-to-noise power ratio varies with aperture diameter. This is perhaps most conveniently expressed in terms of the effective diameter, i.e., that aperture diameter which would produce the same average signal-to-noise power ratio in the absence of turbulence induced wavefront distortion. It can be shown[12] that this effective diameter, $(D_{eff})_{slow}$ is given by the expression

$$(D_{eff})_{slow} = r_0 \, H_{slow}(D/r_0) \quad , \tag{24}$$

where

$$H_{slow}(D/r_0) = \left(\frac{D}{r_0}\right)\left\{\frac{16}{\pi}\int_0^1 u\,du\,[\cos^{-1}u - u(1-u^2)^{1/2}] \times \exp\left[-3.44\left(\frac{D}{r_0}\right)^{5/3}u^{5/3}\right]\right\}^{1/2} \quad . \tag{25}$$

In addition to the information on the effective average receiver diameter, which tells us about the average signal to noise ratio achieved by the heterodyne receiver, we would also like to know something about the fluctuations of the signal power. This is still a poorly-analyzed subject, and while some results are available, they are at best only numerical results obtained from a Monte Carlo evaluation of an eight-dimensional integral. Using these results[13] and defining the normalized heterodyne signal power variance, $(\sigma_N^2)_{slow}$, as

$$(\sigma_N^2)_{slow} = \frac{\langle (S - \langle S\rangle)^2\rangle}{\langle S\rangle^2} \quad , \tag{26}$$

where S is the randomly fluctuating slow operation heterodyne receiver signal power, we can write

$$(\sigma_N^2)_{slow} = H_{var,slow}(D/r_0) \quad , \tag{27}$$

where $H_{var,slow}(D/r_0)$ is most usefully defined in tabular form. In Table 3, we list the values of H_{slow} and $H_{var,slow}$.

Table 3

Slow Operation Heterodyne Receiver

Performance Functions

D/r_0	0.1	0.215443	0.464158	1.0	2.15443	4.64158	10.0
$H_{slow}(D/r_0)$	0.09889	0.20717	0.4061	0.667429	0.849963	0.932984	0.969713
$H_{var,slow}(D/r_0)$	0.0219	0.0787	0.20	0.616	1.31	1.47	1.23

As can be seen, the effective diameter for a slow operation heterodyne receiver has a limiting value of r_0 . The signal power variance gets to be of the order of unity for a diameter much larger than r_0 , and seems to peak at about 1.5 for a diameter about equal to $5\ r_0$. (It can be shown[14] that the signal power variance reaches a limiting value of unity for D/r_0 very large.)

In examining the performance of a fast operation optical heterodyne receiver, we would be concerned with 1) its effective diameter (i.e., the receiver diameter which in the absence of turbulence-induced wavefront distortion would result in a signal-to-noise power ratio equal to the actual average signal-to-noise power ratio), 2) the angular tracking range over which the alignment system would have to track the dither in angle of arrival of the distorted wavefront (taking the "range" to refer to twice the rms excursion), and 3) the normalized signal power variance. Unfortunately, there are no available theoretical results which we can use to calculate the signal power variance for a fast operation optical heterodyne receiver.

It can be seen[13] that the effective diameter of a fast operating optical heterodyne receiver is given by the expression

$$(D_{eff})_{het} = r_0\ H_{fast}\ (D/r_0) \quad , \tag{28}$$

where the function $H_{Fast}(D/r_0)$ has a value given by the equation

$$H_{Fast}(D/r_0) = \left(\frac{D}{r_0}\right)\left\{\frac{16}{\pi}\int_0^1 u\,du\,[\cos^{-1}u - u(1-u^2)^{1/2}] \times \exp\left[-3,44\left(\frac{D}{r_0}\right)^{5/3} u^{5/3}(1-u^{1/3}\right]\right\}^{1/2}. \quad (29)$$

The fast operation optical heterodyne receiver angular alignment, in tracking the dither in the angle of arrival of the turbulence tilted wavefront, will have to operate over a range (range ≡ two times rms) , $\delta\theta_{Dither}$,

$$\delta\theta_{Dither} = \theta_{min}\, R_{Jitter}(D/r_0) \quad . \quad (30)$$

Here θ_{min} and $R_{Jitter}(D/r_0)$ are as defined in Eq.'s (4) and (23). In Table 4, we list a set of numerical values for H_{Fast} and R_{Jitter} for various values of D/r_0 .

Table 4

Fast Operation Heterodyne Receiver

Performance Functions

D/r_0	0.1	0.215443	0.464159	1.0	2.15443	4.64159	10.0
$H_{Fast}(D/r_0)$	0.0998127	0.214013	0.453237	0.918652	1.60239	1.8306	1.44241
$R_{Jitter}(D/r_0)$	1.3658	1.211	1.0935	1.0192	0.99737	0.92218	0.76341

As can be seen from Table 4, here as in the case of the fast operation imager and the fast operation laser transmitter, the performance peaks at an aperture diameter around $4\ r_0$. The angular dither is seen to be a weakly-decreasing function of aperture diameter.

2.2.4 Predetection Compensation Imagery

The concept of predetection compensation imagery relates to an imaging system which can, in real time, sense the details of the wavefront distortion of the waves from an object in its field-of-view, and in real time apply correction signals to a deformable mirror so as to cancel this distortion. If everything works perfectly, the imaging system ought to achieve diffraction-limited performance. In practice, there is a basic limitation associated with isoplanatism. The wavefront distortion is not constant over the entire field-of-view and as a consequence, whatever wavefront distortion correction is made will not be entirely applicable for some part of the field-of-view. Normally one considers a working field-of-view of only a few arc-seconds or less, but even over this small a field-of-view there can be isoplanatism problems.

The effect of lack of isoplanatism can be measured in terms of a reduction in the modulation transfer function of the compensated imaging system for all the high spatial frequencies. The magnitude of this reduction is related to the angular spread between the detail being imaged and the region in the field-of-view that was used to sense what wavefront distortion corrections were required.

There are two somewhat distinct approaches to the matter of sensing the required wavefront distortion correction. In the first approach, a point source distinct from but close by the region of interest is used as an "external reference," to determine the wavefront correction. The degradation of the modulation transfer function is a function of the angular separation, δ, between the reference and the region of interest, if we are imaging radiation from an infinite plane wave source, and a function of the linear separation, ℓ, between the reference and the region of interest if we are dealing with a point source. It can be shown[9] that the degradation is given by

$$(\text{MTF-Degradation})_{\text{Ext Ref}} = \exp\left[-6.88\,(\vartheta/\vartheta_0)^{5/3}\right] \quad , \tag{31}$$

for imaging of radiation from an infinite plane-wave source, and

$$(\text{MTF-Degradation})_{\text{Ext Ref}} = \exp\left[-6.88\,(\ell/x_0)^{5/3}\right] \quad , \tag{32}$$

for imaging of radiation from a point source. In Eq. (31), the quantity ϑ_0 is as defined in Eq. (13), and x_0 in Eq. (32) is defined by the equation

$$\begin{aligned} x_0 &= \vartheta_0 \mathcal{L} \\ &= \tfrac{1}{2}\, r_0\, (\mathcal{L}/H_0) \end{aligned} \quad . \tag{33}$$

It is worth noting that by virtue of the reciprocity between transmitter and receiver[11], the isoplanatism problems of compensated imaging can be equated with that of a Coherent Optical Adaptive Transmitter (COAT) laser transmitter. In such a system, the transmitter antenna is distorted in a manner controlled by some sensor servo loop that senses the optical propagation distortion in the propagation path to some reference point on the plane being illuminated. (Often this reference point is a glint point.) The antenna gain of the COAT system can be expected to be reduced from the diffraction-limited antenna gain by an amount equal to the factor given in Eq. (31) or (32), where ϑ or ℓ is the separation between the glint (i.e., reference) point and the aimpoint.

In addition to the external reference approach to predetection compensation imaging, it is also possible to use the object of interest as its own reference. In this case, the isoplanatism problem arises from the finite extent of the object. The degree of degradation of the MTF is then a function of Θ, the angular extent, or L, the linear extent in the case of a point source, of the area acting as its reference, and of ϑ, the angular separation, or ℓ, the linear separation in the case of a

point source, of the subregion being imaged, from the center of the region being used as the reference. If the reference region is circular with an angular diameter Θ , or a linear diameter L , in the case of a point source, then it has been shown[9] that the degradation of the modulation transfer function is given by the expression

$$(\text{MTF-Degradation})_{\text{Self Ref}} = \exp\left[-\alpha\,(\theta/\vartheta_0)^{5/3}\right] \quad , \tag{34}$$

for imaging of an infinite plane wave source, and by the expression

$$(\text{MTF-Degradation})_{\text{Self Ref}} = \exp\left[-\alpha\,(L/x_0)^{5/3}\right] \quad , \tag{35}$$

for imaging of a plane wave source. In Eq.'s (34) and (35), the quantity α is a function of (ϑ/θ) if we are imaging an infinite plane wave source, or of (ℓ/L) if we are dealing with imaging of a point source. The value of α is given by the expression

$$\alpha = \left(0.69 \int_{|\vec{x}'| \le 1} d\vec{x}' \, |\vec{x} - \vec{x}'|^{5/3}\right) - 1.03 \quad , \tag{36}$$

where

$$|\vec{x}| = 2\,\vartheta/\theta \quad , \tag{37}$$

or

$$\vec{x} = 2\,\ell/L \quad . \tag{38}$$

In Table 5, we show the value of α for various values of $|\vec{x}|$.

Table 5

Isoplanatism Function for Self-Referenced

Predetection Compensation

$\lvert\vec{x}\rvert$	0.00	0.25	0.50	0.75	1.00
location	center	$\frac{1}{4}$ radius from center	$\frac{1}{2}$ radius from center	$\frac{3}{4}$ radius from center	edge
α	0.165	0.278	0.615	1.166	1.914

The data in Table 5, together with Eq.'s (34) and (37), or with Eq.'s (35) and (38), provide a basis for calculating the degradation of the modulation transfer function for self-referenced predetection compensation.

The aperture diameter of the predetection compensation system does not figure in the degradation of the modulation transfer function in terms of the isoplanatism problem. It only appears in the determination of the diffraction-limited modulation transfer function. The diffraction-limited modulation transfer function for a circular aperture of diameter D, for image frequency f is given by the expression

$$MTF_{DL}(f) = \frac{2}{\pi}\left\{\cos^{-1}\left(\frac{f}{f_0}\right) - \left(\frac{f}{f_0}\right)\left[1 - \left(\frac{f}{f_0}\right)^2\right]^{1/2}\right\} , \qquad (39)$$

where for imaging of an infinite plane-wave source, f is measured in units of cycles per radian, and

$$f_0 = D/\lambda , \qquad (40)$$

while for imaging of a point source, f is measured in cycles per meter on the plane of the source, and

$$f_0 = D/(\lambda\rho) . \qquad (41)$$

If we solve Eq. (39) for the value of (f/f_0) for various values of the diffraction-limited modulation transfer function, we get the results shown in Table 6.

Table 6

Diffraction-Limited Modulation Transfer Function

MTF_{DL}	0.50	0.25	0.10
(f/f_0)	0.403972	0.634704	0.805384
$2\pi (f_0/f)$	15.5535	9.89939	7.80148

2.2.5 Aperture Averaging Intensity Receivers

The signal collected by an intensity detection receiver will be subject to some fluctuation due to the turbulence-induced variations of the wavefront intensity at the aperture plane. The variance of the total signal collected will be controlled first of all by the intensity variance associated with the fluctuations at a point on the aperture plane, i.e., the variations seen by a very small diameter receiver. This variance expressed in normalized form is given by σ_I^2, as defined in terms of the log-amplitude variance in Eq. (7). If the receiver diameter, D, is non-trivial, then the total signal will have a normalized variance, σ_s^2, where with S denoting the randomly fluctuating signal

$$\sigma_s^2 = \frac{\langle (S - \langle S \rangle)^2 \rangle}{\langle S \rangle^2} \quad , \tag{42}$$

given by the expression[7]

$$\sigma_s^2 = \sigma_I^2 [1 + (D/d_0)^{7/6} + (D/d_0)^{7/6}]^{-1}$$

$$= [\exp (4\sigma_\chi^2) - 1][1 + (D/d_0)^{7/6} + (D/d_0)^{7/6}]^{-1} \quad , \tag{43}$$

where d_0 and σ_ℓ^2 are as defined in Eq.'s (9) and (10).

2.2.6 Spatial Power Spectrum of Log-Amplitude and Phase Variations

The fundamental measures of spatial variation of log-amplitude and phase, as developed in the published literature, are the covariance functions

$$C_\ell(\rho) = \langle [\ell(\vec{r}) - \langle \ell(\vec{r}) \rangle][\ell(\vec{r}') - \langle \ell(\vec{r}') \rangle] \rangle \quad , \tag{44}$$

and

$$C_\phi(\rho) = \langle [\phi(\vec{r}) - \langle \phi(\vec{r}) \rangle][\phi(\vec{r}') - \langle \phi(\vec{r}') \rangle] \rangle \quad , \tag{45}$$

where

$$\rho = |\vec{r} - \vec{r}'| \quad . \tag{46}$$

It has been shown[3,16] that these two covariance functions can be expressed in terms of an integral over the propagation path as

$$C_\ell(\rho) = \frac{8.16}{4\pi} k^2 \int_{\text{Path}} ds\, C_N^2 \int_0^\infty du\, u^{-8/3} J_0(\rho u Q_0(s)) \times \{1 - \cos[u^2(\ell - s) Q_0(s)/k]\} \quad , \tag{47}$$

and

$$C_\phi(\rho) = \frac{8.16}{4\pi} k^2 \int_{\text{Path}} ds\, C_N^2 \int_0^\infty du\, u^{-8/3} J_0(\rho u Q_0(s)) \times \{1 + \cos[u^2(\ell - s) Q_0(s)/k]\} \quad , \tag{48}$$

where $Q_0(s)$ is a function whose form depends on whether the source is a point source or an infinite plane wave source. The form of $Q_0(s)$ is given by the expression

$$Q_0(s) = \begin{cases} 1 & , \text{ for an infinite plane wave source} \\ s/\ell & , \text{ for a point source} \end{cases} \tag{49}$$

In Eq.'s (47) and (48), the integration over s along the propagation path runs from the source (at $s = 0$) to the measurement plane (at $s = \ell$).

Strictly speaking, Eq. (48) can not be valid as the integral is divergent. The divergence is due to the very large contribution for very low values (frequencies) of u. In the physical world, there is a cut-off (the outer scale of turbulence) which suppresses this divergence by introducing an additional factor into the integrand of Eq. (48) which reduces the contribution of the low values of u. In practice, it is customary to get around this problem by working with the phase structure function, thus replacing $J_0(\rho u Q_\ell(s))$ by $[1 - J_0(\rho u Q_\ell(s))]$ and suppressing the divergence, at least for finite values of ρ. For our purposes here there is no difficulty involved in using Eq. (48) just as given with the proviso that we remember that there is a missing factor in the integrand which would suppress the very low frequency (small values of u) contribution.

To calculate the log-amplitude and phase power spectra, we make use of the fact that the spectra can be defined in terms of the two-dimensional fourier transform as

$$B'_\ell(p,q) = \int_{-\infty}^{+\infty} dx \int_{-\infty}^{+\infty} dy\, C_\ell\left(\sqrt{x^2+y^2}\right) \exp\left[-i(px+qy)\right] , \quad (50)$$

$$B'_\phi(p,q) = \int_{-\infty}^{+\infty} dx \int_{-\infty}^{+\infty} dy\, C_\ell\left(\sqrt{x^2+y^2}\right) \exp\left[-i(px+qy)\right] , \quad (51)$$

where p and q represent spatial frequencies along the x and y axes, respectively. Because the covariance functions are isotropic, the spectra can be expressed in terms of a radial function, namely,

$$B_\ell(\mu) = B'_\ell(p,q) , \quad (52)$$

$$B_\phi(\mu) = B'_\phi(p,q) , \quad (53)$$

where

$$\mu = (p^2 + q^2)^{1/2} \quad . \tag{54}$$

It is possible to show, making use of the isotropy of the problem, that

$$B_\chi(\mu) = 2\pi \int_0^\infty \rho\, C_\chi(\rho)\, J_0(\mu\rho)\, d\rho \quad , \tag{55}$$

$$B_\phi(\mu) = 2\pi \int_0^\infty \rho\, C_\phi(\rho)\, J_0(\mu\rho)\, d\rho \quad . \tag{56}$$

If we substitute Eq. (47) into Eq. (55), or Eq. (48) into Eq. (56), and make use of the standard property of repeated Hankel transforms to recover the starting function[17], we obtain the result that

$$B_\chi(\mu) = 4.08\, k^2\, \mu^{-11/3} \int_{\text{Path}} ds\, C_n^2\, Q_1(s) \left\{1 - \cos\left[\frac{\mu^2(\zeta - s)}{k\, Q_1(s)}\right]\right\} \quad , \tag{57}$$

$$B_\phi(\mu) = 4.08\, k^2\, \mu^{-11/3} \int_{\text{Path}} ds\, C_n^2\, Q_1(s) \left\{1 + \cos\left[\frac{\mu^2(\zeta - s)}{k\, Q_1(s)}\right]\right\} \quad . \tag{58}$$

Eq.'s (57) and (58) provide a convenient basis for numerical calculation of the log-amplitude and phase variance, given the distribution of the strength of turbulence along the propagation path. As pointed out previously, we can not expect the phase variation power spectrum, as given by Eq. (58), to be reliable for very low spatial frequencies, i.e., for values of μ smaller than the inverse of the outer scale of turbulence.

It is interesting to comment on the asymptotic dependence of $B_\chi(\mu)$ and $B_\phi(\mu)$ for very small values of μ and for very large values of μ (ignoring, of course, the influence of the outer scale of turbulence). For very small values of μ, the cosine function will be nearly equal to unity.

In evaluating $B_\ell(\mu)$, this will lead to replacing (1-cos) by a μ^4 dependence so that $B_\ell(\mu)$ will vary as $\mu^{1/3}$. In evaluating $B_\phi(\mu)$, this will lead to replacing (1+cos) by a factor of 2 , so that $B_\phi(\mu)$ will vary as $\mu^{-11/3}$. For very large values of μ , the cosine term will vary so rapidly that its contribution to the integral will be negligible. This will lead to replacing (1±cos) by unity in both integrals, and the asymptotic dependence of both $B_\ell(\mu)$ and $B_\phi(\mu)$ will be identical, approaching the same $\mu^{-11/3}$ form. We note that although $B_\phi(\mu)$ varies as $\mu^{-11/3}$ for very small values of μ and for very large values of μ , the two asymptotic limits differ by a factor of two, i.e., the difference between the two replacements for (1+cos) . We expect the factor of two transition to manifest itself in the spatial frequency range $\mu \approx 1/d_0$, where d_0 is as defined in Eq. (10). We expect that in this spatial frequency regime, the value of $B_\ell(\mu)$ will approach that of $B_\phi(\mu)$.

3. Computer Program Structure

The program for calculation of optical propagation effects on optical devices has been prepared in BASIC language in a form suitable for use on a teletype terminal interactive basis. It has been run on a Nova-type minicomputer, but should be easily adaptable to larger machines. The program consists of two parts, the main program which is the bulk of the code, and the turbulence subroutine. Other than noting here that the turbulence subroutine is to be specially prepared by the operator in advance of calling the program and has two entry points, at 9000, called to set up the set of constants required repeatedly by the program and subroutine, and at 9100, called repeatedly to generate values of C_n^2 given an altitude, we defer discussion of the subroutine to the next section.

The main program is listed in Appendix 1, with accompanying remarks in Appendix 2. The main program is conveniently separated into six distinct sections. We categorize these as: 1) set-up, 2) problem parameter definition, 3) propagation path subdivision, 4) C_n^2 evaluation, 5) basic results

computation, and 6) generation of desired special outputs. We discuss each of these in the following six subsections.

3.1 Set-Up

The basic set-up details required before the program computations can start are carried out in instructions 110 to 150. This portion of the program establishes the dimensioning of the arrays required by the main program, defines the output format terms, and goes to the turbulence subroutine at entry 9000. This establishes H9 , the upper altitude limit for the turbulent atmosphere, according to the turbulence model. It also gives the subroutine a chance to carry out whatever preliminary manipulations it requires be performed before it is ever called upon to generate values for C_N^2 . (Some versions of the subroutine require no such manipulations — others do.)

3.2 Problem Parameter Definition

Instructions 1002 to 1230 are concerned with obtaining keyboard inputs from the operator to specify the parameters which will govern the calculation. The nature of these inputs are discussed in detail in Appendix 2, under remark #2 (REM #2).

3.3 Propagation Path Subdivision

Instructions 1240 to 1450 are concerned with establishing the propagation path segments through the turbulent portion of the atmosphere. The calculations start with H1 and H2 , the altitudes at the two ends of the path, Z , the total path length, and N the number of segments we wish to divide the part of the path that is in the turbulent atmosphere into. The calculations also make use of H9 the altitude established by the initial calling of the subroutine as the "top" of the turbulent atmosphere. The program establishes the two altitudes, H3 and H4 , which limit the propagation path in the turbulent atmosphere, taking account as necessary

of H9 . It also establishes the propagation path length to the two limits, namely, Z1 and Z2 , which correspond to H3 and H4 . The program then establishes the altitude increment H5 , and path length increment Z3 which control the N steps between Z1 and Z2 over which the propagation integrals will be evaluated.

3.4 Turbulence Strength Evaluation

Instructions 1460 to 1520 are concerned with establishing a matrix C( ) of N values of C_N^2 at the midpoint of each of the N intervals utilized in evaluation of the propagation integrals. The program in sequence establishes the altitude H of each interval's midpoint, H , and then calls the turbulence subroutine which returns the value C of C_N^2 at that altitude. This value is stored in the matrix C( ) for later use.

3.5 Basic Results Computation

The evaluation of most of the effects of atmospheric turbulence on optical devices requires the evaluation of the four basic parameters, r_0 , σ_ℓ^2 , d_0 , and H_0 -- whose values are defined by the propagation integrals in Eq.'s (2), (9), (10), and (14). Instructions 1610 to 1880 cause the evaluation of the necessary four propagation integrals, called I2 , I3 , I4 , and I5 . The basic parameters r_0 , σ_ℓ^2 , d_0 , and H_0 are calculated (called R1 , R3 , R4 , and R5 , respectively) and printed out by instructions 1910 to 2080.

If the value of σ_ℓ^2 is greater than 0.5 , the program prints out a comment to the effect that it will not printout any further results concerning intensity variations. (The program will later suppress printout of the intensity variance and of the aperture averaged signal variations.) This is accomplished by instructions 2090 to 2140.

Having printed out the values of r_0 , σ_ℓ^2 , d_0 , and H_0 , the program next calculates and prints out the values of θ_{atm} , calculated from Eq. (4)

[or x_{sin} , if we are dealing with a point source, calculated from Eq. (5)], which is called P1; the value of ϑ_0 calculated from Eq. (13) [or x_0 if we are dealing with a point source, calculated from Eq. (33)] , which is called P2 ; and the value of σ_I^2 , calculated from Eq. (7), which is called P3. These results are calculated and printed out in instructions 2220 to 2430. Whether the calculations are performed on the basis of infinite plane wave source or point source is governed by the value of Q , a flag set at the keyboard to 0 or 1 at the start of the program.

Beyond this point, all computer outputs are optional, controlled by the six-digit binary number input by the operator at the start of the program. These optional outputs are discussed in the next subsection.

3.6 Optional Outputs

There are six options for detailed outputs, any or all of which the operator can request by his determination of the six-digits of the binary number he input at the keyboard at the start of the program. The nature of these six outputs is discussed in the following subsections. Which output options will be exercised is determined by the six-digit binary number Q1 , which is manipulated as Q2 in the program. The preparation of these optional outputs is covered by instructions 2510 to 4960.

3.6.1 Ordinary Imaging and Laser Transmitter Output Option

The calculations of the performance of an ordinary imaging system and of a laser transmitter, and the outputting of detailed results are accomplished by instructions 2510 to 3063. (Instructions 2515 to 2530 check to see if this output is desired and set up Q2 from Q1 in a form suitable for controlling the subsequent output options.) The nature of the ordinary imaging device performance is discussed in Section 2.2.1. The governing equations are Eq.'s (15), (18), and (21) [or in the case of a point source, Eq.'s (16), (19), and (22)], with pertinent numerical values given by Table 2.

The nature of the laser transmitter performance is discussed in Section 2.2.2. The governing equations are the same as for the ordinary imaging device, i.e., Eq.'s (15), (18), and (21) if a collimated beam is transmitted [or Eq.'s (16), (19), and (22) if the laser beam is focused at the aimpoint].* Here also Table 2 provides the necessary numerical values.

Because of the identity between the ordinary imaging device performance and the laser transmitter performance, only a single output set is provided. It is labeled primarily in terms of the ordinary imaging device performance, but carries secondary labels which allow interpretation of the results in terms of laser transmitter performance.

3.6.2 Heterodyne Receiver Output Option

The calculation of the performance of an optical heterodyne receiver is carried out in instructions 3065 to 3152. (Instructions 3066 and 3067 are concerned with the binary control number governing whether this or the subsequent output options will be carried out.) The nature of the optical heterodyne receiver performance is discussed in Section 2.2.3. The governing equations are Eq.'s (24), (27), (28), and (30), and the necessary numerical values required to prepare the outputs are contained in Tables 3 and 4.

3.6.3 Predetection Compensation Imagery Output Option

The calculations of the performance of a predetection compensation imaging system is carried out in instructions 3233 to 3870. (Instructions 3234 and 3235 are concerned with the binary control number governing whether this or subsequent output options will be carried out.) The nature of the predetection compensation imaging performance degradation due to turbulence, and the expected diffraction-limited performance in the absence

---

* The numerical calculations are carried out as though the aimpoint were the source and the operator input "source altitude" is actually the aimpoint altitude. The operator inputs the response that he is dealing with a "point source," if the laser beam is focused at the aimpoint.

of turbulence or if compensation is perfect is discussed in Section 2.2.4. The key equations governing the generation of the printout data are Eq.'s (31) and (34) [or Eq.'s (32) and (35) in the case of a point source], together with the numerical data in Tables 5 and 6.

3.6.4 Aperture Averaging Intensity Receiver Output Option

The calculation of the performance of an aperture averaging intensity receiver is carried out in instructions 3980 to 4260. (Instructions 3990 and 4000 are concerned with the binary control number governing whether this or subsequent output options will be exercised.) It should be noted that instruction 4100 checks to see if σ_ℓ^2 (denoted by R3) is greater than 0.5 -- in which case, the output of this option will be suppressed. The calculations are carried out on the basis of Eq. (43), using P3 for σ_I^2 and R4 for d_0 .

3.6.5 Spatial Power Spectra Output Option

The calculation of the log-amplitude and phase power spectra are carried out in instruction 4310 to 4730. (Instructions 4320 and 4330 are concerned with the binary control number governing whether this or the subsequent output options will be carried out.) The outputs are prepared for a six-decade spatial frequency range nominally centered about $(d_0)^{-1}$. The calculations are carried out using Eq.'s (57) and (58). They represent results based on the assumption that the source as specified in the keyboard inputs is literally a source, and that the wavefront distortion statistics, i.e., spatial power spectra, are those which would be measured on the plane containing the aperture of the optics.

The calculation of the log-amplitude and phase variation power spectra involves the evaluation of 62 (somewhat interrelated) propagation path integrals, namely, I1( ) and I2( ) . This is a much larger task than the evaluation of the four propagation path integrals, I2 , I3 , I4 , and I5 , carried out near the start of the program, and when exercised is generally the

longest part of the program execution time. These 62 propagation integrals are evaluated using the same set, C( ), of values of C_N^2 distribution along the propagation path as was used for the evaluation of I2 , I3 , I4 , and I5 .*

3.6.6 Turbulence Strength Output Option

In instructions 4810 to 4960, the program allows the user the option of requesting a printout of the values of C_N^2 along the propagation path that were used in the evaluation of the various propagation integrals. (Exercise of the printout option is evaluated in instruction 4820 and 4830.) The values of C_N^2 listed are those stored in the C( ) matrix, along with the associated altitudes.

4. Strength of Turbulence Subroutines

In order to run the main program, it is necessary to provide the computer with a subroutine which the main program can call on for values of the refractive-index structure constant, C_N^2 . This subroutine has two entry points, at instruction address 9000, which we call the "initiation entry," and at 9010, which we call the "production entry."

A number of different versions of the turbulence subroutine have been prepared based on different turbulence models, and no doubt others will be prepared based on various modifications of the turbulence model. The basic constraints on the subroutine are as follows: 1) It is to be written in BASIC. 2) The subroutine is to be located at instruction addresses 9000 and up. 3) The subroutine is to have an initiation entry at instruction address 9000 and a production entry at instruction address 9010. 4) Return from the

* It was to insure this fact when working with a random turbulence strength generation subroutine that the program was written to initially evaluate the matrix C( ) of values of C_N^2 , rather than call the turbulence subroutine each time a value of C_N^2 was needed in evaluating a propagation integral.

subroutine is to be by means of the BASIC instruction "RETURN." 5) The subroutine will be entered at the initiation entry only once during a program run. This entry will occur before any production entries. When entered at the initiation entry, the subroutine must assign a value to H9 (corresponding to the top altitude for atmospheric turbulence). When entered at the initiation entry, the subroutine can also set up any parameters it will require repeatedly during the later production entries of the subroutine. 6) The subroutine will be entered many times in succession for successive altitudes, at the production entry. At this point, the main program will have previously called the initiation entry once to allow establishment of certain parameters. The main program will have set the value of H to the altitude of interest before calling the production entry of the subroutine. The subroutine will return with C set equal to C_N^2 at the altitude H .

In Appendix 3, we list five different turbulence subroutines which have been used in operation of the main program. We refer to these as the Bufton Turbulence Model, the Hufnagel Non-Random Turbulence Model, the Hufnagel Random Turbulence Model, the AF 15 May 74 Flight Data Turbulence Model, and the Hufnagel Simplified Turbulence Model. The remarks are contained in Appendix 4. In the following subsections, we comment on each of these subroutines.

4.1 Bufton Turbulence Model

This turbulence model is based on balloon thermosonde data obtained in a series of four flights by J. Bufton,[18] providing data for altitudes above 500 m , and the measurements of Koprov and Tsvang[19] for data below that altitude. The model has been assembled by us[20] and has the form

$$C_N^2 = \begin{cases} 7.0 \times 10^{-14}\ h^{-4/3} & , \quad h < 100\ \text{m} \\ 1.5 \times 10^{-16} & , \quad 100\ \text{m} < h < 500\ \text{m} \end{cases} \quad , (59)$$

for altitudes below 500 m , and is obtained by interpolation of the data in Table 7 for altitudes above 500 m .

Table 7

Bufton Turbulence Model

Altitude (km)	C_N^2 ($m^{-2/3}$)	Altitude (km)	C_N^2 ($m^{-2/3}$)
0.5	1.5×10^{-16}	9.0	0.210×10^{-16}
1.0	0.375	10.0	0.305
2.0	1.170	11.0	0.370
3.0	0.585	12.0	0.420
4.0	0.435	13.0	0.385
5.0	0.245	14.0	0.295
6.0	0.100	15.0	0.133
7.0	0.130	16.0	0.063
8.0	0.160	17.0	0.038

The top of the turbulent portion of the atmosphere is considered to be (H9 =) 17 km.

At the initiation entry, the subroutine reads the values of Table 7 out of DATA instructions, which are later used in all production entries to calculate C_N^2 .

4.2 Hufnagel Non-Random Turbulence Model

A turbulence model has been generated by R. E. Hufnagel[21] which can be used to generate random sample realization of the vertical distribution of the optical strength of turbulence, C_N^2 , through the atmosphere. A direct derivative of this model is a non-random version. The non-random version has the form

$$C_N^2 = 6.0 \times 10^{-53} h^{10} (W/27)^2 \exp(-h/1000) + 2.7 \times 10^{-16} \exp(-h/1500) \quad , \quad 3000 < h < 24000 \quad , \tag{60}$$

where W is the rms wind in the 5000 m to 2000 m altitude range, i.e.,

$$W = \left\{(15000)^{-1} \int_{5000}^{20000} dh\, [V(h)]^2\right\}^{1/2} \quad . \tag{61}$$

(All quantities above are in MKS units.)

For altitudes below 3000 m , we have used a model developed from the Koprov and Tsvang[19] data and the Bufton data.[20] We have used the formulation,

$$C_N^2 = \begin{cases} 7 \times 10^{-14} h^{-4/3} & , \ h < 100 \text{ m} \\ 1.5 \times 10^{-16} & , \ 100 \text{ m} < h < 500 \text{ m} \\ 1.5 \times 10^{-16} - 1.125 \times 10^{-16} \left(\frac{h-500}{500}\right) & , \ 500 \text{ m} < h < 1000 \text{ m} \\ 3.75 \times 10^{-17} + 7.95 \times 10^{-17} \left(\frac{h-1000}{1000}\right) & , \ 1000 \text{ m} < h < 2000 \text{ m} \\ 1.17 \times 10^{-16} - 5.85 \times 10^{-17} \left(\frac{h-2000}{1000}\right) & , \ 2000 \text{ m} < h < 3000 \text{ m.} \end{cases} \tag{62}$$

The subroutine sets the upper limit of the turbulent atmosphere at an altitude of (H9=) 24,000 m. The initialization portion of the subroutine sets up both H9 and W .

4.3 Hufnagel Random Turbulence Model

The random turbulence version of the Hufnagel turbulence model has the form

$$C_N^2 = \{2.2 \times 10^{-53}\, h^{10} (W/27)^2 \exp(-h/1000) + 10^{-16} \exp(-h/1500)\} \exp[r(h,t)] \quad ,$$
$$\text{for} \quad 3000 \text{ m} < h < 24000 \text{ m} \quad . \qquad (63)$$

Here W is defined exactly as before, i.e., by Eq. (61). The quantity $r(h,t)$ is a gaussian random variable which depends on altitude and time. As defined by Hufnagel, r has a zero mean and a correlation function

$$\langle r(h+h', t+\tau)\, r(h,t) \rangle = A(h'/100) \exp(-\tau/300) + A(h'/2000) \exp(-\tau/4800) \quad , \qquad (64)$$

where t is time measured in seconds. The function A is defined by Hufnagel as a triangular function, i.e.,

$$A(x) = \begin{cases} 1 - |x| & , \quad |x| < 1 \\ 0 & , \quad |x| > 1 \end{cases} \quad . \qquad (65)$$

We have, however, found it more convenient to use an exponential decay function, i.e.,

$$A(x) = \exp(-x) \quad . \qquad (66)$$

In our development of the subroutine for this model, we have not had to consider the temporal dependence. In calculating $r(h)$, we have assumed that the main program would call the production entry with an ordered series of altitudes and assumed that H5 is available as the altitude difference

between the current value of H and the value at the previous entry. The subroutine in the production entry made also assumes that the random value, R , which was used for r(h) for calculation of C_N^2 at the previous entry is still available to be used in generating a new value of r(h) which will have a correlation with the previous value that is in accord with Eq. (64). Instructions 9310 to 9360 of this version of the subroutine generate this new value of r(h) , called R1 . R is set equal to R1 before returning so that it will be available at the next production entry.

One of the functions of the initiation entry is to generate a random value for R that can be used in the first production entry. Also, during the initiation entry, the top altitude of the turbulent atmosphere, H9 , is set equal to 24,000 m .

4.4 AF 15 May 74 Flight Data Turbulence Model

As one example of the general versatility of this subroutine approach to generation of a turbulence model, we have taken an extensive set of balloon thermosonde data and converted it to a subroutine. Data was available at various irregularly-spaced altitudes. The altitudes and the values of C_N^2 were prepared as a set of DATA instructions. These values were read by the subroutine during its initiation entry operation. During the production entry phase of subroutine operation, evaluation of C_N^2 was merely a matter of table look-up and interpolation.

4.5 Hufnagel Simplified Turbulence Model

As a very simplified turbulence model, Hufnagel has suggested[28] a model based on the equation

$$C_N^2 = 1.2 \times 10^{-17} \, (10^4/h)^{1+\alpha} \quad , \quad 1 < h < 20000 \text{ m} \quad , \qquad (67)$$

where α is a constant whose value is determined by the time-of-day.

$$\alpha = \begin{cases} 0.3 & \text{midday} \\ 0.0 & \text{night} \\ -0.2 & \text{dawn/dusk} \end{cases} \quad . \qquad (68)$$

This model has been very easily converted into a subroutine. The initiation entry sets the top altitude for turbulence to (H9 =) 20000 m , and requests an input from the operator as to the time-of-day conditions for Eq. (68). The production entry simply utilizes Eq. (67) to return appropriate values of C_N^2 .

5. Program User's Instructions

This section is written with the intent that it should more or less be able to stand by itself as a guide to the program user. For deeper understanding of what really is implied by various of the program results and how they are obtained, the user will have to refer to the preceding sections and to the program listing in Appendix 1. However, if all that is required is the ability to use the program at the level of understanding that goes with the notation accompanying the computer printouts (which, by the way, have been designed to provide an explanation of the data's meaning as free from ambiguity as possible, within the space constraints), then a study of this section should suffice for the user's needs.

We assume that a suitable subroutine has been prepared for generation of strength of turbulence data and integrated into the main program. (The necessary information for preparation of such a subroutine will be found in Section 4, along with information on a variety of subroutines, listed in Appendix 3, any of which might be used with the main program if the user accepts the suitability of the turbulence model used in generating that subroutine.) With the program loaded into the computer, the user at a teletype console types in "RUN", which instruction will start the execution of the program. At this point, the program starts to type out requests for information which will be used in controlling the calculations it will

perform. There are seven items requested. The meaning of the question and the nature of the appropriate reply to each is discussed in the following subsections.

5.1 Number of Integration Intervals Input

To carry out its calculations, the program has to evaluate several integrals. The range of integration will cover the portion of the propagation path in the turbulent portion of the atmosphere. These integrals will be evaluated by a method involving subdivision of the total range of integration into a set of intervals. Generally, the more intervals used, i.e., the smaller the individual interval length, the more accurate the integral evaluation and the final computer results will be.

The maximum number of intervals allowed is 1000. However, the user is cautioned that using such a large number can result in a severe operating-time penalty. We have found that for the problems we have run using 200 intervals seems to give very good accuracy, and that in many cases, use of even as few as 20 intervals gives tolerable accuracy. In general, the more varied the distribution of the optical strength of turbulence, C_n^2 , along the propagation path, the greater the number of intervals that should be used. If in doubt as to how find a subdivision to use, i.e., how many intervals to specify, the operator can run the program twice, once with N intervals and once with 2N intervals, and estimate by how much the printout results change whether or not sufficient accuracy has been achieved.

5.2 Wavelength Input

After the number of integration intervals has been input, the computer will request the wavelength for which the calculations are to be performed. Only a single wavelength can be input. It should be entered in units of meters, i.e., 5500 $\mathring{A}$ would be input as 0.55×10^{-6} .

5.3 Point-Source Input

After the wavelength information has been input, the program will ask if the source is a point source. If a "1" is input by the operator, the program will understand the source to be a point source, and will proceed accordingly in its propagation calculations. If any number other than "1" is input, the computer will print out a statement to the effect that it will consider the source to be an infinite plane wave source, and the program will act accordingly in its computations.

The question of whether to classify the source as a point source or an infinite plane wave source deserves some comment here. First, however, we remark on what is considered to be the source in various cases. In most cases, the term "source" refers to just what we would normally consider to be the source. For imaging, it is the object being imaged. For heterodyne reception or intensity detection reception, it is the radiator emitting the detectable, presumably information-carrying photon stream. However, for the laser transmitter, the program uses the word "source" to refer not to the transmitter but rather to the aimpoint.*

For total propagation path lengths in excess of 100 km (source to optical device range), to avoid serious round-off errors in the program operation, if the source is in space and the optical device on the ground, the source should be specified as an infinite plane wave source. If the "source" is emitting a collimated beam or if we are dealing with a laser transmitter which is projecting a collimated beam, then the "source" should be specified as an infinite plane wave source. For problems involving imaging of an object in space at a range under 100 km, or if the object is in the atmosphere, the source should be specified as a point source. If

---

* The logic behind this seemingly strange notation relates to the use of reciprocity between transmitter and coherent receiver. This need not concern the program user, whose only concern need be to keep his inputs, and his interpretation of the data, in conformance with the stated interpretation to be applied to the term "source."

the object is truly a point source emitting a divergent wave, it should be specified as a point source, providing it is not in space and at a range in excess of 100 km, in which case it should be classified as an infinite plane wave source.* If we are dealing with a laser transmitter which is projecting a beam that is focused on the aimpoint, then the "source" should be considered to be a point source.

If the program is told that the source is a point source, it will produce output such as those dealing with resolution and beam spread, measured in meters at the "source," and image frequencies measured in cycles per meter at the "source." Thus laser transmitter beam spread for a focused beam will be given in meters beam spot size as projected on the target, and resolution size will be in terms of meters width of a resolvable element on the object being imaged.†

If the program is told that the source is an infinite plane wave source, then the corresponding values will be presented in terms of angles. In each case, the angle corresponds to an angular subtense as seen from the optical device position looking toward the "source."

In the case of the optical heterodyne receiver's performance output for fast operation, the dither of the alignment system due to turbulence is presented in angular units of subtense as seen from the receiver looking towards the source, whether or not the radiation source is specified as a point source.

The only linear measurement units output by the program which do not refer to length measured on the plane of the source are in the output of the log-amplitude and phase power spectra. In this case, the spatial

---

* By the time the radiation from such a source reaches the turbulent atmosphere, the portion of the radiation that will be detected by the device of interest is so nearly planar that it can be considered a plane wave.

† It should be noted that beam spot size, resolvable length and jitter size are presented in terms that are most easily described as twice the rms value.

frequency, always given in cycles per meter no matter what the type of source, refers to spatial frequencies at the end of the propagation path away from the source.

5.4 Path Length Input

After inputting information on the nature of the source, the computer will request the operator to input the propagation path length. This should be input in meters, including the entire distance from one end of the path to the other (not just the portion in the atmosphere.)

5.5 Optics and Source Altitude Input

The computer will next request information on the optics altitude and then on the altitude of the source. Both are to be input in meters. The term "optics" as used here refers to the device with some aperture diameter of interest, or else to the plane on which the log-amplitude and phase power spectra are to be specified. Except for the case of the laser transmitter, which is also considered the "optics," the "optics" receive the radiation. The other end of the link is the "source."

5.6 Output Options Binary Control Input

After all of the basic parameters covering the propagation problem have been input, the computer will request the input of a six-digit binary number* which it will interpret to determine which special data output options are to be exercised. Each of the six-digits independently control one of the six outputs. If the digit is a "zero," the output will be suppressed. If it is a "one," then the data will be printed.

The first digit controls the output of information on ordinary imaging systems and laser transmitter performance. (Because of reciprocity between

---

* The number is binary in the sense that all non-zero digits are interpreted as "one." Thus if the operator inputs 012345, it would be interpreted as 011111, and if he input 908000, it would be interpreted as 101000.

coherent transmitter and receiver performance, the same output data applies to both types of devices, as indicated in the printout captions.)

The second digit controls the output of information on the performance of an optical heterodyne receiver.

The third digit controls the output of information on the performance of a predetection compensated imaging device. [By reciprocity arguments, the output can be related to the expected performance of a coherent optical adaptive array transmitter (COAT). However, information pertaining to this is not provided in the printouts.]

The fourth digit controls the output of information pertaining to the performance of an intensity detecting receiver.

The fifth digit controls the output of information about the log-amplitude and phase spatial power spectra.

The sixth digit controls the printout of the values of C_N^2 used in evaluation of the propagation integrals. The listing is of the points in the turbulent portion of the atmosphere, listed proceeding from the "source" to the other end of the propagation path. The listing gives altitude and C_N^2 at the center of each interval used in evaluating the propagation integrals.

6. Discussion of Sample Results

As an example of the type of results that will be produced by the propagation code, in Table 8 we show the computer printout associated with a rather comprehensive sample run. Table 8a shows the operation of the first part of the program. The operator-generated characters are indicated by being shaded. Initially the operator types "RUN". This starts the execution of the program, and the computer responds by printing out the nature of the turbulence model being used. (This output is

part of the turbulence subroutine and not part of the main program. Depending on the subroutine used, this output may be missing.) After this, the program asks how many intervals to use in carrying out the integrations. In this case, the operator instructs the program to use 50. When asked for the wavelength of interest, the operator inputs 1.06 μm to the computer. He states that he considers the source to be a point source, and that the propagation path length is 5 km. This path runs between optics on the ground, i.e., at 1 m , and a source at 1 km altitude. This could correspond to ground optics imaging an aircraft at 1 km altitude, or to a ground-based laser transmitter projecting a focused beam on the aircraft. It could also correspond to an optical point source (perhaps a diverged laser beam) emanating from the aircraft at 1 km altitude and being detected by a receiver on the ground. The operator inputs a 111111 binary control digit to the computer in response to the last question, which will cause the program to print out all possible data options.

Shortly thereafter, the computer prints out the Basic General Results and the Subsidiary General Results. These printouts can not be suppressed no matter what six-digit binary control number has been input by the operator. The Basic General Results tell us that in this propagation problem

$$r_0 = 0.0362 \text{ m}$$
$$\sigma_\ell^2 = 0.0992 \text{ neper}^2$$
$$d_0 = 0.0683 \text{ m}$$
$$H_0 = 433 \text{ m} ,$$

The Subsidiary General Results tell us that the limiting resolution on the aircraft is

$$\varkappa_{\text{lim}} = 0.164 \text{ m} ,$$

that the isoplanatism size on the aircraft is

$$x_0 = 0.209 \text{ m} \quad ,$$

and that the intensity variance associated with observing a (point) source on the aircraft with a zero diameter intensity detector will be

$$\sigma_I^2 = 0.487 \quad .$$

1) This means, in general terms, that about the best we will be able to do in resolving details on the aircraft will be to see items of about 16.4 cm size, or that if we are focusing a laser on the aircraft, the spot size as limited by turbulence will be about 16.4 cm. 2) If we form a compensated image of the aircraft, the region in which we can expect to achieve adequate compensation is about 20.9 cm in diameter.* 3) If we were observing a 1.06 μm beacon on the aircraft, unless we had a large enough receiver to provide sufficient aperture averaging, we would find the beacon intensity had a 69.8% rms fluctuation. [Note: $0.487 = (0.698)^2$]

Table 8b shows the portion of the computer output generated because the first digit of the binary control number was "one" rather than "zero." These results pertain to long and short exposure (i.e., fast and slow operation) ordinary imaging systems, and to low and high servo bandwidth (i.e., fast and slow operation) laser transmitters of various diameters. We see, for example, that a high bandwidth laser transmitter focused on the aimpoint and having a 7.8 cm aperture diameter will project a 10.2 cm diameter spot on the aircraft. The tracking servo will have to track out a random dither due to turbulence which would correspond to a range (i.e., two times rms) of 16.4 cm on the aircraft. If it could not track this out, performance would degrade toward the low bandwidth limit of a 19.4 cm diameter laser spot on the target aircraft. If we consider a

---

* If we had a COAT laser transmitter at 1.06 μm working off of a glint point, meaningful COAT performance could only be achieved if the glint point were well within a range of 20.9 cm of the desired aimpoint.

photographic system of only 0.78 cm aperture diameter, we see that the resolution as limited by turbulence and diffraction would be almost unaffected by whether the camera produced a long exposure or a short exposure. The long exposure resolution would correspond to 79.6 cm on the aircraft, while the short exposure resolution would correspond to 77.0 cm on the aircraft.

Table 8c shows the portion of the computer output generated because the second digit of the six-digit binary control number was "one" rather than "zero." The results pertain to the performance of an optical heterodyne receiver on the ground collecting the signal from a wide angle (i.e., many milliradians) divergent 1.06 μm laser beam source on the aircraft at 1 km altitude. We see that if the heterodyne receiver has a low servo bandwidth, so that it can not track out the dither in the apparent angle of arrival of the received wavefront (i.e., slow operation), then if the receiver diameter is 16.8 cm, its effective diameter will be only 3.38 cm and the signal power detected will manifest a 147% rms fluctuation. (The average signal-to-noise power ratio detected will be equal to that which would be produced by a heterodyne receiver with a 3.38 cm diameter, if there were no turbulence effects.) If the heterodyne receiver has a high servo bandwidth so that it can track out the dither in the apparent angle of arrival of the wavefront caused by turbulence, and if the receiver diameter is 3.62 cm, then the servo tracking range (range = two times rms) would be about 33.6 μrad. The average signal-to-noise power ratio will be equal to that which would be produced by a heterodyne receiver with 3.32 cm diameter operating in the absence of any turbulence effects.

Table 8d shows the portion of the computer output generated because the third digit of the six-digit binary control number was "one" rather than "zero." The results pertain to the performance of a predetection compensation imaging system, with the imaging system on the

ground viewing a target object at 1 km altitude and 5 km range. If self-referenced predetection compensation is utilized and the target object is circular with a 45 cm diameter, we see that the compensated image will, because of isoplanatism considerations and the finite size of the target object, have an MTF equal to 55.2% of the diffraction-limited MTF for imaging of details at the center of the target object, but only 10.9% of the diffraction-limited MTF for imaging of details half-way between the center and the edge of the target object. If the predetection compensation imaging system had a 1 m aperture diameter and the pattern details at the center were black and white lines with a line pair every 0.835 cm, the diffraction-limited MTF for imaging these lines would be 25%. With the inherent 55.2% degradation associated with the isoplanatism considerations and the finite size of the target object, we see that these lines would actually be imaged with an expected MTF of 25% x 55.2% = 13.8% . For imaging of black and white lines located half-way between the center and the edge (i.e., 10.125 cm from the center) with a line pair every 1.31 cm, the diffraction-limited MTF would be 50% and the compensated imaging system would achieve an MTF of 50% x 10.9% = 5.1% .

If there is an external reference, such as an intense, very small area optical source near the region to be imaged, which can act as an external reference, we see from Table 8d that if the separation between this external reference and the region to be imaged is 9.71 cm, the degradation of the compensated MTF relative to diffraction-limited imaging will be 14.7%. With 2 m diameter compensated imaging optics, a line pair pattern with a periodicity of 0.655 cm could be imaged with an expected MTF of 50% x 14.7% = 7.35% .

Table 8e shows the portion of the computer output generated because the fourth digit of the six-digit binary control number was "one" rather than "zero." The results pertain to the performance of an intensity

detection receiver on the ground viewing a small (point source) 1.06 μm beacon at 1 km altitude and 5 km range. If the receiver diameter is very small (6.83 mm or less), the signal will fluctuate with a normalized variance of 0.454, i.e., an rms fluctuation of 67.4%. If the receiver diameter is 31.7 cm, the normalized signal variance will be 0.0113, i.e., an rms fluctuation of 10.6%.

Table 8f shows the portion of the computer output generated because the fifth digit of the six-digit binary control number was "one" rather than "zero." The results pertain to the spatial power spectra of log-amplitude and of phase of the wave arriving at the ground end of a 5 km long propagation link from a 1.06 μm point source at an altitude of 1 km. The exact definition of the power spectra* given in terms of a fourier transform on a covariance function are to be found in Eq.'s (50) and (51) with the phase and log-amplitude covariance functions defined in Eq.'s (44) and (45). The spatial frequencies listed are those for which the corresponding power spectrum values are applicable, and are given in units of cycles per meter. All values given refer to measurements made on a hypothetical screen at the ground end of the propagation path, the screen being oriented perpendicular to the line-of-sight associated with the propagation path. We see from the printout that at a spatial frequency of 0.1 cycles per meter, the log-amplitude power spectrum has a value of 4.16×10^{-8} and the phase power spectrum has a value of 2.25×10^{7}. The dimensions of the power spectra are not indicated in the printout. They are neper^2/(cycle/meter) for the log-amplitude power spectrum, and radian^2/(cycle/meter) for the phase power spectrum.

Table 8g shows the portion of the computer output generated because the sixth digit of the six-digit binary control number was a "one"

* Different definitions of a power spectra can differ by factors of 2π, and even in the two-dimensional space case with radial symmetry, by a power of spatial frequency. The user is cautioned to refer to the referenced definition.

Table 8a

Propagation Code Sample Run, Part 1

```
RUN

        CALCULATIONS WILL BE PERFORMED USING THE
        AF 15 MAY 74 (ASCENT) C-SUB-N SQ. DATA


NUMBER OF INTERVALS IN INTEGRATION = ? 50
WAVELENGTH (METERS) = ? 1.06E-6
IS SOURCE A POINT SOURCE? (1=YES) ? 1
PATH LENGTH (METERS) = ? 5E3
OPTICS ALTITUDE (METERS) = ? 1
REMOTE END ALTITUDE (METERS) = ? 1E3
INPUT 6-DIGIT BINARY NUMBER TO CONTROL OUTPUT. ? 111111


                BASIC GENERAL RESULTS

RECEIVER COHERENCE DIAMETER, R-SUB-ZERO = 3.62E-02 (METERS)
LOG-AMPLITUDE VARIANCE,SIGMA-SUB-L SQUARED = 9.92E-02 (NEPERS-SQ)
SCINTILLATION AVERAGING LENGTH, D-SUB-ZERO = 6.83E-02 (METERS)
ISOPLANATISM EFFECTIVE PATH LENGTH, H-SUB-ZERO = 4.33E+02 (METERS)


             SUBSIDIARY GENERAL RESULTS

LIMITING RESOLUTION SOURCE LENGTH X-SUB-MIN = 1.64E-01 (METERS)
ISOPLANATISM SOURCE SIZE, X-SUB-ZERO = 2.09E-01 (METERS)
NORMALIZED INTENSITY VARIANCE, SIGMA-SUB-I SQUARED = 4.87E-01
```

Table 8b

Propagation Code Sample Run, Part 2

IMAGING-OPTICS RESOLUTION
(OR TRANSMITTER BEAM SPREAD)
FOR VARIOUS OPTICS DIAMETERS

OPTICS DIAMETER (METERS)	SLOW OPERATION RESOLUTION (METERS)	FAST OPERATION RESOLUTION (METERS)	FAST OPERATION DITHER (METERS)
3.62E-03	1.66E+00	1.65E+00	2.25E-01
7.80E-03	7.96E-01	7.70E-01	1.99E-01
1.68E-02	4.06E-01	3.64E-01	1.80E-01
3.62E-02	2.47E-01	1.79E-01	1.69E-01
7.80E-02	1.94E-01	1.02E-01	1.64E-01
1.68E-01	1.76E-01	9.01E-02	1.52E-01
3.62E-01	1.70E-01	1.14E-01	1.25E-01

Table 8c

Propagation Code Sample Run, Part 3

HETERØDYNE RECEIVER PERFØRMANCE

SLØW ØPERATIØN PERFØRMANCE

ØPTICS DIAMETER (METERS)	EFFECTIVE DIAMETER (METERS)	RMS SIGNAL-PØWER VARIATIØN (%)
3.62E-03	3.58E-03	2.19E+00
7.80E-03	7.50E-03	7.87E+00
1.68E-02	1.47E-02	2.00E+01
3.62E-02	2.41E-02	6.16E+01
7.80E-02	3.08E-02	1.31E+02
1.68E-01	3.38E-02	1.47E+02
3.62E-01	3.51E-02	1.23E+02

FAST ØPERATIØN PERFØRMANCE

ØPTICS DIAMETER (METERS)	EFFECTIVE DIAMETER (METERS)	TRACKING DITHER (RADIANS)
3.62E-03	3.61E-03	4.50E-05
7.80E-03	7.75E-03	3.99E-05
1.68E-02	1.64E-02	3.60E-05
3.62E-02	3.32E-02	3.36E-05
7.80E-02	5.80E-02	3.29E-05
1.68E-01	6.63E-02	3.04E-05
3.62E-01	5.22E-02	2.51E-05

Table 8d

Propagation Code Sample Run, Part 4

PREDETECTION COMPENSATION

EFFECT OF LACK OF ISOPLANATISM ON COMPENSATED MTF FOR SELF-REFERENCED OPERATION, FOR VARIOUS (NOMINALLY CIRCULAR) SOURCE DIAMETERS.

SOURCE SIZE (METERS)	LOCATION ON THE SOURCE OF THE IMAGED REGION				
	CENTER	1/4	1/2	3/4	EDGE
	MTF DEGREDATION				
2.09E-02	9.96E-01	9.94E-01	9.86E-01	9.75E-01	9.59E-01
4.50E-02	9.87E-01	9.78E-01	9.53E-01	9.13E-01	8.62E-01
9.71E-02	9.55E-01	9.25E-01	8.42E-01	7.22E-01	5.87E-01
2.09E-01	8.47E-01	7.57E-01	5.40E-01	3.11E-01	1.47E-01
4.50E-01	5.52E-01	3.68E-01	1.09E-01	1.51E-02	1.02E-03
9.71E-01	1.18E-01	2.75E-02	3.55E-04	2.88E-07	1.83E-11
2.09E+00	4.71E-04	2.48E-06	4.00E-13	3.12E-24	2.61E-39

EFFECT OF LACK OF ISOPLANATISM ON COMPENSATED MTF FOR EXTERNALLY-REFERENCED OPERATION, FOR VARIOUS IMAGE-TO-REFERANCE SEPERATIONS.

SEPERATION (METERS)	MTF DEGREDATION
4.50E-03	9.88E-01
9.71E-03	9.59E-01
2.09E-02	8.62E-01
4.50E-02	5.87E-01
9.71E-02	1.47E-01
2.09E-01	1.02E-03
4.50E-01	1.83E-11

THE DIFFRACTION LIMITED MTF IS 50%, 25%, 10%
WITH THE INDICATED OPTICS DIAMETERS, FOR THE
SOURCE PATTERN PERIODICITIES LISTED.

OPTICS DIAMETER (METERS)	SOURCE PATTERN PERIOD FOR 50% MTF (METERS)	25% MTF (METERS)	10% MTF (METERS)
2.50E-01	5.24E-02	3.34E-02	2.63E-02
5.00E-01	2.62E-02	1.67E-02	1.31E-02
7.50E-01	1.74E-02	1.11E-02	8.77E-03
1.00E+00	1.31E-02	8.35E-03	6.58E-03
1.25E+00	1.04E-02	6.68E-03	5.26E-03
1.50E+00	8.74E-03	5.56E-03	4.38E-03
1.75E+00	7.49E-03	4.77E-03	3.76E-03
2.00E+00	6.55E-03	4.17E-03	3.29E-03
2.25E+00	5.83E-03	3.71E-03	2.92E-03
2.50E+00	5.24E-03	3.34E-03	2.63E-03
2.75E+00	4.77E-03	3.03E-03	2.39E-03
3.00E+00	4.37E-03	2.78E-03	2.19E-03

Table 8e

Propagation Code Sample Run, Part 5

NØRMALIZED, APERTURE AVERAGED
INTENSITY VARIANCE AS A FUNCTIØN
ØF APERTURE DIAMETER.

ØPTICS DIAMETER (METERS)	INTENSITY VARIANCE
6.83E-03	4.54E-01
1.47E-02	4.08E-01
3.17E-02	3.09E-01
6.83E-02	1.62E-01
1.47E-01	5.16E-02
3.17E-01	1.13E-02
6.83E-01	2.10E-03

Table 8f

Propagation Code Sample Run, Part 6

SPATIAL PØWER-SPECTRUM FØR
LØG-AMPLITUDE AND PHASE VARIATIØNS

SPATIAL FREQUENCY (1/METERS)	LØG-AMPLITUDE PØWER-SPECTRUM	PHASE PØWER-SPECTRUM
1.00E-04	4.16E-06	2.25E+18
1.58E-04	4.85E-06	4.16E+17
2.51E-04	5.66E-06	7.70E+16
3.98E-04	6.60E-06	1.42E+16
6.30E-04	7.69E-06	2.62E+15
1.00E-03	8.97E-06	4.85E+14
1.58E-03	1.04E-05	8.97E+13
2.51E-03	1.22E-05	1.65E+13
3.98E-03	1.42E-05	3.06E+12
6.30E-03	1.65E-05	5.66E+11
1.00E-02	1.93E-05	1.04E+11
1.58E-02	2.25E-05	1.93E+10
2.51E-02	2.62E-05	3.57E+09
3.98E-02	3.06E-05	6.60E+08
6.30E-02	3.57E-05	1.22E+08
1.00E-01	4.16E-05	2.25E+07
1.58E-01	4.85E-05	4.16E+06
2.51E-01	5.66E-05	7.70E+05
3.98E-01	6.60E-05	1.42E+05
6.30E-01	7.69E-05	2.62E+04
1.00E+00	8.97E-05	4.85E+03
1.58E+00	1.04E-04	8.97E+02
2.51E+00	1.21E-04	1.65E+02
3.98E+00	1.39E-04	3.06E+01
6.30E+00	1.50E-04	5.66E+00
1.00E+01	1.58E-04	1.04E+00
1.58E+01	1.58E-04	1.93E-01
2.51E+01	1.41E-04	3.56E-02
3.98E+01	9.00E-05	6.51E-03
6.30E+01	3.82E-05	1.18E-03
1.00E+02	1.74E-05	2.08E-04

Table 8g

Propagation Code Sample Run, Part 7

TURBULENCE DISTRIBUTION ALONG
THE PROPAGATION PATH

ALTITUDE (M)	C-SUB N SQ (M**-2/3)
9.900E+02	5.08E-16
9.700E+02	4.25E-16
9.500E+02	3.42E-16
9.300E+02	2.59E-16
9.100E+02	3.06E-16
8.901E+02	3.53E-16
8.701E+02	4.00E-16
8.501E+02	4.47E-16
8.301E+02	4.94E-16
8.101E+02	5.41E-16
7.902E+02	5.88E-16
7.702E+02	6.35E-16
7.502E+02	6.83E-16
7.302E+02	7.30E-16
7.102E+02	7.77E-16
6.903E+02	8.24E-16
6.703E+02	8.71E-16
6.503E+02	8.64E-16
6.303E+02	8.26E-16
6.103E+02	7.88E-16
5.904E+02	7.51E-16
5.704E+02	7.13E-16
5.504E+02	6.75E-16
5.304E+02	6.61E-16
5.104E+02	6.65E-16
4.905E+02	6.69E-16
4.705E+02	6.73E-16
4.505E+02	6.77E-16
4.305E+02	6.81E-16
4.105E+02	6.85E-16
3.906E+02	6.89E-16
3.706E+02	6.93E-16
3.506E+02	6.91E-16
3.306E+02	6.76E-16
3.106E+02	6.60E-16
2.907E+02	6.45E-16
2.707E+02	6.29E-16
2.507E+02	6.13E-16
2.307E+02	5.98E-16
2.107E+02	5.76E-16

ALTITUDE (M)	C-SUB N SQ (M**-2/3)
1.908E+02	4.62E-16
1.708E+02	3.47E-16
1.508E+02	2.33E-16
1.308E+02	1.73E-16
1.108E+02	8.40E-15
9.091E+01	1.66E-14
7.093E+01	2.48E-14
5.095E+01	3.31E-14
3.097E+01	4.13E-14
1.099E+01	4.95E-14

rather than a "zero." The data listed corresponds to the altitude and value of C_N^2 at the midpoint of each of the 50 intervals utilized in the evaluation of the propagation integrals.

7. Computer Results

As an example of the application of the propagation code, we have utilized it to carry out three investigations. The first of these was concerned with the question of how large an isoplanatic region the Hufnagel Simplified Turbulence Model would lead to for visible light satellite imaging. The second application is concerned with an assessment of the general credibility of the turbulence measurement data utilized to generate the "AF 15 MAY 74 (ASCENT) C-SUB-N SQ DATA." The third application we have considered is a general assessment of the implications of the Hufnagel Random Turbulence and Non-Random Turbulence Models, with particular emphasis on the log-amplitude and phase power spectra. These applications are treated in the following three subsections.

7.1 Hufnagel Simplified Turbulence Model

Using the appropriate turbulence subroutine for the Hufnagel Simplified Turbulence Model, as listed in Appendix 3, we ran the computer code for ground-based viewing of a visible light illuminated satellite passing directly overhead at 300 km altitude. We assumed that 5500 Å was representative of visible light, and since we only had special interest in the isoplanatism aspect of the propagation problem, the binary control number was chosen to only provide for the isoplanatism printout option. The computer printouts are given in Table 9.

As can be seen from a study of the data in Table 9, the turbulence model predicts reasonable values for r_0 and σ_χ^2. It also predicts an isoplanatism angle $\vartheta_0 \approx 2$ arc seconds. This means that if we are using self-referenced predetection compensation, we can not get usefully compensated results for imaging of details near the edge of the satellite if the

Table 9

Satellite Compensated Imaging Evaluation

Using The

Hufnagel Simplified Turbulence Model

```
CALCULATIØNS WILL BE PERFØRMED USING THE
HUFNAGEL SIMPLIFIED TURBULENCE MØDEL

INPUT TIME ØF DAY; 1=MID-DAY,2=NIGHT,3=DAWN/DUSK? 2


NUMBER ØF INTERVALS IN INTEGRATIØN = ? 200
WAVELENGTH (METERS) = ? .55E-6
IS SØURCE A PØINT SØURCE? (1=YES) ? 0

(SØURCE WILL BE TREATED AS AN INFINITE PLANE WAVE.)

PATH LENGTH (METERS) = ? 3E5
ØPTICS ALTITUDE (METERS) = ? 1
REMØTE END ALTITUDE (METERS) = ? 3E5
INPUT 6-DIGIT BINARY NUMBER TØ CØNTRØL ØUTPUT. ? 001000


                BASIC GENERAL RESULTS


RECEIVER CØHERENCE DIAMETER, R-SUB-ZERØ = 9.78E-02 (METERS)
LØG-AMPLITUDE VARIANCE,SIGMA-SUB-L SQUARED = 5.30E-02 (NEPERS-SQ)
SCINTILLATIØN AVERAGING LENGTH, D-SUB-ZERØ = 6.90E-02 (METERS)
ISØPLANATISM EFFECTIVE PATH LENGTH, H-SUB-ZERØ = 4.47E+03 (METERS)


             SUBSIDIARY GENERAL RESULTS


LIMITING RESØLUTIØN ANGLE, THETA-SUB-MIN = 6.34E-06 (RADIANS)
ISØPLANATISM FIELD-ANGLE, THETA-SUB-ZERØ = 1.09E-05 (RADIANS)
NØRMALIZED INTENSITY VARIANCE, SIGMA-SUB-I SQUARED = 2.36E-01
```

PREDETECTION COMPENSATION

EFFECT OF LACK OF ISOPLANATISM ON COMPENSATED MTF FOR SELF-REFERENCED OPERATION, FOR VARIOUS (NOMINALLY CIRCULAR) SOURCE DIAMETERS.

SOURCE SIZE (RADIANS)	MTF DEGREDATION LOCATION ON THE SOURCE OF THE IMAGED REGION CENTER	1/4	1/2	3/4	EDGE
1.09E-06	9.96E-01	9.94E-01	9.86E-01	9.75E-01	9.59E-01
2.35E-06	9.87E-01	9.78E-01	9.53E-01	9.13E-01	8.62E-01
5.07E-06	9.55E-01	9.25E-01	8.42E-01	7.22E-01	5.87E-01
1.09E-05	8.47E-01	7.57E-01	5.40E-01	3.11E-01	1.47E-01
2.35E-05	5.52E-01	3.60E-01	1.09E-01	1.51E-02	1.02E-03
5.07E-05	1.18E-01	2.75E-02	3.55E-04	2.88E-07	1.63E-11
1.09E-04	4.71E-04	2.48E-06	4.00E-13	3.12E-24	2.61E-39

EFFECT OF LACK OF ISOPLANATISM ON COMPENSATED MTF FOR EXTERNALLY-REFERENCED OPERATION, FOR VARIOUS IMAGE-TO-REFERANCE SEPERATIONS.

SEPERATION (RADIANS)	MTF DEGREDATION
2.35E-07	9.88E-01
5.07E-07	9.59E-01
1.09E-06	8.66E-01
2.35E-06	5.87E-01
5.07E-06	1.47E-01
1.09E-05	1.02E-03
2.35E-05	1.82E-11

THE DIFFRACTION LIMITED MTF IS 50%, 25%, 10% WITH THE INDICATED OPTICS DIAMETERS, FOR THE SOURCE PATTERN PERIODICITIES LISTED.

OPTICS DIAMETER (METERS)	SOURCE PATTERN PERIOD FOR 50% MTF (RADIANS)	25% MTF (RADIANS)	10% MTF (RADIANS)
2.50E-01	5.44E-06	3.46E-06	2.73E-06
5.00E-01	2.72E-06	1.73E-06	1.36E-06
7.50E-01	1.81E-06	1.15E-06	9.10E-07
1.00E+00	1.36E-06	8.66E-07	6.82E-07
1.25E+00	1.08E-06	6.93E-07	5.46E-07
1.50E+00	9.07E-07	5.77E-07	4.55E-07
1.75E+00	7.77E-07	4.95E-07	3.90E-07
2.00E+00	6.80E-07	4.33E-07	3.41E-07
2.25E+00	6.05E-07	3.85E-07	3.03E-07
2.50E+00	5.44E-07	3.46E-07	2.73E-07
2.75E+00	4.95E-07	3.15E-07	2.48E-07
3.00E+00	4.53E-07	2.88E-07	2.27E-07

satellite diameter is greater than about 2 arc seconds, i.e., about 3 m at this range. However, if we are willing to restrict attention to the central part of the satellite, we could work with a satellite angular diameter of about 4 arc seconds. This corresponds to about 6 m diameter. This is about twice as large as what we have previously estimated was the case using the Bufton Turbulence Model. The difference in results is strictly a function of the data in the turbulence model.

7.2 Assessment of the "AF 15 MAY . . ." Turbulence Model

A set of thermosonde readings for C_N^2 collected on 15 May 74 at Fairbanks, Alaska, was available for propagation analysis, and a turbulence subroutine has been generated from this data. However, there had been some suspicion by the experimenters that there was a defect in the instrumentation and that the data was not valid; that, in fact, the reported values of C_N^2 were much too high.

To check this conjecture, we used the subroutine to make some predictions of what an aircraft at about 60,000 ft. (i.e., 18.6 km) altitude would see if it were to look down at a divergent (i.e., point source) argon laser source at 4880 $\mathring{A}$. Because of the nature of our interest, no optional output features were exercised, and the six-digit binary control number was 000000 . The computer printout for this run is listed in Table 10.

As can be seen from a brief study of Table 10, the predicted effects of turbulence are generally too strong to appear credible. In particular, we note that the predicted value of σ_χ^2 is greater than unity. This large a log-amplitude variance is clearly in disagreement with any of our observations -- and this large a log-amplitude variance would be easily noticeable even to a casual observer.

Table 10

Test Calculation for the

"AF 15 May . . . " Turbulence Model

```
RUN

        CALCULATIØNS WILL BE PERFØRMED USING THE
        AF 15 MAY 74 (ASCENT) C-SUB-N SQ. DATA



NUMBER ØF INTERVALS IN INTEGRATIØN = ?  200
WAVELENGTH (METERS) = ?  .488E-6
IS SØURCE A PØINT SØURCE? (1=YES)  ?  1
PATH LENGTH (METERS) = ?  18600
ØPTICS ALTITUDE (METERS) = ?  18601
REMØTE END ALTITUDE (METERS) = ?  1
INPUT 6-DIGIT BINARY NUMBER TØ CØNTRØL ØUTPUT.  ?  000000


                BASIC GENERAL RESULTS


RECEIVER CØHERENCE DIAMETER, R-SUB-ZERØ = 4.37E-01 (METERS)
LØG-AMPLITUDE VARIANCE, SIGMA-SUB-L SQUARED = 1.05+00 (NEPERS-SQ)
SCINTILLATIØN AVERAGING LENGTH, D-SUB-ZERØ = 2.66E-01 (METERS)
ISØPLANATISM EFFECTIVE PATH LENGTH, H-SUB-ZERØ = 8.68E+03 (METERS)


THE CØMPUTED VALUE ØF LØG-AMPLITUDE VARIANCE IS SØ LARGE
AS TØ CAST DØUBT ØN ALL INTENSITY FLUCTUATIØN RESULTS.
PRINT-ØUT ØF THESE RESULTS WILL BE SUPPRESSED.


             SUBSIDIARY GENERAL RESULTS


LIMITING RESØLUTIØN SØURCE LENGTH X-SUB-MIN = 2.34E-01 (METERS)
ISØPLANATISM SØURCE SIZE, X-SUB-ZERØ = 4.68E-02 (METERS)
```

We therefore conclude that the C_N^2 data that went into the "AF 15 MAY . . ." turbulence model is almost certainly too large and ought not to be used for prediction of optical effects of turbulence.

7.3 Assessment of the Hufnagel Random and Non-Random Turbulence Models

Subroutines representing the Hufnagel Random Turbulence Model and the Hufnagel Non-Random Turbulence Model are presented in Appendix 3. Using these two subroutines, we have carried out a series of calculations of propagation effects, emphasizing evaluation of the expected log-amplitude and phase power spectra. Two propagation paths were considered. Each case represented an aircraft flying through the illumination from a ground-based point source (i.e., widely diverged) laser beacon located 1 m above the ground. The aircraft viewed the laser radiation when virtually directly over the beacon. Aircraft altitudes of 35,000 ft. (10,660 m) and 62,000 ft. (18,600 m) were utilized. The laser operated at 4880 Å.

In running either of these two Hufnagel turbulence models, it is necessary to specify the rms wind, W , in the altitude range of 5 km to 15 km. A number of flights have been made involving optical experiments (which we shall not discuss here) for conditions related to these described above. The vertical wind profile data is available for these cases, and from this data we have calculated values of W . These values are listed in Table 11.

Table 11

RMS Wind, W , For Various Flights

Flight	RMS Wind
Fairbanks, Alaska; 15 May 74	6.89 m/sec
Albuquerque, New Mexico; 25 Mar 74	13.1 m/sec
Dayton, Ohio; 17 Nov 73	15.3 m/sec
Amarillo, Texas; 18 Oct 67	14.4 m/sec
Amarillo, Texas; 18 Oct 67	12.6 m/sec
Amarillo, Texas; 17 Oct 67	18.4 m/sec

We note that these values are significantly below the 27 m/sec nominal value suggested by Hufnagel[31] when he presented his Random Turbulence Model and his Non-Random Turbulence Model.

We have run both a 35,000 ft. flight altitude case and a 62,000 ft. flight altitude case using the non-random turbulence model with the rms wind parameter, W = 5 , 10 , 15 , . . . , 50 m/sec , and made ten runs for each altitude using the random turbulence model with W = 25 m/sec. As a reference point, we have also run the 62,000 ft. flight altitude case using the Bufton Turbulence Model with the corresponding subroutine as listed in Appendix 3. The computer printout for this reference case is presented in Table 12.

A plot of the log-amplitude and phase power spectra for the Bufton turbulence model is shown in Fig. 1. It can be seen that the phase power spectra decreases as the (-11/3)-power with an additional factor of two reduction transition introduced at a spatial frequency about equal to $2\pi/d_0 \approx 23$ cycles per meter. The log-amplitude power spectra first rises as the 1/3-power, and then starts to decrease as the (-11/3)-power joining the phase power spectra after it has undergone its factor of two reduction in magnitude. It is possible to parametrize these two power spectra by writing the low-frequency behavior in the form

$$\Psi_\phi(f) \approx A_\phi f^{-11/3} \quad , \quad (f \ll f_t) \quad . \tag{69}$$

for the phase power spectra, and

$$\Psi_\chi(f) \approx A_\chi f^{11/3} \quad , \quad (f \ll f_t) \quad . \tag{70}$$

The factor of two transition in the phase power spectra occurs in the vicinity of where these two asymptotic dependencies intersect, i.e., at the transition frequency

Table 12

Reference Case

Computer Run with Bufton Turbulence Model

```
NUMBER ØF INTERVALS IN INTEGRATIØN = ? 200
WAVELENGTH (METERS) = ? .488E-6
IS SØURCE A PØINT SØURCE? IF YES INPUT 1.? 1
PATH LENGTH (METERS) = ? 18600
ØPTICS ALTITUDE (METERS) = ? 18600
REMØTE END ALTITUDE (METERS) = ? 1
INPUT 6-DIGIT BINARY NUMBER TØ CØNTRØL ØUTPUT. ? 000100

                BASIC GENERAL RESULTS

RECEIVER CØHERENCE DIAMETER, R-SUB-ZERØ = 2.67E-01 (METERS)
LØG-AMPLITUDE VARIANCE,SIGMA-SUB-L SQUARED = 4.94E-02 (NEPERS-SQ)
SCINTILLATIØN AVERAGING LENGTH, D-SUB-ZERØ = 2.33E-01 (METERS)
ISØPLANATISM EFFECTIVE PATH LENGTH, H-SUB-ZERØ = 7.74E+03 (METERS)

             SUBSIDIARY GENERAL RESULTS

LIMITING RESØLUTIØN SØURCE LENGTH X-SUB-MIN = 3.83E-02 (METERS)
ISØPLANATISM SØURCE SIZE, X-SUB-ZERØ = 3.20E-01 (METERS)
NØRMALIZED INTENSITY VARIANCE, SIGMA-SUB-I SQUARED = 2.18E-01
```

SPATIAL PØWER-SPECTRUM FØR
LØG-AMPLITUDE AND PHASE VARIATIØNS

SPATIAL FREQUENCY (1/METERS)	LØG-AMPLITUDE PØWER-SPECTRUM	PHASE PØWER-SPECTRUM
9.99E-05	3.63E-05	8.07E+16
1.58E-04	4.24E-05	1.49E+16
2.51E-04	4.94E-05	2.75E+15
3.98E-04	5.77E-05	5.09E+14
6.30E-04	6.72E-05	9.41E+13
9.99E-04	7.84E-05	1.73E+13
1.58E-03	9.14E-05	3.21E+12
2.51E-03	1.06E-04	5.93E+11
3.98E-03	1.24E-04	1.09E+11
6.30E-03	1.44E-04	2.02E+10
9.99E-03	1.68E-04	3.74E+09
1.58E-02	1.97E-04	6.92E+08
2.51E-02	2.29E-04	1.27E+08
3.98E-02	2.67E-04	2.36E+07
6.30E-02	3.12E-04	4.36E+06
1.00E-01	3.63E-04	8.07E+05
1.58E-01	4.24E-04	1.49E+05
2.51E-01	4.94E-04	2.75E+04
3.98E-01	5.76E-04	5.09E+03
6.30E-01	6.71E-04	9.41E+02
1.00E+00	7.77E-04	1.73E+02
1.58E+00	8.66E-04	3.21E+01
2.51E+00	8.29E-04	5.93E+00
3.98E+00	8.39E-04	1.09E+00
6.30E+00	7.83E-04	2.02E-01
1.00E+01	6.50E-04	3.68E-02
1.58E+01	4.48E-04	6.47E-03
2.51E+01	1.87E-04	1.09E-03
3.98E+01	8.84E-05	1.47E-04
6.30E+01	2.32E-05	1.53E-05
1.00E+02	4.00E-06	4.06E-06

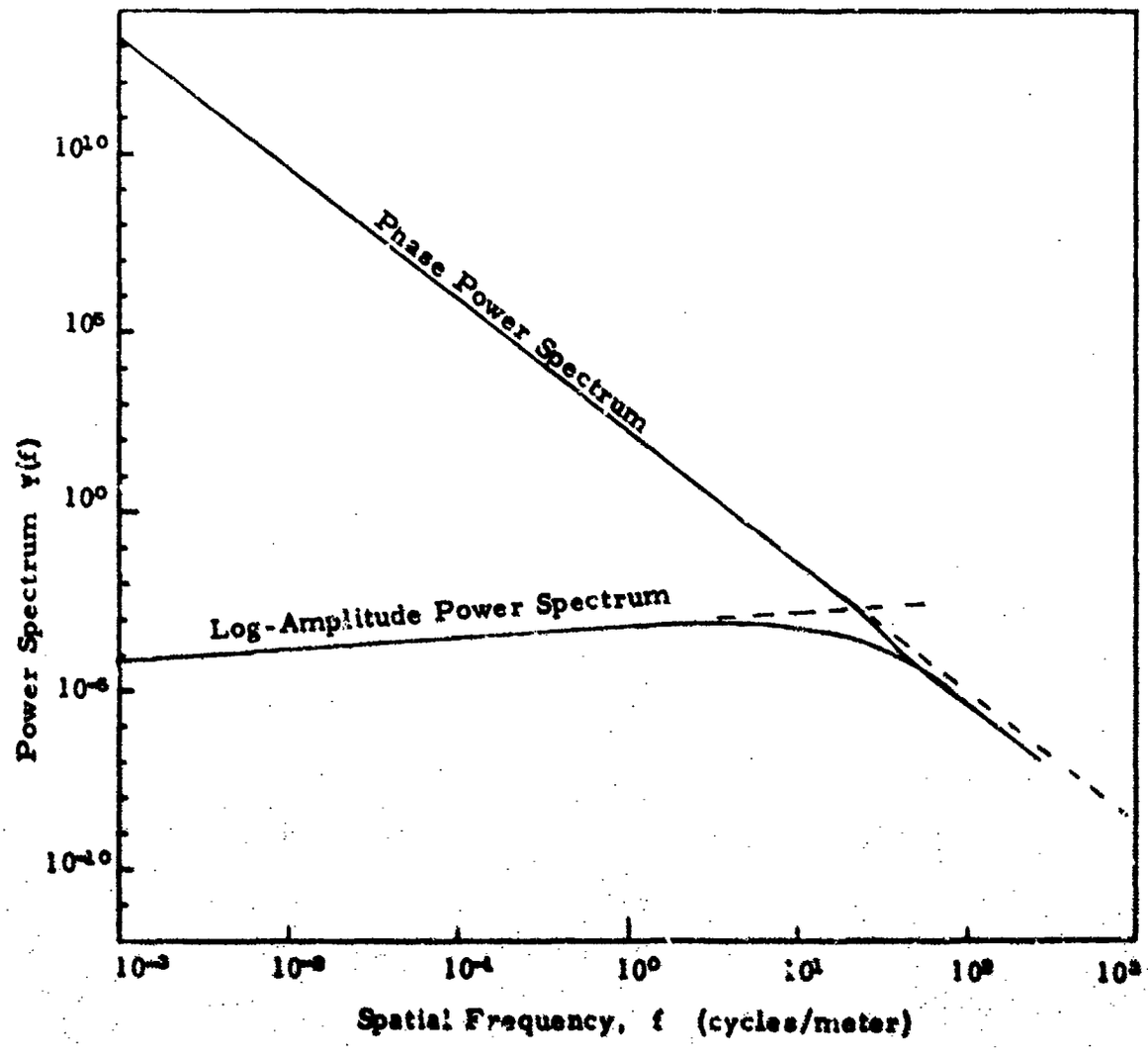

Figure 1. Bufton Turbulence Model Power Spectra. Calculations are for an aircraft at 62,000 ft. looking straight down at a 4880 Å point-source beacon. The extension of the low frequency asymptotic behavior, Eq.'s (69) and (70), is shown as the broken lines.

$$f_\tau = (A_\phi / A_\ell)^{1/4} \quad . \tag{71}$$

For high spatial frequencies, the asymptotic limit for the two power spectra appear to have the form

$$W_\phi(f) \approx \tfrac{1}{2} A_\phi f^{-11/3} \quad , \qquad (f >> f_\tau) \quad , \tag{72}$$

$$W_\ell(f) \approx \tfrac{1}{2} A_\phi f^{-11/3} \quad , \qquad (f >> f_\tau) \quad . \tag{73}$$

Thus we see that presenting values for A_ϕ and A_ℓ, and for convenience also for f_τ, appears to completely characterize the phase and log-amplitude power spectra.

The forty runs performed using the Hufnagel Random Turbulence Model and the Hufnagel Non-Random Turbulence Model give results in good general agreement with the asymptotic representation of the power spectra presented. In Fig.'s 2 and 3, we present plots of the phase and log-amplitude power spectra for the rms wind parameter W having the two extreme values of 5 and 50 m/sec, for cases run with aircraft flight altitudes of 62,000 ft. and 35,000 ft., respectively, using the Hufnagel Non-Random Turbulence Model. As can be seen, the results are clearly in conformance with the asymptotic behavior suggested in Eq.'s (69)-(73). The ten power spectra runs with the Hufnagel Random Turbulence Model for each aircraft altitude were averaged, and the results plotted in Fig.'s 4 and 5. Here again, it is obvious that the power spectra follow the asymptotic dependencies presented in Eq.'s (69)-(73). Moreover, we note from a comparison of Fig.'s 4 with 2, and 5 with 3, that the power spectra obtained from the random turbulence model with W = 25 is in reasonably good general agreement with what we get with the same value of W from the non-random turbulence model.

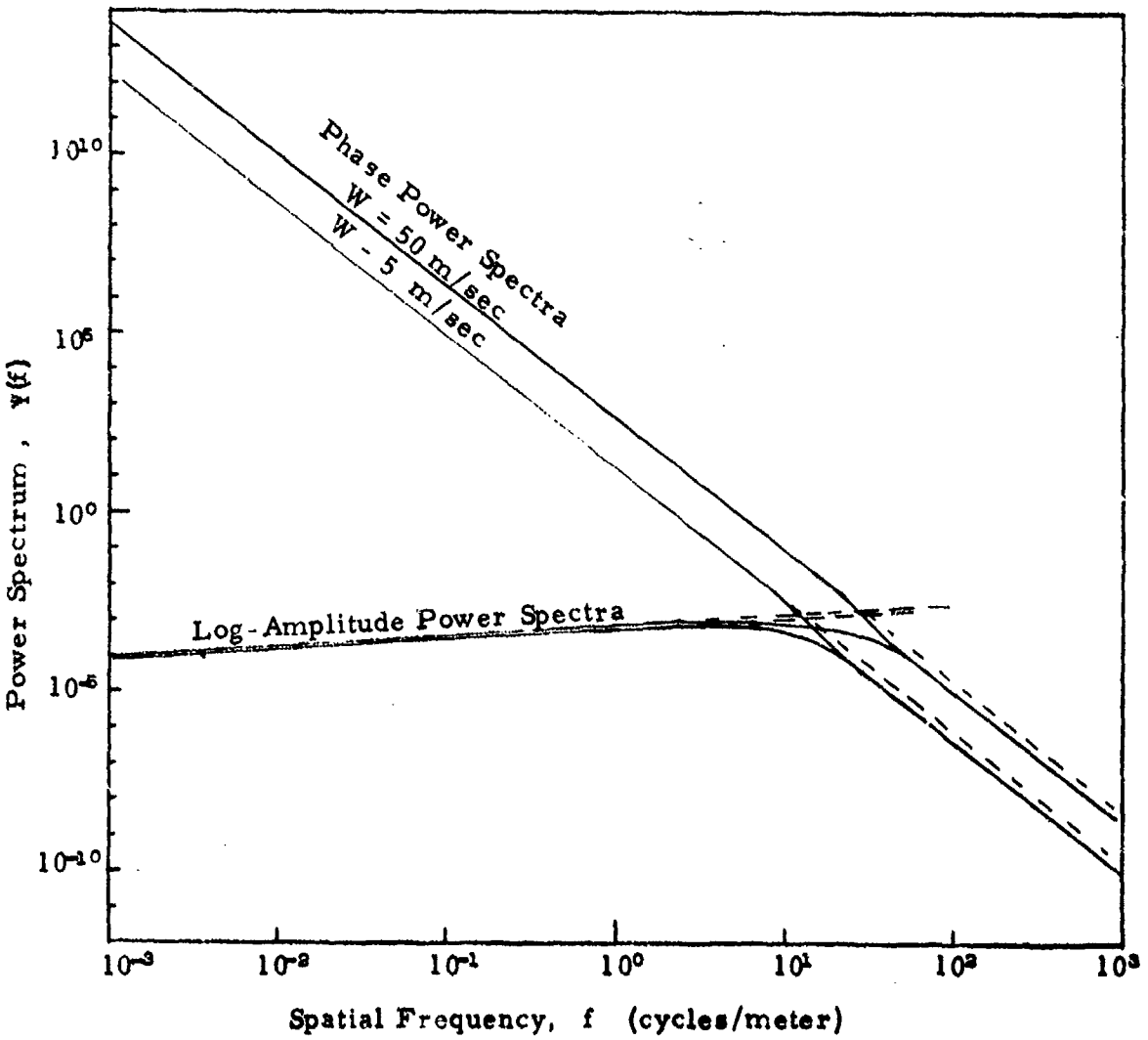

Figure 2. Hufnagel Non-Random Turbulence Model Power Spectra, 62,000 ft. Calculations are for an aircraft at 62,000 ft. looking straight down at a 4880 Å point-source beacon. Results are shown for the turbulence model run with rms wind values of W = 5 m/sec and W = 50 m/sec. For very low spatial frequencies, there is only a very small difference in the log-amplitude power spectra for these two cases. The broken lines represent the extension to high frequencies of the low frequency asymptotic dependencies given in Eq.'s (69) and (70).

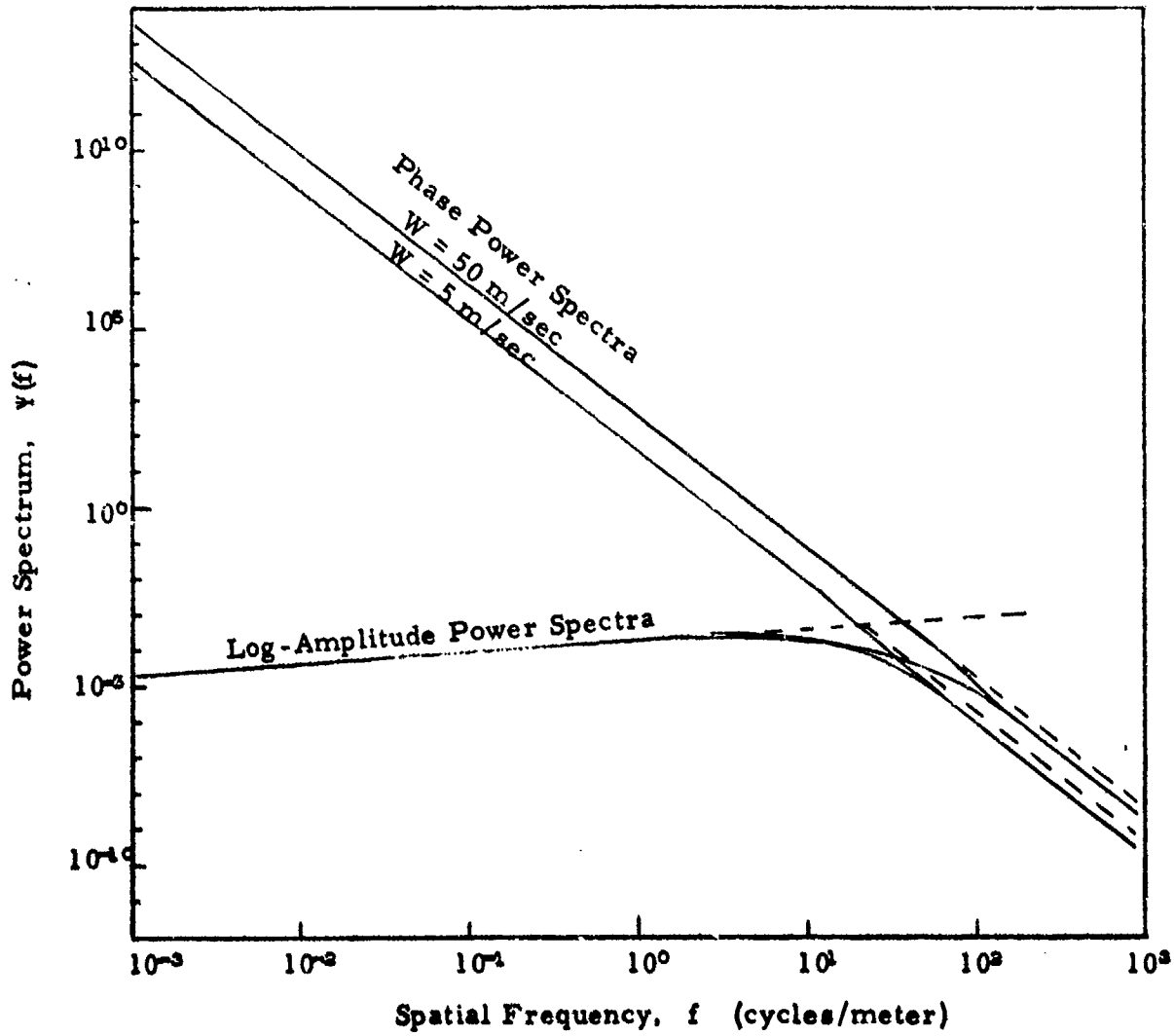

Figure 3. Hufnagel Non-Random Turbulence Model Power Spectra, 35,000 ft. All comments here are the same as for Fig. 2, except that the aircraft altitude is 35,000 ft.

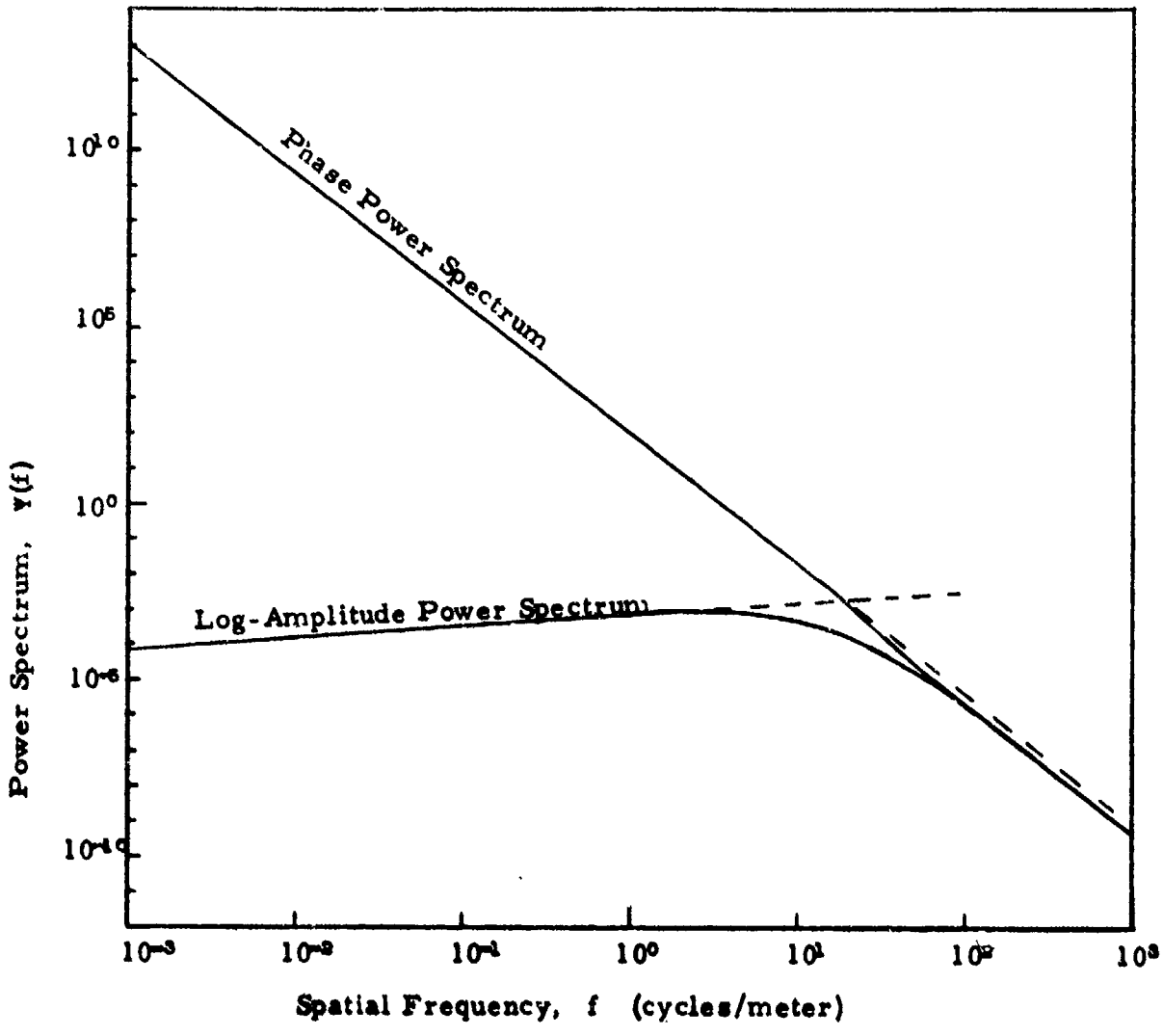

Figure 4. Hufnagel Random Turbulence Model Power Spectra, 62,000 ft. Calculations are for an aircraft at 62,000 ft. looking straight down at a 4880 Å point-source beacon. Results shown are the average of the results of ten runs, all carried out with an rms wind parameter value W = 25 m/sec. The broken lines represent an extension of the low frequency asymptotic dependencies, given in Eq.'s (69) and (70), into the high spatial frequency range.

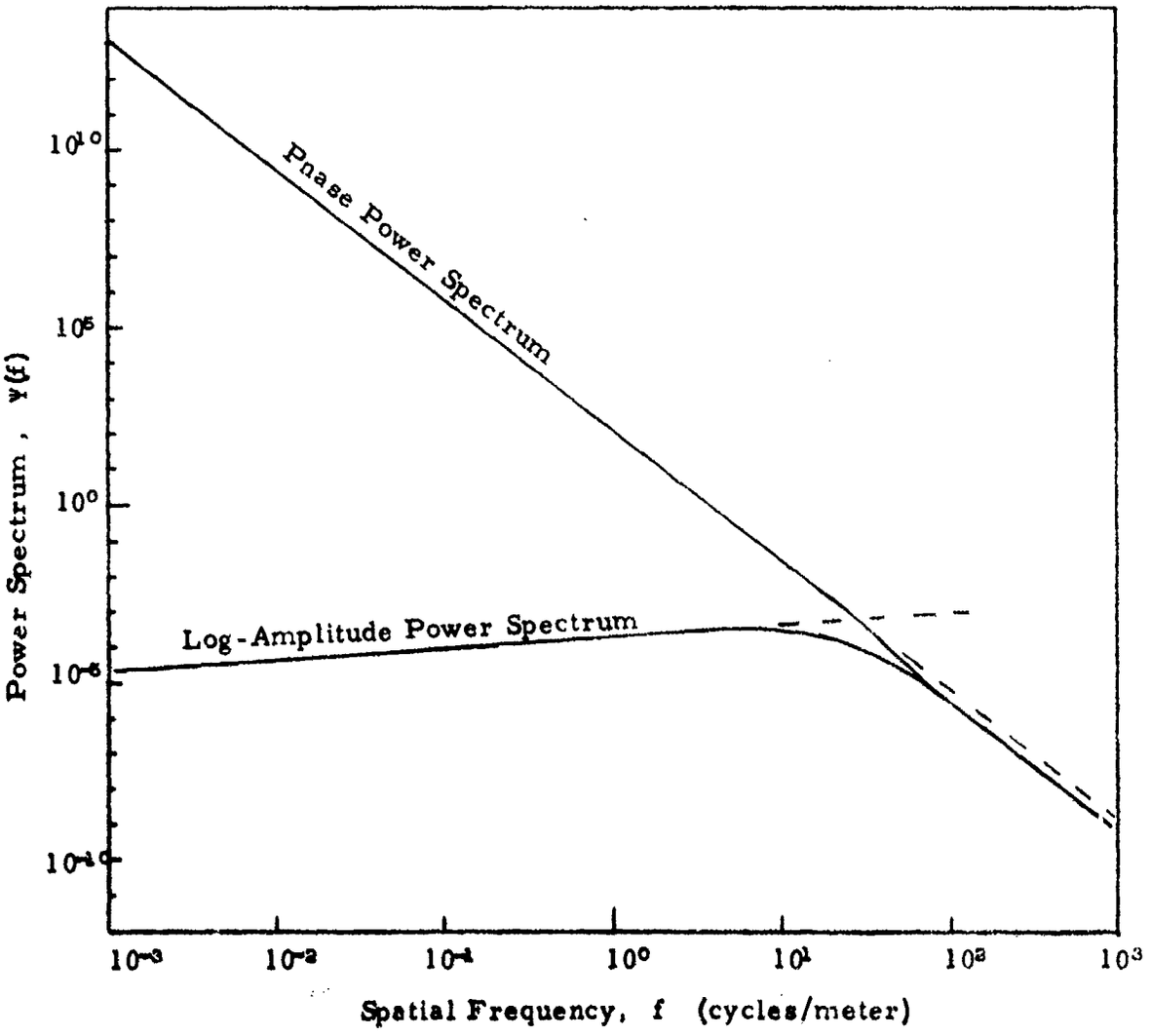

Figure 5. Hufnagel Random Turbulence Model Power Spectra, 35,000 ft. All comments here are the same as for Fig. 4, except that the aircraft altitude is 35,000 ft.

In Tables 13 and 14, we present the values of the parameters governing the asymptotic dependencies, i.e., A_ϕ , A_ℓ , and f_τ for the Bufton turbulence model and 62,000 ft. aircraft flight altitude, for the ten W-values obtained with the non-random turbulence model at 62,000 ft. and 35,000 ft. aircraft flight altitudes, and for the average of the ten random turbulence runs with W = 25 m/sec and 62,000 ft. and 35,000 ft. aircraft flight altitudes. As can be seen from an inspection of these tables, there appears to be no very great significance to be attached to the random as distinct from the non-random Hufnagel turbulence model -- at least as far as computation of the phase and log-amplitude power spectra are concerned. The values of A_ϕ , A_ℓ , and f_τ obtained with the random model match the values obtained with the non-random model for the same value of the rms wind parameter, i.e., W = 25 m/sec , to within one standard deviation. We note also that the ability to distinguish between different turbulence models, in this case between the Bufton Turbulence Model and the Hufnagel Non-Random Turbulence Model is not provided by phase and log-amplitude power spectra taken at a single altitude.

In Tables 15 and 16, we show the values of the basic propagation parameters, r_0 , σ_ℓ^2 , d_0 , and H_0 for each of the cases considered. Here again, we note the good agreement between the average of the random turbulence results and the results of the non-random turbulence for the same rms wind speed parameter, W = 25 m/sec . It is not clear from any of these results that any particular virtue or utility should be attached to the Hufnagel Random Turbulence Model in comparison to the Hufnagel Non-Random Turbulence Model. We prefer the latter because of its ease in use.

None of our results, however, can be interpreted as in any way validating either model. What is clear from our results is that validation

Table 13

Power Spectra Parameters, 62,000 ft.

The parameters listed are defined by Eq.'s (69)-(73). The data is for an aircraft at 62,000 ft. looking straight down at a 4880 Å point-source beacon on the ground.

Turbulence Model	A_ϕ	A_ℓ	f_T
Bufton	1.73×10^{3}	7.84×10^{-4}	21.7
Hufnagel Non-Random			
W = 5 m/sec	1.77×10^{1}	6.90×10^{-4}	12.7
W = 10	3.01×10^{1}	6.94×10^{-4}	14.4
W = 15	5.08×10^{1}	7.06×10^{-4}	16.4
W = 20	7.98×10^{1}	7.16×10^{-4}	18.3
W = 25	1.17×10^{2}	7.28×10^{-4}	20.0
W = 30	1.62×10^{2}	7.43×10^{-4}	21.6
W = 35	2.16×10^{2}	7.60×10^{-4}	23.1
W = 40	2.79×10^{2}	7.81×10^{-4}	24.4
W = 45	3.49×10^{2}	8.04×10^{-4}	25.7
W = 50	4.27×10^{2}	8.29×10^{-4}	26.8
Hufnagel Random Average of 10 runs with			
W = 25 m/sec	$(1.01 \pm 0.25)\times10^{2}$	$(7.10 \pm 0.15)\times10^{-4}$	19.4 ± 1.2

Table 14

Power Spectra Parameters, 35,000 ft.

The comments here are the same as for Table 13, except that the aircraft altitude is 35,000 ft.

Turbulence Model	A_ϕ	A_ℓ	f_r
Hufnagel Non-Random			
W = 5 m/sec	3.72×10^{1}	2.06×10^{-4}	20.6
W = 10	4.74×10^{1}	2.07×10^{-4}	21.9
W = 15	6.46×10^{1}	2.07×10^{-4}	23.6
W = 20	8.86×10^{1}	2.07×10^{-4}	25.6
W = 25	1.19×10^{2}	2.08×10^{-4}	27.5
W = 30	1.57×10^{2}	2.09×10^{-4}	29.4
W = 35	2.01×10^{2}	2.10×10^{-4}	31.3
W = 40	2.53×10^{2}	2.11×10^{-4}	33.1
W = 45	3.11×10^{2}	2.12×10^{-4}	34.8
W = 50	3.76×10^{2}	2.13×10^{-4}	36.5
Hufnagel Random Average of 10 runs with			
W = 25 m/sec	$(1.14 \pm 0.38)\times10^{2}$	$(2.13 \pm 0.24)\times10^{-4}$	27.0 ± 9.5

Table 15

Basic Propagation Parameters, 62,000 ft.

All data is for an aircraft at 62,000 ft. looking straight down at a 4880 Å point-source beacon on the ground

Turbulence Model	r_o (m)	σ_ℓ^2 (neper²)	d_o (m)	H_o (km)
Bufton	0.267	0.0494	0.233	7.74
Hufnagel Non-Random				
W = 5 m/sec	1.05	0.0173	0.347	13.2
W = 10	0.765	0.0197	0.329	10.9
W = 15	0.559	0.0238	0.305	9.43
W = 20	0.426	0.0295	0.280	8.57
W = 25	0.338	0.0368	0.256	8.06
W = 30	0.278	0.0457	0.235	7.75
W = 35	0.234	0.0562	0.218	7.54
W = 40	0.201	0.0684	0.202	7.40
W = 45	0.175	0.0821	0.189	7.30
W = 50	0.155	0.0975	0.178	7.23
Hufnagel Random Average of 10 runs with W = 25 m/sec	0.383 ± 0.069	0.0325 ± 0.0055	0.270 ± 0.020	8.14 ± 0.54

Table 16

Basic Propagation Parameters, 35,000 ft.

All data is for an aircraft at 35,000 ft. looking straight down at a 4880 Å point-source beacon on the ground.

Turbulence Model	r_o (m)	σ_ℓ^2 (neper^2)	d_o (m)	H_o (km)
Hufnagel Non-Random				
W = 5 m/sec	0.674	0.0147	0.221	6.72
W = 10	0.588	0.0153	0.218	5.94
W = 15	0.484	0.0162	0.212	5.13
W = 20	0.400	0.0175	0.206	4.46
W = 25	0.334	0.0191	0.198	3.95
W = 30	0.283	0.0211	0.190	3.57
W = 35	0.244	0.0235	0.182	3.29
W = 40	0.213	0.0263	0.174	3.08
W = 45	0.188	0.0294	0.166	2.92
W = 50	0.168	0.0329	0.159	2.79
Hufnagel Random Average of 10 runs with				
W = 25 m/sec	0.382 ± 0.099	0.0206 ± 0.0101	0.202 ± 0.023	4.42 ± 1.00

or rejection of any particular turbulence model will require more than merely straightforward optical measurements* made at a single altitude. The virtue of single altitude measurements is that they may be translated to prediction of the results of other types of measurements at the same altitude at the same time, but clearly they will not by themselves provide the basis for generating a description of the distribution of turbulence in the atmosphere.

---

* Certain rather special measurements made at a single altitude may be able to give data on the altitude distribution of C_n^2, but these are not ordinary measurements.

References for Part I

1. D. L. Fried, "Statistics of a Geometric Representation of Wavefront Distortion," J. Opt. Soc. Am. 55, 1427 (1965)

2. I. Goldstein, P. A. Miles, and A. Chabot, "Heterodyne Measurements of Light Propagation Through Atmospheric Turbulence," Proc. IEEE 53, 1172 (1965)

3. D. L. Fried, "Propagation of a Spherical Wave in a Turbulent Medium," J. Opt. Soc. Am. 57, 175 (1967)

4. D. L. Fried, "Limiting Resolution Looking Down Through the Atmosphere," J. Opt. Soc. Am. 56, 1380 (1966)

5. D. L. Fried, "Aperture Averaging of Scintillation," J. Opt. Soc. Am. 57, 169 (1967)

6. M. E. Gracheva and A. S. Gurvich, "Strong Fluctuations of Light Intensity in Propagation in the Ground Air Layer," Izvestiya Vazov (Radiofizika) 8, 717 (1965)

7. D. L. Fried, "Theoretical Analysis of Aperture Averaging," Optical Science Consultants Report No. DR-015, Final Report on NASA Contract NAS5-23272

8. M. Born and E. Wolf, "Principles of Optics," Third (Revised) Edition, Pergamon Press, (New York, 1965)

9. D. L. Fried, "Theoretical Study of Non-Standard Imaging Concepts," Interim Technical Report on RADC Contract No. F30602-74-C-0115, RADC Report No. TR-74-185, May 1974, and RADC Report No. TR-74-276, October 1974 (783 276) & (A002 160)

10. D. L. Fried, "Optical Resolution Through a Randomly Inhomogeneous Medium for Very Long and Very Short Exposures," J. Opt. Soc. Am. 56, 1372 (1966)

11. D. L. Fried and H. T. Yura, "Telescope Performance Reciprocity for Propagation in a Turbulent Medium," J. Opt. Soc. Am. 62, 600 (1972)

12. D. L. Fried, "Optical Heterodyne Detection of an Atmospherically Distorted Signal Wavefront," Proc. IEEE 55, 57 (1967)

References (Continued)

13. D. L. Fried, "Atmospheric Turbulence-Induced Signal Variance in an Optical Heterodyne Receiver," Optical Science Consultants Report No. TR-158, Nov. 1974

14. J. R. Kerr, R. A. Elliott, P. A. Pincus, and M. H. Lee, "Propagation of Multiwavelength Laser Radiation Through Atmospheric Turbulence," Final Technical Report on RADC Contract No. F30602-74-C-0082, RADC Report No. RADC-TR-74-320, November 1974, Section III. B (A003 340)

15. D. M. Chase, "Power Loss in Propagation Through a Turbulent Medium for an Optical Heterodyne System with Angle Tracking," J. Opt. Soc. Am. 56, 33 (1966)

16. V. I. Tatarski, "Wave Propagation in a Turbulent Medium," McGraw-Hill (New York, 1961)

17. A. Erdelyi, et al, "Table of Integral Transforms," Vol. II, McGraw-Hill (New York, 1954), p. 5, Eq. (1)

18. J. L. Bufton, "Comparison of Vertical Profile Turbulence Structure with Stellar Observations," Appl. Opt. 12, 1785 (1973)

19. V. M. Koprov and L. R. Tsvang, "Characteristics of Very Small Scale Turbulence in a Stratified Boundary Layer," Atmos. and Oceanic Phys. 22, 1142 (1966)

20. op cit, ref. 9, Chapter II of RADC-TR-74-185 dated May 1974 (783 276)

21. R. E. Hufnagel, "Variations of Atmospheric Turbulence," presented at the OSA Topical Meeting on Optical Propagation Through Turbulence, Boulder, Colorado, July 9-11, 1974

22. R. E. Hufnagel, private communications.

Appendix 1

Main Program Listing

(Copies of this program can be obtained on 8-bit wide paper tape, on request to Optical Science Consultants.)

```
110 REM   #1
120 DIM C[1000],M[30],I1[30],I2[30],M1[30],M2[30]
121 DIM A$[8],B$[18]
130 LET A$="#.##↑↑↑↑"
131 LET B$="#.###↑↑↑↑ #.##↑↑↑↑"
150 GOSUB  9000
1002 FOR I=1 TO 5
1004 PRINT
1006 NEXT I
1010 REM   #2
1012 PRINT "NUMBER OF INTERVALS IN INTEGRATION = ";
1014 INPUT N
1016 PRINT
1020 PRINT "WAVELENGTH (METERS) = ";
1030 INPUT K
1040 PRINT
1050 LET K=6.28319/K
1060 PRINT "IS SOURCE A POINT SOURCE? (1=YES) ";
1070 INPUT Q
1080 PRINT
1090 IF Q<>1 PRINT
1091 IF Q<>1 PRINT "(SOURCE WILL BE TREATED AS AN INFINITE ";
1092 IF Q<>1 PRINT "PLANE WAVE.)"
1093 IF Q<>1 PRINT
1100 PRINT "PATH LENGTH (METERS) = ";
1110 INPUT Z
1120 PRINT
1160 PRINT "OPTICS ALTITUDE (METERS) = ";
1170 INPUT H2
1180 PRINT
1182 PRINT "REMOTE END ALTITUDE (METERS) = ";
1184 INPUT H1
1186 PRINT
1190 PRINT "INPUT 6-DIGIT BINARY NUMBER TO CONTROL OUTPUT. ";
1230 INPUT Q1
1240 FOR I=1 TO 5
1250 PRINT
1260 NEXT I
1310 REM   #3
1330 LET H3=H1
1340 IF H3>H9 LET H3=H9
1350 LET H4=H2
1360 IF H4>H9 LET H4=H9
1370 IF H3<>H4 GOTO  1410
1380 IF H3<H9 GOTO 1410
1390 PRINT "PROPAGATION ENTIRELY OUT OF THE TURBULENT ATMOSPHERE."
1400 STOP
```

```
1410 LET Z1=0
1412 LET Z2=Z
1414 IF H1=H2 GØTØ 1440
1416 LET Z1=Z*(H1-H3)/(H1-H2)
1420 LET Z2=Z*(H1-H4)/(H1-H2)
1440 LET Z3=(Z2-Z1)/N
1450 LET H5=(H4-H3)/N
1460 REM   #4
1470 LET H=H3-H5/2
1480 FØR I=1 TØ N
1490 LET H=H+H5
1500 GØSUB 9010
1510 LET C[I]=C
1520 NEXT I
1610 REM   #5
1630 LET I2=1E-60
1640 LET I3=1E-60
1650 LET I4=1E-60
1660 LET I5=1E-60
1670 LET S=Z1-Z3/2
1680 FØR I=1 TØ N
1690 LET S=S+Z3
1700 LET S1=Z-S
1710 LET S2=S1↑(5/6)
1720 LET S3=1
1730 LET S4=1
1740 LET S5=1
1750 IF Q=1 LET S3=(S/Z)↑(5/6)
1760 IF Q=1 LET S4=S3*S3
1770 IF Q=1 LET S5=S4*(Z/S)*(Z/S)
1790 LET I2=I2+C[I]*S4
1800 LET I3=I3+C[I]*S2*S3
1810 LET I4=I4+C[I]*S2*S2*S4
1820 LET I5=I5+C[I]*S1*S1*S5
1830 NEXT I
1850 LET I2=I2*Z3
1860 LET I3=I3*Z3
1870 LET I4=I4*Z3
1880 LET I5=I5*Z3
1910 REM   #6
1920 LET R1=(.423*K*K*I2)↑(-3/5)
1940 LET R3=.56
1960 LET R3=R3*K↑(7/6)*I3
1970 LET R4=2.399*K↑(-.5)*(I5/I3)↑(3/7)
1980 LET R5=(I4/I2)↑(3/5)
1982 PRINT " ","BASIC GENERAL RESULTS"
1984 PRINT
```

```
1985 PRINT
1990 PRINT  USING A$;"RECEIVER C0HERENCE DIAMETER, R-SUB-ZER0 = ";R1;
2000 PRINT " (METERS)"
2030 PRINT "L0G-AMPLITUDE VARIANCE,SIGMA-SUB-L SQUARED = ";
2040 PRINT  USING A$;R3;" (NEPERS-SQ)"
2050 PRINT "SCINTILLATI0N AVERAGING LENGTH, D-SUB-ZER0 = ";
2060 PRINT  USING A$;R4;" (METERS)"
2070 PRINT "IS0PLANATISM EFFECTIVE PATH LENGTH, H-SUB-ZER0 = ";
2080 PRINT  USING A$;R5;" (METERS)"
2090 IF R3<.5 G0T0 2220
2100 PRINT
2110 PRINT
2120 PRINT "THE C0MPUTED VALUE 0F L0G-AMPLITUDE VARIANCE IS S0 LARGE"
2130 PRINT "AS T0 CAST D0UBT 0N ALL INTENSITY FLUCTUATI0N RESULTS."
2140 PRINT "PRINT-0UT 0F THESE RESULTS WILL BE SUPPRESSED."
2220 PRINT
2230 PRINT
2231 PRINT
2232 PRINT " ","SUBSIDIARY GENERAL RESULTS"
2234 PRINT
2235 PRINT
2240 IF Q=1 G0T0 2320
2250 LET P1=7.08982/(K*R1)
2260 PRINT "LIMITING RES0LUTI0N ANGLE, THETA-SUB-MIN = ";
2270 PRINT  USING A$;P1;" (RADIANS)"
2280 LET P2=.5*R1/R5
2290 PRINT "IS0PLANATISM FIELD-ANGLE, THETA-SUB-ZER0 = ";
2300 PRINT  USING A$;P2;" (RADIANS)"
2310 G0T0  2380
2320 LET P1=7.08982*Z/(K*R1)
2330 PRINT "LIMITING RES0LUTI0N S0URCE LENGTH X-SUB-MIN = ";
2340 PRINT  USING A$;P1;" (METERS)"
2350 LET P2=.5*R1*Z/R5
2360 PRINT "IS0PLANATISM S0URCE SIZE, X-SUB-ZER0 = ";
2370 PRINT  USING A$;P2;" (METERS)"
2380 IF R3>.5 G0T0 2420
2390 LET P3= EXP (4*R3)-1
2400 PRINT "N0RMALIZED INTENSITY VARIANCE, SIGMA-SUB-I SQUARED = ";
2410 PRINT  USING A$;P3
2420 F0R I=1 T0 5
2425 PRINT
2430 NEXT I
2510 REM   #7
2515 LET Q2=Q1
2520 IF Q1<100000 G0T0 3066
2530 LET Q2=Q1-100000* INT (Q1/100000)
2540 PRINT " "," IMAGING-0PTICS RES0LUTI0N"
```

```
2541 PRINT " ","(ØR TRANSMITTER BEAM SPREAD)"
2542 PRINT " ","FØR VARIØUS ØPTICS DIAMETERS"
2543 PRINT
2544 PRINT
2550 PRINT " ","  SLØW","           FAST"
2551 PRINT " ","ØPERATIØN","          ØPERATIØN"
2552 PRINT
2560 PRINT " ØPTICS","RESØLUTIØN","RESØLUTIØN"," DITHER"
2562 PRINT "DIAMETER",
2570 IF Q=1 PRINT " (METERS)"," (METERS)","(METERS)"
2580 IF Q<>1 PRINT "(RADIANS)","(RADIANS)","(RADIANS)"
2590 PRINT "(METERS)"
2595 PRINT
3000 PRINT  USING A$;.1*R1,10.111*P1,10.019*P1,1.3658*P1
3010 PRINT  USING A$;.215443*R1,4.827*P1,4.6726*P1,1.211*P1
3020 PRINT  USING A$;.464159*R1,2.4625*P1,2.2064*P1,1.0935*P1
3030 PRINT  USING A$;R1,1.4983*P1,1.0886*P1,1.0295*P1
3040 PRINT  USING A$;2.15443*R1,1.1765*P1,.62407*P1,.99737*P1
3050 PRINT  USING A$;4.64159*R1,1.0718*P1,.54627*P1,.92218*P1
3060 PRINT  USING A$;10*R1,1.0312*P1,.69329*P1,.76341*P1
3061 FØR I=1 TØ 5
3062 PRINT
3063 NEXT I
3065 REM   #8
3066 IF Q2<10000 GØTØ  3234
3067 LET Q2=Q2-10000* INT (Q2/10000)
3070 PRINT  TAB (15);"HETERØDYNE RECEIVER PERFØRMANCE"
3075 FØR I=1 TØ 3
3076 PRINT
3077 NEXT I
3078 PRINT  TAB (17);"SLØW ØPERATIØN PERFØRMANCE"
3080 PRINT
3081 PRINT
3082 PRINT  TAB (11);"ØPTICS"; TAB (23);"EFFECTIVE";
3083 PRINT  TAB (38);"RMS SIGNAL-"
3084 PRINT  TAB (10);"DIAMETER"; TAB (23);"DIAMETER";
3085 PRINT  TAB (36);"PØWER VARIATIØN"
3086 PRINT  TAB (10);"(METERS)"; TAB (23);"(METERS)";
3087 PRINT  TAB (42);"(%)"
3090 PRINT
3091 PRINT  USING A$; TAB (10);.1*R1; TAB (23);9.889E-02*R1;
3092 PRINT  USING A$; TAB (40);2.19
3093 PRINT  USING A$; TAB (10);.215443*R1; TAB (23);
3094 PRINT  USING A$;.20717*R1; TAB (40);7.87
3095 PRINT  USING A$; TAB (10);.464158*R1; TAB (23);
3096 PRINT  USING A$;.4061*R1; TAB (40);20
3097 PRINT  USING A$; TAB (10);R1; TAB (23);.667429*R1;
```

```
3098 PRINT  USING A$; TAB (40);61.6
3099 PRINT  USING A$; TAB (10);2.15443*R1; TAB (23);
3100 PRINT  USING A$;.849963*R1; TAB (40);131
3101 PRINT  USING A$; TAB (10);4.64158*R1; TAB (23);
3102 PRINT  USING A$;.932984*R1; TAB (40);147
3103 PRINT  USING A$; TAB (10);10*R1; TAB (23);.969713*R1;
3104 PRINT  USING A$; TAB (40);123
3110 FØR I=1 TØ 4
3111 PRINT
3112 NEXT I
3113 PRINT  TAB (17);"FAST ØPERATIØN PERFØRMANCE"
3114 PRINT
3115 PRINT
3116 PRINT  TAB (14);"ØPTICS"; TAB (26);"EFFECTIVE";
3117 PRINT  TAB (38);"TRACKING"
3118 PRINT  TAB (13);"DIAMETER"; TAB (26);"DIAMETER";
3119 PRINT  TAB (39);"DITHER"
3120 PRINT  TAB (13);"(METERS)"; TAB (26);"(METERS)";
3121 PRINT  TAB (38);"(RADIANS)"
3125 PRINT
3126 LET X=P1
3127 IF Q=1 LET X=P1/Z
3130 PRINT  USING A$; TAB (13);.1*R1; TAB (26);
3131 PRINT  USING A$;9.98127E-02*R1; TAB (40);1.3658*X
3132 PRINT  USING A$; TAB (13);.215443*R1; TAB (26);
3133 PRINT  USING A$;.214013*R1; TAB (40);1.211*X
3134 PRINT  USING A$; TAB (13);.464159*R1; TAB (26);
3135 PRINT  USING A$;.453237*R1; TAB (40);1.0935*X
3136 PRINT  USING A$; TAB (13);R1; TAB (26);
3137 PRINT  USING A$;.918652*R1; TAB (40);1.0192*X
3138 PRINT  USING A$; TAB (13);2.15443*R1; TAB (26);
3139 PRINT  USING A$;1.60239*R1; TAB (40);.99737*X
3140 PRINT  USING A$; TAB (13);4.64159*R1; TAB (26);
3141 PRINT  USING A$;1.8306*R1; TAB (40);.92218*X
3142 PRINT  USING A$; TAB (13);10*R1; TAB (26);
3143 PRINT  USING A$;1.44241*R1; TAB (40);.76341*X
3150 FØR I=1 TØ 5
3151 PRINT
3152 NEXT I
3233 REM   #9
3234 IF Q2<1000 GØTØ 3990
3235 LET Q2=Q2-1000* INT (Q2/1000)
3236 PRINT  TAB (18);"PREDETECTIØN CØMPENSATIØN"
3237 PRINT
3238 PRINT
3239 PRINT
3240 PRINT  TAB (11);"EFFECT ØF LACK ØF ISØPLANATISM ØN";
```

```
3241 PRINT " COMPENSATED"
3250 PRINT  TAB (11);"MTF FOR SELF-REFERENCED OPERATION, ";
3251 PRINT "FOR VARIOUS"
3260 PRINT  TAB (13);"(NOMINALLY CIRCULAR) SOURCE DIAMETERS."
3270 PRINT
3280 PRINT
3290 PRINT  TAB (31);"MTF DEGREDATION"
3300 PRINT
3310 PRINT  TAB (6);"SOURCE"; TAB (17);"LOCATION ON THE SOURCE";
3320 PRINT " OF THE IMAGED REGION"
3330 PRINT  TAB (7);"SIZE"; TAB (16);"CENTER"; TAB (26);"1/4"; TAB (36);

3340 PRINT "1/2"; TAB (46);"3/4"; TAB (56);"EDGE"
3350 IF Q=1 PRINT  TAB (5);"(METERS)"
3360 IF Q<>1 PRINT  TAB (5);"(RADIANS)"
3370 PRINT
3380 FOR I=-3 TO 3
3390 PRINT  USING A$; TAB (5);10↑(I/3)*P2;"  ";
3391 PRINT  USING A$; EXP (-.165*10↑(5*I/9));"  ";
3400 PRINT  USING A$; EXP (-.278*10↑(5*I/9));"  ";
3401 PRINT  USING A$; EXP (-.615*10↑(5*I/9));"  ";
3410 PRINT  USING A$; EXP (-1.166*10↑(5*I/9));"  ";
3411 PRINT  USING A$; EXP (-1.914*10↑(5*I/9))
3420 NEXT I
3430 FOR I=1 TO 5
3440 PRINT
3450 NEXT I
3500 PRINT  TAB (11);"EFFECT OF LACK OF ISOPLANATISM ON COMPENSATED"
3510 PRINT  TAB (11);"MTF FOR EXTERNALLY-REFERENCED OPERATION,"
3520 PRINT  TAB (11);"FOR VARIOUS IMAGE-TO-REFERANCE SEPERATIONS."
3530 PRINT
3540 PRINT
3550 PRINT  TAB (18);"SEPERATION"; TAB (38);"MTF"
3560 IF Q=1 PRINT  TAB (19);"(METERS)";
3570 IF Q<>1 PRINT  TAB (19);"(RADIANS)";
3580 PRINT  TAB (34);"DEGREDATION"
3590 PRINT
3600 FOR I=-5 TO 1
3610 PRINT  USING A$; TAB (19);10↑(I/3)*P2; TAB (35);
3611 PRINT  USING A$; EXP (-6.88*10↑(5*I/9))
3620 NEXT I
3630 FOR I=1 TO 5
3640 PRINT
3650 NEXT I
3680 PRINT  TAB (9);"THE DIFFRACTION LIMITED MTF IS 50%, 25%, ";
3681 PRINT "10%"
3690 PRINT  TAB (9);"WITH THE INDICATED OPTICS DIAMETERS, ";
3691 PRINT "FOR THE"
```

```
3700 PRINT  TAB (9);"SOURCE PATTERN PERIODICITIES LISTED."
3710 PRINT
3720 PRINT
3730 PRINT  TAB (5);"OPTICS"; TAB (27);"SOURCE PATTERN PERIOD FOR"
3740 PRINT  TAB (4);"DIAMETER"; TAB (21);"50% MTF"; TAB (36);
3741 PRINT "25% MTF"; TAB (51);"10% MTF"
3750 PRINT  TAB (4);"(METERS)"; TAB (20);
3760 IF Q=1 PRINT  TAB (4);"(METERS)"; TAB (35);"(METERS)";
3761 IF Q=1 PRINT  TAB (50);"(METERS)"
3770 IF Q<>1 PRINT  TAB (4);"(RADIANS)"; TAB (35);"(RADIANS)";
3771 IF Q<>1 PRINT  TAB (50);"(RADIANS)"
3780 PRINT
3790 FOR I=.25 TO 3 STEP .25
3800 PRINT  USING A$; TAB (4);I; TAB (19);
3810 IF Q=1 LET K1=K*I/Z
3820 IF Q<>1 LET K1=K*I
3830 PRINT  USING A$;15.5535/K1; TAB (34);9.89939/K1; TAB (49);
3831 PRINT  USING A$;7.80148/K1
3840 NEXT I
3850 FOR I=1 TO 5
3860 PRINT
3870 NEXT I
3980 REM   #10
3990 IF Q2<100 GOTO  4320
4000 LET Q2=Q2-100* INT (Q2/100)
4100 IF R3>.5 GOTO 4320
4110 PRINT  TAB (16);"NORMALIZED, APERTURE AVERAGED"
4120 PRINT  TAB (15);"INTENSITY VARIANCE AS A FUNCTION"
4130 PRINT  TAB (20);"OF APERTURE DIAMETER."
4140 PRINT
4150 PRINT
4160 PRINT  TAB (22);"OPTICS"; TAB (34);"INTENSITY"
4170 PRINT  TAB (21);"DIAMETER"; TAB (34);"VARIANCE"
4180 PRINT  TAB (21);"(METERS)"
4190 PRINT
4200 FOR I=-3 TO 3
4210 PRINT  USING A$; TAB (21);10↑(I/3)*R4;
4220 PRINT  USING A$; TAB (34);P3/(1+10↑(7*I/18)+10↑(7*I/9))
4230 NEXT I
4240 FOR I=1 TO 5
4250 PRINT
4260 NEXT I
4310 REM   #11
4320 IF Q2<10 GOTO 4520
4330 LET Q2=Q2-10* INT (Q2/10)
4335 LET S=10↑( INT ( LOG (3.16228/R4)/ LOG (10)))
4340 FOR J=0 TO 30
```

```
4350 LET M[J]=10↑((J-15)/5)/S
4360 LET M1[J]=M[J]↑(-11/3)
4370 LET M2[J]=M[J]*M[J]
4380 LET I1[J]=1E-60
4390 LET I2[J]=1E-60
4400 NEXT J
4410 LET S=Z1-Z3/2
4420 FØR I=1 TØ N
4430 LET S=S+Z3
4440 LET S1=1
4450 IF Q=1 LET S1=(S/Z)↑(5/3)
4460 LET S2=(Z-S)/K
4470 IF Q=1 LET S2=Z*(Z-S)/(K*S)
4480 FØR J=0 TØ 30
4488 LET M3=M2[J]*S2
4490 LET I3= CØS (M3)
4496 LET I4=1-I3
4497 IF M3>1 GØTØ  4500
4498 IF I3>.99 LET I4=M3*M3/2-M3*M3*M3*M3/24
4500 LET I1[J]=I1[J]+C[I]*S1*I4
4510 LET I2[J]=I2[J]+C[I]*S1*(1+I3)
4520 NEXT J
4530 NEXT I
4540 FØR J=0 TØ 30
4550 LET I1[J]=4.08*K*K*Z3*M1[J]*I1[J]
4560 LET I2[J]=4.08*K*K*Z3*M1[J]*I2[J]
4570 NEXT J
4580 PRINT  TAB (16);"SPATIAL PØWER-SPECTRUM FØR"
4590 PRINT  TAB (12);"LØG-AMPLITUDE AND PHASE VARIATIØNS"
4600 PRINT
4610 PRINT
4620 PRINT  TAB (11);"SPATIAL     LØG-AMPLITUDE";
4630 PRINT  TAB (44);"PHASE"
4640 PRINT  TAB (10);"FREQUENCY    PØWER-SPECTRUM";
4650 PRINT  TAB (39);"PØWER-SPECTRUM"
4660 PRINT  TAB (10);"(1/METERS)"
4670 PRINT
4680 FØR J=0 TØ 30
4690 PRINT  USING A$; TAB (10);1.00001*M[J]; TAB (27);
4691 PRINT  USING A$;I1[J]; TAB (43);I2[J]
4700 NEXT J
4710 FØR I=1 TØ 5
4720 PRINT
4730 NEXT I
4810 REM   #12
4820 IF Q2<1 GØTØ  4970
4830 LET Q2=Q2- INT (Q2)
```

```
4840 FØR I=1 TØ 5
4850 PRINT
4860 NEXT I
4870 PRINT "                TURBULENCE DISTRIBUTIØN ALØNG"
4871 PRINT "                   THE PRØPAGATIØN PATH"
4872 PRINT
4873 PRINT
4880 PRINT "                   ALTITUDE       C-SUB N SQ"
4890 PRINT "                     (M)           (M↑-2/3)"
4900 PRINT
4910 LET H=H3-H5/2
4920 FØR I=1 TØ N
4930 LET H=H+H5
4940 PRINT  USING B$; TAB (17);H; TAB (33);C[I]
4950 NEXT I
4960 PRINT
4970 STØP
```

Appendix 2

Program Remarks

In the Main Program, the notation REM #____ is utilized to indicate a discussion of some aspect of the operation of the program at that point. These comments, mostly too long for inclusion in the program itself, are presented in this appendix.

REM #1

The program's operation is initiated at this point. The computer program will accept the definition of an optical propagation problem and the pertinent propagation path and source information, and calculate the value of the various propagation integrals. From this, the program will calculate and report the value of the basic parameters which quantitatively describe the effects of turbulence on optical propagation for the propagation problem specified. The user has the option of requesting detailed information concerning any particular aspect of the problem. Before the program can be run, the user must provide a subroutine (described later) to allow calculation of the refractive-index structure constant along the propagation path.

REM #2

At this point, the program starts the process of requesting keyboard entry from the operator of the parameters governing the propagation problem, as well as a definition of the degree of detail to be provided in the result reported. (For batch operation, this section would have to be modified.) Most of the data input requests are self-explanatory in terms of the printout accompanying each request. However, the following three input requests deserve comment.

1) Number of intervals in integration -- All integrals are evaluated by first identifying the extent of the portion of the propagation path that is in the significantly turbulent part of the atmosphere. (The subroutine for generation of the refractive-index structure constant also defines the upper limit of the turbulent atmosphere.) The portion of the propagation path that is within the atmosphere is then subdivided into N equal length intervals. Each integral is evaluated as the sum over the set of N-intervals of the value of the integrand at the mid-point of each interval times the length of each interval. The user can specify integral evaluation using subdivision of the path into as few as N equals one (1) interval to as many as N equals one-thousand (1000) intervals.

2) In order to carry out propagation calculations, the program must be told whether to consider the "source" to be a point-source or an infinite plane wave source. If the user wants the program to consider the source to be a point-source, he inputs a one (1). Inputting any other value will cause the computer to consider the source to be an infinite plane-wave source. What is treated as the source can correspond to a true source, if we are concerned with such things as an optical system that receives a photon stream from a source (such as an imaging system, a heterodyne receiver, or an intensity receiver). However, if the optical system is a laser transmitter, then the program considers the aimpoint region to be the (virtual) source. We classify the problem as a point-source case if the laser beam is focused on the target.

If the source is a point-source, then imaging resolution results are given in units of length of the source, and for a laser transmitter, results are given in units of length at the target. For an infinite plane-wave source, such results are given in terms of angular subtense as seen from the system's optics, i.e., by the imaging aperture, or the laser transmitter's aperture.

3) The program will output detailed information concerning such things as imaging resolution or transmitter beam spread, heterodyne receiver performance, isoplanatism, aperture averaging of intensity fluctuations, etc., if so instructed. To cause computer printout of any of these options, the computer allows the operator to input a six-digit binary number. (Though the binary digits are nominally "zero" and "one", actually they are "zero" and "any non-zero digit.") Each digit refers to a particular output option. These are explained below.

First Digit: Causes output of resolution of an ordinary imaging system. (The results are also applicable for laser transmitter beam spread.)

Second Digit: Causes output of performance of an optical heterodyne receiver.

Third Digit: Causes output of information on predetection compensation imaging.

Fourth Digit: Causes output of performance of an intensity detection receiver in terms of signal fluctuations.

Fifth Digit: Causes output of the log-amplitude and phase fluctuation power spectrum.

Sixth Digit: Causes output of the turbulence distribution along the propagation path.

REM #3

The portion of the program starting here causes the portion of the propagation path within the turbulent atmosphere to be identified. This portion is between the path length ranges Z1 to Z2 (at altitudes H3 to H4 .)

REM #4

The portion of the program starting here calls on the refractive-index structure constant subroutine to generate values of the refractive-index structure constant at the center of each of the N-intervals involved in the integral evaluation.

REM #5

The portion of the program starting here evaluates the four basic propagation integrals, I2 , I3 , I4 , and I5 .

REM #6

The portion of the program starting here uses the propagation integrals to evaluate the four basic propagation parameters, r_0 , σ_ℓ^2 , d_0 , H_0 . It then prints out these values as the "Basic General Results," after which it prints out a set of "Subsidiary General Results" calculated directly from these basic parameters.

REM #7

If the first digit in the six-digit binary control number is not zero, the following portion of the program will be executed. This portion of the program will print out the resolution of various diameter imaging optics.

For a point-source, results are given in terms of a length at the source. For an infinite plane-wave source, results are given in terms of angular spread. Long exposure and short exposure results (called slow operation and fast operation, respectively) are both given. For the short exposure, results are in terms of both the resolution per se, and the jitter in the apparent position of a point source.

The same results, as indicated in the printout, are also applicable to the subject of laser transmitter beam spread. In this interpretation of the results, the term "slow operation" refers to a laser transmitter with a pointing servo too slow to follow the turbulence-induced rapid motion of the target. The term "fast operation" covers the case in which servo operation is fast enough to follow the turbulence-induced apparent dither of the target position.

REM #8

If the second digit of the six-digit binary control number is not zero, the following portion of the program will be executed. This portion of the program will print out the performance of an optical heterodyne receiver for various diameters of the entrance aperture. The term "slow operation" is used here to characterize a receiver whose pointing system is not capable of following the rapid changes of the apparent angle of arrival of the signal wavefront caused by turbulence. The term "fast operation" implies a system whose pointing system has a high enough servo bandwidth to do this.

REM #9

If the third digit of the six-digit binary control number is not zero, the following portion of the program will be executed. This portion of the program will print out information related to the performance of a

predetection compensation imaging system. For a point-source (the object being imaged is the source), the source size and source separation is given in units of length at the source, but for an infinite plane-wave source, source size and source separation are given in terms of angular subtense as seen from the imaging system's aperture.

For all image frequencies of interest (i.e., high image frequencies) there is a degradation above the normal diffraction-limited degradation. For self-referenced predetection compensation, this degradation depends on source size and how far from the center of the source the field-of-view being compensated is. For externally-referenced predetection compensation, this degradation depends on the separation of the reference and the field-of-view being compensated. For both self-referenced and externally-referenced predetection compensation, the MTF degradation values are printed out. Also as an aid to the user, the MTF per se associated with the diffraction limit is printed out in terms of the optics diameter and the pattern wavelength associated with the image frequency that gives an MTF of 50% , 25% , and 10% . The pattern wavelength of the image frequency is given in units of length for a point source, and in units of angular subtense for an infinite plane-wave source.

REM #10

If the fourth digit of the six-digit binary control number is not zero, the following portion of the program will be executed. This portion of the program will print out the fractional variance of the signal collected by photon-bucket receivers of various diameters.

REM #11

If the fifth digit of the six-digit binary control number is not zero, the following portion of the program will be executed. This portion of the

program will print out the spatial frequency power spectrum of log-amplitude and of phase fluctuations. Here, spatial frequency is in inverse units of length in the measurement plane.

REM #12

If the sixth digit of the six-digit binary control number is not zero, the following portion of the program will be executed. This portion of the program will cause the printout of the midpoint altitude and refractive-index structure constant for each of the N-points utilized in evaluation of the propagation path integrals.

Appendix 3

Sample Turbulence Subroutines

BUFTON TURBULENCE SUBROUTINE

```
9000  REM#S1.1
9001  GØ TØ 9020
9010  REM #S2.1
9011  GØ TØ 9300
9020  PRINT
9030  PRINT
9040  PRINT
9050  PRINT TAB(10);"CALCULATIØNS WILL BE PERFØRMED USING THE"
9060  PRINT TAB(18);"BUFTØN TURBULENCE MØDEL"
9070  PRINT
9080  PRINT
9090  PRINT
9100 DIM C1(17)
9110  LET H9=17000
9120  DATA .375,1.17,.585,.435,.245,.1,.13,.16,.21
9130  DATA .305,.37,.42,.385,.295,.133,.063,.038
9140  FØR I=1 TØ 17
9150  READ C1(I)
9160  LET C1(I)=C1(I)*1E-16
9170  NEXT I
9180  RETURN
9300  IF H>100 GØ TØ 9330
9310  LET C=7E-14*H↑(-4/3)
9320  RETURN
9330  IF H>500 GØ TØ 9360
9340  LET C=1.5E-16
9350  RETURN
9360  IF H>1000  GØ TØ 9390
9370  LET C=(1.5E-16)-((H-500)/500)*1.125E-16
9380  RETURN
9390  LET J=INT(H/1000)
9400  LET C=C1(J)
9410  IF J<>H/1000 LET C=C+(C1(J+1)-C1(J))*(H/1000-J)
9420  RETURN
```

HUFNAGEL NON-RANDOM TURBULENCE SUBROUTINE

```
9000 REM  #S1.2
9001 GØTØ  9020
9010 REM  #S2.2
9011 GØTØ  9200
9020 LET W=27
9030 PRINT
9040 PRINT
9050 PRINT
9060 PRINT  TAB (10);"CALCULATIØNS WILL BE PERFØRMED USING A"
9070 PRINT  TAB (4);"NØNRANDØM HUFNAGEL TURBULENCE MØDEL WITH W ="W
9080 PRINT
9090 PRINT
9100 PRINT
9110 LET H9=24000
9120 RETURN
9200 IF H<3000 GØTØ  9240
9210 LET C=2.2E-53*H↑10*(W/27)*(W/27)* EXP (-H/1000)
9220 LET C=2.71828*(C+1E-16* EXP (-H/1500))
9230 RETURN
9240 IF H>100 GØTØ 9270
9250 LET C=7E-14*H↑(-4/3)
9260 RETURN
9270 IF H>500 GØTØ 9300
9280 LET C=1.5E-16
9290 RETURN
9300 IF H>1000 GØTØ  9330
9310 LET C=(1.5E-16)-((H-500)/500)*1.125E-16
9320 RETURN
9330 IF H>2000 GØTØ  9360
9340 LET C=3.75E-17+((H-1000)/1000)*7.95E-17
9350 RETURN
9360 LET C=1.17E-16-((H-2000)/1000)*5.85E-17
9370 RETURN
```

HUFNAGEL RANDOM TURBULENCE SUBROUTINE

```
9000 REM  #S1.3
9001 GØTØ  9020
9010 REM  #S2.3
9011 GØTØ  9300
9020 LET W=25
9030 PRINT
9040 PRINT
9050 PRINT
9060 PRINT  TAB (10);"CALCULATIØNS WILL BE PERFØRMED USING A"
9070 PRINT  TAB (6);"RANDØM HUFNAGEL TURBULENCE MØDEL WITH W= ";W
9080 LET R= RND (0)*1000000
9090 PRINT  TAB (19);"(RANDØM KEY = ";R;")"
9100 PRINT
9110 PRINT
9120 PRINT
9130 LET R=- LØG ( RND (0))
9140 LET R= SQR (R)* CØS (6.28319* RND (0))
9150 LET R=R+R
9160 LET H9=24000
9170 RETURN
9300 IF H<3000 GØTØ  9410
9310 LET A= EXP (- ABS (H5)/100)+ EXP (- ABS (H5)/2000)
9320 LET A=A/2
9330 LET A2= SQR (1-A*A)
9340 LET R1=- LØG ( RND (0))
9350 LET R1= SQR (R1)* CØS (6.28319* RND (0))
9360 LET R1=R1+R1
9370 LET R=R*A+R1*A2
9380 LET C=(2.2E-53*H↑10*W*W/729)* EXP (-H/1000)
9390 LET C=(C+1E-16* EXP (-H/1500))* EXP (R)
9400 RETURN
9410 IF H>100 GØTØ 9440
9420 LET C=7E-14*H↑(-4/3)
9430 RETURN
9440 IF H>500 GØTØ 9470
9450 LET C=1.5E-16
9460 RETURN
9470 IF H>1000 GØTØ  9500
9480 LET C=(1.5E-16)-((H-500)/500)*1.125E-16
9490 RETURN
9500 IF H>2000 GØTØ  9530
9510 LET C=(3.75E-17)+((H-1000)/1000)*7.95E-17
9520 RETURN
9530 LET C=(1.17E-16)-((H-2000)/1000)*5.85E-17
9540 RETURN
```

AF 15 MAY 74 TURBULENCE SUBROUTINE

```
9000 REM  #S1.4
9001 GØTØ  9020
9010 REM  #S2.4
9011 GØTØ  9500
9020 LET H9=15381
9030 DIM H1[80],C1[80]
9040 DATA 0,131,212,357,542,663,930,1341
9050 DATA 1510,1639,1905,2155,2317,2446,2720,2881,3123
9060 DATA 3260,3397,3494,3639,3768,3930,4059,4196,4405
9070 DATA 4736,5010,5228,5542,5704,5897,6083,6381,6534
9080 DATA 6913,7059,7317,7534,7680,7841,8091,8204,8550
9090 DATA 8680,8849,9236,9494,9889,9986,10139,10268,10470
9100 DATA 10986,11139,11510,11720,11825,12155,12349,12478,12639
9110 DATA 12841,12962,13010,13204,13317,13413,13752,13930,14042
9120 DATA 14171,14325,14413,14526,14647,14809,14905,14933,15381
9130 DATA 541.2,1.197,5.839,6.965,6.592,8.887,2.593,19.65
9140 DATA 1.468,1.965,3.076,1.625,1.588,2.32,1.141,3.365,1.663
9150 DATA 3.322,1.384,5.877,3.052,5.222,2.407,2.798,2.259,7.495
9160 DATA 3.35,10.65,3.079,10.71,3.37,10.3,5.754,24.73,7.261
9170 DATA 8.971,8.175,18.63,9.791,13.46,9.555,7.394,23.18,7.808
9180 DATA 9.192,5.547,20.03,6.192,4.622,7.793,3.516,4.564,3.817
9190 DATA 12.06,4.203,3.191,13.45,3.056,8.06,4.392,6.601,2.416
9200 DATA 4.909,2.165,5.591,2.064,5.984,1.586,7.605,2.569,7.493
9210 DATA 2.117,2.511,1.767,2.573,1.989,7.425,1.463,6.213,1.733
9220 FØR I=1 TØ 80
9230 READ H1[I]
9240 NEXT I
9250 FØR I=1 TØ 80
9260 READ C1[I]
9270 LET C1[I]=C1[I]*1E-16
9280 NEXT I
9290 PRINT
9300 PRINT
9310 PRINT
9320 PRINT  TAB (10);"CALCULATIØNS WILL BE PERFØRMED USING THE"
9330 PRINT  TAB (11);"AF 15 MAY 74 (ASCENT) C-SUB-N SQ. DATA"
9340 PRINT
9350 PRINT
9360 PRINT
9370 RETURN
9500 LET J=0
9510 LET J=J+1
9520 IF H1[J]<H GØTØ 9510
9530 LET C=(C1[J-1]*(H1[J]-H)+C1[J]*(H-H1[J-1]))/(H1[J]-H1[J-1])
9540 RETURN
```

HUFNAGEL SIMPLIFIED TURBULENCE SUBROUTINE

```
9000 REM  #S1.5
9001 GØTØ  9020
9010 REM  #S2.5
9011 GØTØ  9300
9020 PRINT
9030 PRINT
9040 PRINT
9050 PRINT  TAB (10);"CALCULATIØNS WILL BE PERFØRMED USING THE"
9060 PRINT  TAB (12);"HUFNAGEL SIMPLIFIED TURBULENCE MØDEL"
9070 PRINT
9080 PRINT  TAB (5);"INPUT TIME ØF DAY; 1=MID-DAY,2=NIGHT,";
9081 PRINT "3=DAWN/DUSK";
9090 INPUT E
9100 LET E1=1
9110 IF E=1 LET E1=0
9120 IF E=1 LET E=1.3
9130 IF E=2 LET E1=0
9140 IF E=2 LET E=1
9150 IF E=3 LET E1=0
9160 IF E=3 LET E=.8
9170 IF E1=1 GØTØ  9070
9180 PRINT
9190 PRINT
9200 PRINT
9210 LET H9=20000
9220 RETURN
9300 LET C=1.2E-17*(10000/H)↑E
9310 RETURN
```

Appendix 4

Subroutine Remarks

(The same remarks apply to all of the subroutines.)

REM #S1. --

This point is the entrance to the initial portion of the refractive-index structure constant generating subroutine. This portion of the subroutine is to be called only once, at the start of execution of the Main Program. It serves to set up all the basic constants that will be used later in the evaluation of the refractive-index structure constant. It also establishes the altitude limit corresponding to the top of the turbulent atmosphere.

REM #S2. --

This point is the entrance to the main working portion of the refractive-index structure constant generating subroutine. This portion of the subroutine is called repeatedly, each time with a new value of altitude, H , and returns with the corresponding value of the refractive-index structure constant, C .

PART II

Angle-of-Arrival Isoplanatism and the Calculation of the Isoplanatic Dependence of Predetection Compensation Imagery from Measurements of the Isoplanatic Dependence of Angle-of-Arrival

1.0 Angle-of-Arrival Isoplanatism

1.1 Introduction

The subject of isoplanatism is a relatively exotic matter, originally introduced by Linfoot[1] in the consideration of the optical transfer function of a lens. The isoplanatic patch size was defined as that region in the field-of-view of a lens over which the optical transfer function could be considered to be essentially constant. It was necessary to introduce this concept of isoplanatism in the development of the theory of the optical transfer function as, without it, the normal definition of the transfer function is mathematically unsatisfactory. The situation is rather akin to that involved in the discussion of the transfer function of a time varying electronic filter. One has to assume that the transfer function varies slowly compared to the frequencies involved if the concept of a transfer function is to have any meaning -- and even then the situation is mathematically awkward. The practical engineer is, however, generally not so much of a mathematical purist as to be bothered by this rather subtle and somewhat exotic mathematical difficulty.

The concept of isoplanatism, originally defined in terms of a lens and its transfer function, was applied by Hufnagel[2] to the subject of atmospheric turbulence as an optical system. Because the concept was used only as "the name of the reason given for ignoring a mathematical difficulty," it was not necessary to give a precise definition of isoplanatism. Isoplanatism was simply understood to be something that had to do with the relative constancy of an imaging system's aberration with field-of-view, and considered to be about as meaningful for use in studies of imaging through atmospheric turbulence as in studies of lens design. Recently, however, with detailed attention being paid to the subject of correcting for turbulence effects, both by predetection compensation and by post-detection compensation, the matter of isoplanatism has entered into our considerations in a quantitative way. It has become important to develop precise, quantitative definitions, theory, and experimental data related to the subject of isoplanatism.

We start by noting that there is no reason to believe that there is a uniquely definable isoplanatic patch size or isoplanatism angle to be associated with imaging over a given propagation path. In fact, we shall argue that accordingly as we are concerned with 1) post-detection compensation of a long exposure image, with 2) post-detection compensation of a short exposure image, or with 3) predetection compensated imaging, there are three different values to be associated with the isoplanatic patch size. We shall demonstrate this heuristically in the next section.

Unfortunately, the lack of a simple relationship between the isoplanatic patch size for post-detection compensation of short exposure imagery and the isoplanatic patch size for predetection compensation imagery means that while we can make measurements of the former, such measurements are not applicable to the latter. Since we are currently very interested in knowing about what the isoplanatic patch size may be expected to be for predetection compensation, we have studied the possibility of using short exposure imagery isoplanatism data to form a basis for calculating in some indirect manner the predetection compensation isoplanatic patch size. We have found that such a possibility exists if, rather than concern ourselves with the isoplanatic aspects of the short exposure image's resolution and modulation transfer function, we turn our attention to the concept of isoplanatism for angle-of-arrival fluctuation. (This represents a fourth area in imaging through turbulence for which we shall have a separate definition of isoplanatism.)

The angle-of-arrival isoplanatism is no more directly related to predetection compensation imagery isoplanatism than post-detection compensation short exposure imagery isoplanatism is. However, unlike the situation for post-detection compensation, for angle-of-arrival isoplanatism we can develop a rather simple linear theory which relates

measurements of the isoplanatic dependence of angle-of-arrival statistics to a weighted integral over the vertical distribution of turbulence in the atmosphere. This would then allow angle-of-arrival measurement data to be inverted to provide an estimate of the vertical distribution of the strength of turbulence. Since the available theory for isoplanatic dependence in predetection compensation is well advanced,[3] requiring only a knowledge of the vertical distribution of the strength of turbulence to allow quantitative results to be generated, we should be able to go from angle-of-arrival isoplanatism measurement data to quantitative predictions of the isoplanatic dependence of predetection compensation imagery. The main part of this paper will be concerned with the development of the theory of angle-of-arrival isoplanatism, with the objective of obtaining results expressed in terms of an integral over the vertical distribution of turbulence. We shall not be concerned in this report with the processing of any actual measurement data, or with formulation of the details of the integral inversion procedure by which we would obtain the turbulence distribution from the angle-of-arrival isoplanatism measurements. These matters will be treated separately at a later time.

Before taking up the development of the theory of angle-of-arrival isoplanatism, we shall first explain why we have to consider isoplanatism to be different, with distinct numerical values, for different processes of imaging through turbulence. We take this up in the next section.

1.2 Difference in Isoplanatism

As indicated above, though the term "isoplanatism" is used in regard to turbulence effects without any further limiting modifier, we shall show here that there are several distinct and generally unequal meanings to be associated with the term. We shall offer heuristic arguments to demonstrate this based on the rather simple model of all

significant turbulence located in a single layer some distance from the aperture of a telescope. We consider a pair of point sources located at an essentially infinite distance from the aperture. We shall let ϑ denote the angular separation of the two sources, as seen by the telescope, let L denote the range from the telescope aperture to the turbulence layer, and let D denote the telescope diameter. We assume that the optical wavelength and strength of turbulence are such that the wavefront reaching the telescope aperture has a coherence diameter, r_c . In Fig. 1, we depict this situation, showing the "projection" of the aperture on the turbulence layer for rays oriented toward the two point sources, and also indicate how the wavefront distortion generated by the turbulence layer will project onto the telescope aperture -- the projection being shown for light from the two point sources.

The question that is central to our considerations here is whether or not the two different wavefront distortion patterns projected onto the telescope aperture by the two point sources are related to each other closely enough. If they are, then we would say that the two point sources, separated by the angle ϑ , lie within a single isoplanatic patch. But this question, rather than providing the basis for evaluating the isoplanatic patch size, simply highlights our lack of definition of the problem -- for the fact is that the question can not be answered until we say what we mean by "related . . . closely enough." In attempting to formulate an answer to such a question, we find we must first decide which type of imaging we are concerned about, i. e., 1) predetection compensated imaging, 2) post-detection compensated short-exposure imagery, or 3) post-detection compensated long-exposure imagery.

If we are interested in predetection compensated imagery, in which we would use measurements of the wavefront distortion for light from source #1 to control the compensation for the wavefront distortion of light from

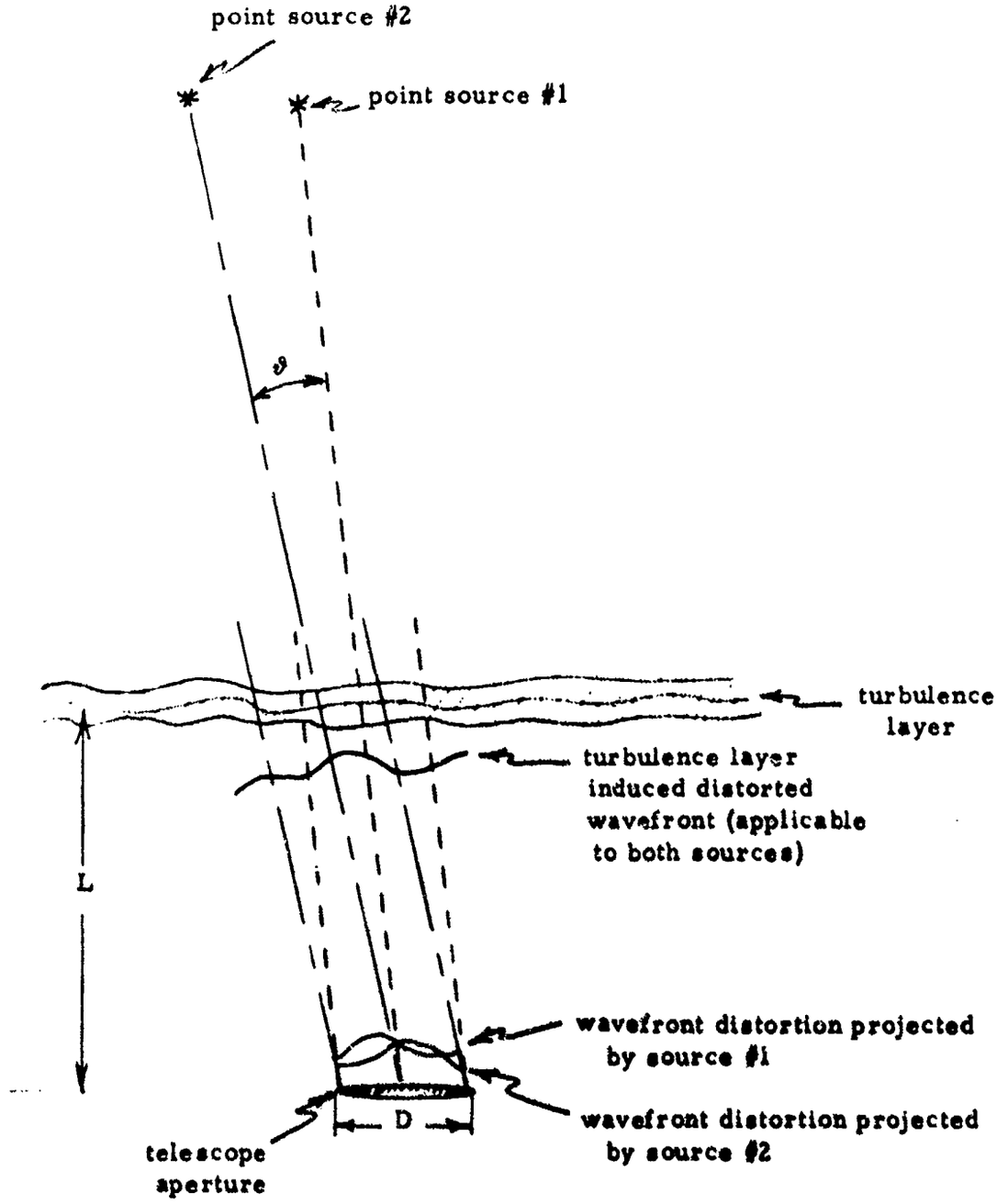

Figure 1.1, Generalized View of Imaging Isoplanatism Related Effects for a Single Turbulence Layer. The significant point to be noted here is that the same turbulence pattern is projected by the two point sources as two different wavefront distortion patterns at the telescope aperture. If the wavefront distortion patterns are related closely enough, then the angular separation of the two sources, ϑ , is within the isoplanatic patch. The key question is exactly what do we mean by "related closely enough."

source #2, then we must have the two wavefront distortion patterns match reasonably well on a point-by-point basis across the telescope aperture. (By "matching reasonably well," we mean that the rms difference should be about one radian.) If $\phi_t(\vec{r})$ denotes the wavefront distortion pattern at position $\vec{r}$ just below the turbulence layer, then the wavefront distortion patterns projected onto the telescope aperture by sources #1 and #2 will be $\phi_1(\vec{r})$ and $\phi_2(\vec{r})$, respectively. It is obvious that

$$\phi_1(\vec{r}) = \phi_t(\vec{r} + \vec{R}) \quad , \tag{1}$$

$$\phi_2(\vec{r}) = \phi_t(\vec{r} + \vec{R} + \vec{\vartheta}L) \quad , \tag{2}$$

where $\vec{R}$ is some displacement vector associated with the fact that source #1 is not at the zenith.

Our condition that the two wavefront distortion patterns projected on the telescope aperture match well enough is represented mathematically by the requirement

$$\langle [\phi_1(\vec{r}) - \phi_2(\vec{r})]^2 \rangle \leq 1 \quad . \tag{3}$$

Making use of Eq.'s (1) and (2), this can be rewritten as

$$\langle [\phi_t(\vec{r} + \vec{R}) - \phi_t(\vec{r} + \vec{R} + \vec{\vartheta}L)]^2 \rangle \leq 1 \quad , \tag{4}$$

but here the ensemble average can be recognized as the ordinary phase structure function, which for the coherence diameter r_0 can be written as

$$\langle [\phi_t(\vec{r} + \vec{R}) - \phi_t(\vec{r} + \vec{R} + \vec{\vartheta}L)]^2 \rangle = 6.88 \left(\frac{\vartheta L}{r_0}\right)^{5/3} \tag{5}$$

Combining Eq.'s (4) and (5), we see that the requirement for isoplanatism in predetection compensation imaging will be satisfied if we require that

$$\vartheta \leq \frac{r_0}{3.18\ L} \tag{6}$$

(where $3.18 = 6.88^{3/5}$). This is in good agreement with exact results derived previously for isoplanatism in predetection compensation.[4]

Eq. (6) is subject to a very simple physical interpretation. This interpretation is that if ϑ is too large, i.e., greater than the value given in Eq. (6), then the two wavefront distortion patterns will be shifted so much with respect to each other that although they are fundamentally the same distortion pattern, the amount sensed at a point (from source #1) will be only poorly correlated with the amount of correction required at that point (for imaging source #2). If the shift is of order r_0, then the two wavefront distortion patterns will not be related to each other closely enough.

For predetection compensation, we see then that the answer to the question we asked before about the required closeness of the relation has to do with the exact matching of the two distortion patterns at the same point on the aperture. Quantitatively it leads to an isoplanatism angle determined by the coherence diameter r_0 and the distance L to the turbulence.

For post-detection compensation of a short-exposure image, we intend to use modulation transfer function measurements obtained by processing the short-exposure image of source #1 to compensate the short-exposure image of source #2. Our basic requirement is that the two short-exposure images be aberrated in exactly the same way. This is a requirement on the aberration realization in any one picture, and not a statistical requirement. If the two aberrated short-exposure images are essentially

the same, then post-detection compensation will function almost perfectly (at least to the limit allowed by noise considerations) and a validly compensated image of source #2 will be formed using compensation values derived from the image of source #1. If post-detection compensated short-exposure imagery isoplanatism conditions are not satisfied, however, then the aberrations in the short-exposure image of source #1 will not be well related to the aberration in the short-exposure image of source #2. As a consequence, the post-detection compensation process will introduce spurious details into the compensated image of source #2.

The basic condition for the aberration of two images to be at least approximately the same is that the wavefront distortion patterns entering the telescope aperture for the two sources be essentially the same. If due to the angle ϑ the two wavefront distortion patterns are displaced by a distance ϑL which is much less than the aperture diameter D, then for the most part the two distortion patterns will be the same. There will be minor regions, crescent-shaped on two sides of the aperture, for which one of the distortion patterns will not have any match in the other distortion pattern, but over most of the aperture region the wavefront distortion from one source can be perfectly matched to the wavefront distortion entering the aperture from the other source. The matching portions of the two wavefront distortion patterns will not lie on top of each other -- the match will involve a displacement ϑL, but the wavefront distortion pattern entering the aperture from the two sources will be essentially the same and the images formed will, as a consequence, be essentially identical. The modulation transfer function developed from the image of source #1 will be suitable for compensation of the image of source #2. So long as the displacement ϑL is much less than the aperture diameter D, we would be able to consider that isoplanatism applies for post-detection compensation of a short-exposure image. Taking 30% to correspond to "much less than", this condition could be written as the requirement

that

$$\vartheta \leq \frac{.3\,D}{L} = \frac{D}{3.33\,L} \tag{7}$$

It is worthwhile to compare this result with Eq. (6). We see that the two equations have the same form for the size of the isoplanatic patch, except that the role of the coherence diameter, r_0 , in predetection compensation imaging is played by the aperture diameter in post-detection short-exposure imagery. (We acknowledge that the agreement between the numerical coefficients of Eq.'s (6) and (7) is somewhat contrived, and not to be taken too seriously.) We see that the isoplanatic patch size is quite distinct in these two cases, and that measurement of isoplanatism for short-exposure imagery can not be directly applied to predetection compensation imagery. It might be possible to obtain an order of magnitude type estimate of the size of the isoplanatic patch for predetection compensation imagery by making measurements of the isoplanatic patch size for post-detection compensated short-exposure imagery and scaling by a factor of r_0/D -- but this would only yield what would at best be an order of magnitude estimate.

If we now turn our attention to the isoplanatic patch size for post-detection compensated long-exposure imagery, we first note that each realization of the image of a point source is well defined by the statistical description of the propagation path. The nature of the image is not a random variable, it is repeatable from photograph to photograph. Post-detection compensation of a long-exposure image from source #2 on the basis of an image of source #1 would therefore be expected to work since the two images may be expected to suffer from the same turbulence degradation. The only thing that will change the nature of the image is a change in the statistics of the propagation path. For the case depicted in Fig. 1, such a change would exist between the paths from source #1 to the telescope, compared to the path from source #2 to the

telescope, if the angular separation, ϑ , is large enough to change the secant of the zenith angles involved by a significant amount. Nominally we might take

$$\vartheta \leq \frac{1}{3} \tag{8}$$

as a measure of this condition, i.e., as a measure of the isoplanatic patch size for post-detection compensated long-exposure imagery. This is so significantly different from the isoplanatic patch size for predetection compensation, Eq. (6), or for post-detection compensation of short-exposure imagery, Eq. (7), as to require no special comment here.

Having seen that each of the three different types of imagery leads to a different criteria and different numerical values for the isoplanatic patch size, we see that we can not make direct measurements of the isoplanatic patch size for either post-detection compensated short-exposure or long-exposure imagery and expect it to be applicable to the question of isoplanatism for predetection compensated imagery. This would seem to imply that we shall have to operate a predetection compensated imaging system to get measurement data related to its patch size.

Actually, such need not be the case. Since measurements of isoplanatism dependence for post-detection compensated short-exposure imagery can be related to the vertical distribution of turbulence, we could presumably calculate the distribution of turbulence along the propagation path from such measurements. Then, since exact theoretical results already exist[4] for calculating the isoplanatic patch size from knowledge of the distribution of turbulence along the propagation path, it would be possible to calculate the predetection compensation isoplanatic patch size from measurements of post-detection compensated short-exposure imagery isoplanatism.

We have developed the theory for the relationship between post-detection compensated short-exposure imagery isoplanatism and the distribution of turbulence along the propagation path and concluded that it will be very difficult, if not totally impractical, to attempt to work backwards from the isoplanatism measurements to the turbulence distribution. The basic analysis of this situation is presented in Appendix A.

Instead of working with the post-detection compensated short-exposure image, we have noted that a much simpler relationship can be established if we work with angle-of-arrival isoplanatism. The equation relating angle-of-arrival isoplanatism and the distribution of turbulence along the propagation path is rather straightforward and appears to be quite easy to manipulate so as to obtain an estimate of the turbulence distribution from a set of angle-of-arrival isoplanatism measurements. In the next two sections, we provide an exact definition of angle-of-arrival isoplanatism, set up the basic formulation, and carry out its reduction to a rather simple one-dimensional integral formulation.

1.3 Angle-of-Arrival Isoplanatism Definition and Formulation

The angle-of-arrival at the entrance aperture of diameter D of a telescope viewing a point source at angular position $\vec{\theta}$ can be equated with the aperture averaged tilt of the wavefront at the aperture, relative to the direction $\vec{\theta}$. It can be shown[5] that this can be written as

$$\vec{\alpha}(\vec{\theta}) = \frac{32\,\lambda}{\pi^2 D^4} \int d\vec{r}\, W(\vec{r};D)\, \vec{r}\, \phi(\vec{r};\vec{\theta}) \quad , \tag{9}$$

where $\vec{r}$ is a two-dimensional variable over the plane of the aperture, and $W(\vec{r};D)$ is a function which serves to define the extent of the aperture according to the equation

$$W(\vec{r};D) = \begin{cases} 1 \quad , & \text{if } |\vec{r}| \le \frac{1}{2} D \\ 0 \quad , & \text{if } |\vec{r}| > \frac{1}{2} D \end{cases} \quad . \tag{10}$$

In Eq. (9), λ denotes the optical wavelength and $\phi(\vec{r};\vec{\theta})$ denotes the (complex*) phase error at aperture position $\vec{r}$ associated with the wavefront distortion of the radiation from a point source located at $\vec{\theta}$. (The wavefront distortion is, of course, referenced to an undistorted plane whose normal is oriented toward $\vec{\theta}$.)

The components of the angle-of-arrival vector, $\vec{\alpha}$, are

$$\alpha_x(\vec{\theta}) = \frac{32\lambda}{\pi^3 D^4} \int d\vec{r}\, W(\vec{r};D)\, x\, \phi(\vec{r};\vec{\theta}) \quad , \tag{11a}$$

$$\alpha_y(\vec{\theta}) = \frac{32\lambda}{\pi^3 D^4} \int d\vec{r}\, W(\vec{r};D)\, y\, \phi(\vec{r};\vec{\theta}) \quad , \tag{11b}$$

where x and y are the two components of $\vec{r}$.

The isoplanatic aspect of angle-of-arrival can be introduced by considering a pair of point sources located at $\vec{\theta}_1$ and $\vec{\theta}_2$, and considering the angle-of-arrival isoplanatism-structure function

$$\mathcal{D}_{l,\alpha}(\vartheta) = \langle [\vec{\alpha}(\vec{\theta}_1) - \vec{\alpha}(\vec{\theta}_2)] \cdot [\vec{\alpha}(\vec{\theta}_1) - \vec{\alpha}(\vec{\theta}_2)] \rangle \quad , \tag{12}$$

where

$$\vec{\vartheta} = \vec{\theta}_1 - \vec{\theta}_2 \quad . \tag{13}$$

As a practical matter with an eye toward the problems of making related measurements, it is appropriate to treat the statistics of the x- and y-components of angle-of-arrival separately. To make this particularly useful, since we have freedom in our choice of the orientation of the (x, y)-coordinate system, we choose the orientation so that the x-axis is parallel to $\vec{\vartheta}$ and the y-axis is perpendicular to $\vec{\vartheta}$. We write for

---

* To the extent that log-amplitude variations are negligible, the complex phase is equivalent to the ordinary phase. We shall assume that this is the case and shall treat ϕ as either the real or complex phase, in each case as most convenient.

the angle-of-arrival component isoplanatism-structure function

$$D_{l,\alpha_x}(\vartheta) = \langle [\alpha_x(\vec{\theta}_1) - \alpha_x(\vec{\theta}_2)]^2 \rangle \quad , \tag{14a}$$

and

$$D_{l,\alpha_y}(\vartheta) = \langle [\alpha_y(\vec{\theta}_1) - \alpha_y(\vec{\theta}_2)]^2 \rangle \quad . \tag{14b}$$

If we substitute Eq. (9) into Eq. (12), appropriately combine first the sum and then the product of integrals, and finally interchange the order of integration and ensemble averaging, we get

$$D_{l,\alpha}(\vartheta) = \left(\frac{32\,\lambda}{\pi^2 D^4}\right) \iint d\vec{r}\, d\vec{r}\,' \, W(\vec{r};D)\, W(\vec{r}\,';D)\, \vec{r} \cdot \vec{r}\,'$$

$$\times \langle [\phi(\vec{r};\vec{\theta}_1) - \phi(\vec{r};\vec{\theta}_2)][\phi(\vec{r}\,';\vec{\theta}_1) - \phi(\vec{r}\,';\vec{\theta}_2)] \rangle \quad . \tag{15}$$

The ensemble average in Eq. (15) can be simplified to the form

$$\begin{aligned}
&\langle [\phi(\vec{r};\vec{\theta}_1) - \phi(\vec{r};\vec{\theta}_2)][\phi(\vec{r}\,';\vec{\theta}_1) - \phi(\vec{r}\,';\vec{\theta}_2)] \rangle \\
&= \langle \phi(\vec{r};\vec{\theta}_1)\, \phi(\vec{r}\,';\vec{\theta}_1) \rangle - \langle \phi(\vec{r};\vec{\theta}_1)\, \phi(\vec{r}\,';\vec{\theta}_2) \rangle \\
&\quad - \langle \phi(\vec{r};\vec{\theta}_2)\, \phi(\vec{r}\,';\vec{\theta}_1) \rangle + \langle \phi(\vec{r};\vec{\theta}_2)\, \phi(\vec{r}\,';\vec{\theta}_2) \rangle \\
&= -\tfrac{1}{2} \langle [\phi(\vec{r};\vec{\theta}_1) - \phi(\vec{r}\,';\vec{\theta}_1)]^2 \rangle + \tfrac{1}{2} \langle [\phi(\vec{r};\vec{\theta}_1) - \phi(\vec{r}\,';\vec{\theta}_2)]^2 \rangle \\
&\quad + \tfrac{1}{2} \langle [\phi(\vec{r};\vec{\theta}_2) - \phi(\vec{r}\,';\vec{\theta}_1)]^2 \rangle - \tfrac{1}{2} \langle [\phi(\vec{r};\vec{\theta}_2) - \phi(\vec{r}\,';\vec{\theta}_2)]^2 \rangle \\
&= -\tfrac{1}{2} \mathcal{D}_{l,\phi}(\vec{u};0) + \tfrac{1}{2} \mathcal{D}_{l,\phi}(\vec{u};\vec{\vartheta}) + \tfrac{1}{2} \mathcal{D}_{l,\phi}(\vec{u};-\vec{\vartheta}) - \tfrac{1}{2} \mathcal{D}_{l,\phi}(\vec{u};0) \quad ,
\end{aligned} \tag{16}$$

where

$$\vec{u} = \vec{r} - \vec{r}\,' \quad , \tag{17}$$

and the isoplanatic phase structure function $\mathcal{D}_{l,\phi}$ is defined by the equation

$$\mathcal{D}_{l,\phi}(\vec{u};\vec{\vartheta}) = \langle [\phi(\vec{r};\vec{\theta}_1) - \phi(\vec{r}';\vec{\theta}_2)]^2 \rangle \quad . \tag{18}$$

It can be shown[6] that the isoplanatic (complex) phase structure function for propagation over a path of length L is given by the expression

$$\mathcal{D}_{l,\phi}(\vec{u};\vec{\vartheta}) = 2.91\, k^2 \int_{\text{Path}} ds\; C_N^2 \left[\left| \vec{u} + \vec{\vartheta} s \right| \left(\frac{L - s}{L} \right) \right]^{5/3} \quad , \tag{19}$$

where $s = 0$ at the measurement plane and $s = L$ at the location of the point source. As a practical matter, when the source is astronomical (or at least exoatmospheric), which we shall assume to be the case in this work, Eq. (19) reduces to the form

$$\mathcal{D}_{l,\phi}(\vec{u};\vec{\vartheta}) = 2.91\, k^2 \int_{\text{Path}} ds\; C_N^2 \left| \vec{u} + \vec{\vartheta} s \right|^{5/3} \quad . \tag{20}$$

If we substitute Eq. (20) into Eq. (16), we get

$$\begin{aligned} &\langle [\phi(\vec{r};\vec{\theta}_1) - \phi(\vec{r};\vec{\theta}_2)][\phi(\vec{r}';\vec{\theta}_1) - \phi(\vec{r}';\vec{\theta}_2)] \rangle \\ &\quad = 2.91\, k^2 \int_{\text{Path}} ds\; C_N^2 \left(\tfrac{1}{2} \left| \vec{u} + \vec{\vartheta} s \right|^{5/3} + \tfrac{1}{2} \left| \vec{u} - \vec{\vartheta} s \right|^{5/3} - u^{5/3} \right) \end{aligned} \tag{21}$$

and if we substitute this result into Eq. (15), interchanging the order of integration and simplifying as appropriate, we get

$$\begin{aligned} \mathcal{D}_{l,\alpha}(\vartheta) = \int_{\text{Path}} ds\; C_N^2 \Bigg\{ 2.91 \left(\frac{64}{\pi D^4} \right)^2 \iint d\vec{r}\, d\vec{r}'\; W(\vec{r};D)\, W(\vec{r}';D)\, \vec{r} \cdot \vec{r}' \\ \times \left(\tfrac{1}{2} \left| \vec{u} + \vec{\vartheta} s \right|^{5/3} + \tfrac{1}{2} \left| \vec{u} - \vec{\vartheta} s \right|^{5/3} - u^{5/3} \right) \Bigg\} \quad . \end{aligned} \tag{22}$$

If we repeat the same procedure, starting from Eq.'s (14a) or (14b) rather than from Eq. (12), we get in place of Eq. (22) the results that

$$D_{1,\alpha_x}(\vartheta) = \int_{\text{Path}} ds\, C_N^2 \left\{ 2.91 \left(\frac{64}{\pi D^4}\right)^2 \iint d\vec{r}\, d\vec{r}'\, W(\vec{r};D)\, W(\vec{r}';D)\, x\, x' \right.$$

$$\left. \times \left(\tfrac{1}{2} \left|\vec{u} + \vec{\vartheta} s\right|^{5/3} + \tfrac{1}{2} \left|\vec{u} - \vec{\vartheta} s\right|^{5/3} - u^{5/3} \right) \right\} , \qquad (23a)$$

$$D_{1,\alpha_y}(\vartheta) = \int_{\text{Path}} ds\, C_N^2 \left\{ 2.91 \left(\frac{64}{\pi D^4}\right)^2 \iint d\vec{r}\, d\vec{r}'\, W(\vec{r};D)\, W(\vec{r}';D)\, y\, y' \right.$$

$$\left. \times \left(\tfrac{1}{2} \left|\vec{u} + \vec{\vartheta} s\right|^{5/3} + \tfrac{1}{2} \left|\vec{u} - \vec{\vartheta} s\right|^{5/3} - u^{5/3} \right) \right\} . \qquad (23b)$$

If we now introduce the variable

$$\vec{v} = \tfrac{1}{2} (\vec{r} + \vec{r}') , \qquad (24)$$

then the $\vec{r}$- and $\vec{r}'$-integrations in Eq. (22) can be replaced by integrations over $\vec{u}$ and $\vec{v}$. We get

$$D_{1,\alpha}(\vartheta) = \int_{\text{Path}} ds\, C_N^2 \left\{ 2.91 \left(\frac{64}{\pi D^4}\right)^2 \iint d\vec{u}\, d\vec{v}\, W(\vec{v} + \tfrac{1}{2}\vec{u};D) \right.$$

$$\left. \times W(\vec{v} - \tfrac{1}{2}\vec{u};D)(v^2 - \tfrac{1}{4}u^2)\left(\tfrac{1}{2} \left|\vec{u} + \vec{\vartheta} s\right|^{5/3} + \tfrac{1}{2} \left|\vec{u} - \vec{\vartheta} s\right|^{5/3} - u^{5/3} \right) \right\} , \qquad (25)$$

where we have made use of the fact that in accordance with Eq.'s (17) and (24)

$$\vec{r} \cdot \vec{r}' = v^2 - \tfrac{1}{4} u^2 , \qquad (26)$$

It is particularly convenient at this point to replace the variables $\vec{u}$ and $\vec{v}$ by $\vec{u}'$ and $\vec{v}'$, where

$$\vec{u}' = \vec{u}/D , \qquad d\vec{u}' = d\vec{u}/D^2 , \qquad (27a)$$

$$\vec{v}' = \vec{v}/D , \qquad d\vec{v}' = d\vec{v}/D^2 , \qquad (27b)$$

so that Eq. (25) can be rewritten as

$$D_{l,\alpha}(\vartheta) = D^{-1/3} \int_{\text{Path}} ds\, C_N^2 \left\{ 2.91\,(64/\pi)^2 \iint d\vec{u}'\, d\vec{v}'\, W(\vec{v}' + \tfrac{1}{2}\vec{u}';1) \right.$$

$$\left. \times\, W(\vec{v}' - \tfrac{1}{2}\vec{u}';1)(v'^2 - \tfrac{1}{4}u'^2)\left(\tfrac{1}{8}|\vec{u}' + \vec{\xi}|^{5/3} + \tfrac{1}{8}|\vec{u}' - \vec{\xi}|^{5/3} - u'^{5/3}\right)\right\} , \quad (28)$$

where

$$\vec{\xi} = \vec{\vartheta} s/D \quad . \quad (29)$$

If we define the quantity in the curly brackets in Eq. (28) as $F_\alpha(\xi)$, i.e.,

$$F_\alpha(\xi) = 2.91\,(64/\pi)^2 \iint d\vec{u}\, d\vec{v}\, W(\vec{v} + \tfrac{1}{2}\vec{u};1)\, W(\vec{v} - \tfrac{1}{2}\vec{u};1)$$

$$\times\, (v^2 - \tfrac{1}{4}u^2)\left(\tfrac{1}{8}|\vec{u} + \vec{\xi}|^{5/3} + \tfrac{1}{8}|\vec{u} - \vec{\xi}|^{5/3} - u^{5/3}\right) , \quad (30)$$

where, for convenience, we have dropped the primes on the variables of integration, then we can rewrite Eq. (28) in the very compact form

$$B_{l,\alpha}(\vartheta) = D^{-1/3} \int_{\text{Path}} ds\, C_N^2\, F_\alpha(\vartheta s/D) \quad . \quad (31)$$

In a similar way, starting from Eq.'s (23a) and (23b), we get

$$B_{l,\alpha_x}(\vartheta) = D^{-1/3} \int_{\text{Path}} ds\, C_N^2\, F_{\alpha_x}(\vartheta s/D) \quad , \quad (32a)$$

$$B_{l,\alpha_y}(\vartheta) = D^{-1/3} \int_{\text{Path}} ds\, C_N^2\, F_{\alpha_y}(\vartheta s/D) \quad , \quad (32b)$$

where

$$F_{\alpha_x}(\xi) = 2.91\,(64/\pi)^2 \iint d\vec{u}\, d\vec{v}\, W(\vec{v} + \tfrac{1}{2}\vec{u};1)\, W(\vec{v} - \tfrac{1}{2}\vec{u};1)$$

$$\times\, [v^2 \cos^2(\mu+\nu) - \tfrac{1}{4}u^2 \cos^2(\mu)]$$

$$\times\, \left(\tfrac{1}{8}|\vec{u} + \vec{\xi}|^{5/3} + \tfrac{1}{8}|\vec{u} - \vec{\xi}|^{5/3} - u^{5/3}\right) \quad , \quad (33a)$$

$$F_{\alpha_y}(\xi) = 2.91\,(64/\pi)^2 \iint d\vec{u}\, d\vec{v}\, W(\vec{v} + \tfrac{1}{2}\vec{u};1)\, W(\vec{v} - \tfrac{1}{2}\vec{u};1)$$

$$\times\ [v^2 \sin^2(\mu+\nu) - \tfrac{1}{4} u^2 \sin^2(\mu)]$$

$$\times\ \left(\tfrac{1}{2}\left|\vec{u} + \vec{\xi}\right|^{5/3} + \tfrac{1}{2}\left|\vec{u} - \vec{\xi}\right|^{5/3} - u^{5/3}\right) \quad . \tag{33b}$$

Here we have used μ to denote the angle between $\vec{u}$ and the x-axis, and ν to denote the angle between $\vec{v}$ and $\vec{u}$. We made use of the fact that since

$$\vec{r} = \vec{v} + \tfrac{1}{2}\vec{u} \quad , \quad \vec{r}' = \vec{v} - \tfrac{1}{2}\vec{u} \quad , \tag{34}$$

then

$$x = v\cos(\mu + \nu) + \tfrac{1}{2} u \cos(\mu) \tag{35a}$$

$$x' = v\cos(\mu + \nu) - \tfrac{1}{2} u \cos(\mu) \tag{35b}$$

so that

$$x\,x' = v^2 \cos^2(\mu + \nu) - \tfrac{1}{4} u^2 \cos^2(\mu) \tag{36}$$

and similarly,

$$y = v\sin(\mu + \nu) + \tfrac{1}{2} u \sin(\mu) \tag{37a}$$

$$y' = v\sin(\mu + \nu) - \tfrac{1}{2} u \sin(\mu) \tag{37b}$$

so that

$$y\,y' = v^2 \sin^2(\mu + \nu) - \tfrac{1}{4} u^2 \sin^2(\mu) \tag{38}$$

If we consider μ and ν to be the angular components of a polar coordinate representation of $\vec{u}$ and $\vec{v}$, respectively, and recall that $\vec{\xi}$ is parallel to $\vec{\vartheta}$ and that the x-axis is parallel to $\vec{\vartheta}$, then we can rewrite $F_\alpha(\xi)$ in the form

$$F_\alpha(\xi) = 2.91 \int_0^{2\pi} d\mu \int_0^1 u\, du\; K_\alpha(u)$$

$$\times \left\{ \tfrac{1}{2} \left[u^2 + 2u\xi\cos(\mu) + \xi^2\right]^{5/6} \right.$$

$$\left. \tfrac{1}{2}\left[u^2 - 2u\xi\cos(\mu) + \xi^2\right]^{5/6} - u^{5/3} \right\} \quad , \qquad (39)$$

where

$$K_\alpha(u) = (64/\pi)^2 \int_0^{2\pi} d\nu \int dv\; W(\vec{v} + \tfrac{1}{2}\vec{u};1)\; W(\vec{v} - \tfrac{1}{2}\vec{u};1)\,(v^2 - \tfrac{1}{4}u^2) \quad . \qquad (40)$$

In a similar way we get

$$F_{\alpha_x}(\xi) = 2.91 \int_0^{2\pi} d\mu \int_0^1 u\, du\; K_{\alpha_x}(\mu, u)$$

$$\times \left\{ \tfrac{1}{2}\left[u^2 + 2u\xi\cos(\mu) + \xi^2\right]^{5/6} + \tfrac{1}{2}\left[u^2 - 2u\xi\cos(\mu) + \xi^2\right]^{5/6} - u^{5/3} \right\}, \qquad (41a)$$

$$F_{\alpha_y}(\xi) = 2.91 \int_0^{2\pi} d\mu \int_0^1 u\, du\; K_{\alpha_y}(\mu, u)$$

$$\times \left\{ \tfrac{1}{2}\left[u^2 + 2u\xi\cos(\mu) + \xi^2\right]^{5/6} + \tfrac{1}{2}\left[u^2 - 2u\xi\cos(\mu) + \xi^2\right]^{5/6} - u^{5/3} \right\}, \qquad (41b)$$

where

$$K_{\alpha_x}(\mu, u) = (64/\pi)^2 \int_0^{2\pi} d\nu \int v\, dv\; W(\vec{v} + \tfrac{1}{2}\vec{u};1)\; W(\vec{v} - \tfrac{1}{2}\vec{u};1)$$

$$\times \left[v^2\cos^2(\mu+\nu) - \tfrac{1}{4}u^2\cos^2(\mu)\right] \quad , \qquad (42a)$$

$$K_{\alpha_y}(\mu, u) = (64/\pi)^2 \int_0^{2\pi} d\nu \int v\, dv\; W(\vec{v} + \tfrac{1}{2}\vec{u};1)\; W(\vec{v} - \tfrac{1}{2}\vec{u};1)$$

$$\times \left[v^2\sin^2(\mu+\nu) - \tfrac{1}{4}u^2\sin^2(\mu)\right] \quad . \qquad (42b)$$

Our basic results are Eq.'s (31), (32a), and (32b), with the integrands defined by Eq.'s (39), (41a), and (41b), with Eq.'s (40), (42a), and (42b) defining their integrands. These integrals are in a form directly suited to numerical evaluation and provide a basis for establishing a linear relationship between the distribution of turbulence over the propagation path and the isoplanatic angle-of-arrival structure function. Our basic problem is the evaluation of $F_\alpha(\xi)$, $F_{\alpha_x}(\xi)$, and $F_{\alpha_y}(\xi)$ in numerical form, as this is the key to the linear relationship. In the next section, we take up the matter of establishing this numerical result, starting from Eq.'s (39), (41a), (4ab), (40), (42a), and (42b).

1.4 Numerical Evaluation of $F_\alpha(\xi)$, $F_{\alpha_x}(\xi)$, and $F_{\alpha_y}(\xi)$

The functions $K_\alpha(u)$, $K_{\alpha_x}(\mu, u)$, and $K_{\alpha_y}(\mu, u)$ can be evaluated analytically without recourse to numerical techniques. We start by turning our attention to Eq. (40) for $K_\alpha(u)$. We note that the product of the two W-functions, treated as functions in $\vec{v}$-space, provide the bounds for the (ν, v)-integration. The region of integration corresponds to the area of overlap of two circles of unit diameter, with centers located a distance $\pm \frac{1}{2}\vec{u}$ from the origin in $\vec{v}$-space. If, instead of using polar-coordinates for $\vec{v}$, we represent $\vec{v}$ by the rectangular coordinates (p, q) , with the p-axis picked to be parallel to $\vec{u}$, then we can rewrite Eq. (40) as

$$K_\alpha(u) = (64/\pi)^2 \left\{ \int_{-(1-u)/2}^{0} dp \int_{-R_-}^{R_-} dq \; (p^2 + q^2 - \tfrac{1}{4}u^2) \right.$$

$$\left. + \int_{0}^{(1-u)/2} dp \int_{-R_+}^{R_+} dq \; (p^2 + q^2 - \tfrac{1}{4}u^2) \right\} \quad , \tag{43}$$

where

$$R_\pm = \tfrac{1}{2}\left[1 - (u \pm 2p)^2\right]^{1/2} \quad . \tag{44}$$

Making use of the fact that

$$\cos^2(\mu+\nu) = \cos^2\mu\cos^2\nu - 2\cos\mu\sin\mu\cos\nu\sin\nu + \sin^2\mu\sin^2\nu \quad , \tag{45a}$$

$$\sin^2(\mu+\nu) = \sin^2\mu\cos^2\nu + 2\cos\mu\sin\mu\cos\nu\sin\nu + \cos^2\mu\sin^2\nu \quad , \tag{45b}$$

and that since ν is the angle between $\vec{v}$ and $\vec{u}$, and that p is the component of $\vec{v}$ parallel to u

$$p = v\cos\nu \quad , \tag{46a}$$

$$q = v\sin\nu \quad , \tag{46b}$$

we can rewrite Eq.'s (42a) and (42b) as

$$K_{\alpha_x}(\mu,u) = (64/\pi)^2\Bigg\{\int_{-(1-u)/2}^{0} dp \int_{-R_-}^{R_-} dq\,(p^2\cos^2\mu - 2pq\cos\mu\sin\mu + q^2\sin^2\mu - \tfrac{1}{4}u^2\cos^2\mu)$$

$$+ \int_{0}^{(1-u)/2} dp \int_{-R_+}^{R_+} dq\,(p^2\cos^2\mu - 2pq\cos\mu\sin\mu + q^2\sin^2\mu - \tfrac{1}{4}u^2\cos^2\mu)\Bigg\} \quad , \tag{47a}$$

$$K_{\alpha_y}(\mu,u) = (64/\pi)^2\Bigg\{\int_{-(1-u)/2}^{0} dp \int_{-R_-}^{R_-} dq\,(p^2\sin^2\mu + 2pq\cos\mu\sin\mu + q^2\cos^2\mu - \tfrac{1}{4}u^2\sin^2\mu)$$

$$+ \int_{0}^{(1-u)/2} dp \int_{-R_+}^{R_+} dq\,(p^2\sin^2\mu + 2pq\cos\mu\sin\mu + q^2\cos^2\mu - \tfrac{1}{4}u^2\sin^2\mu)\Bigg\} \quad . \tag{47b}$$

If in Eq. 's (43), (47a), and (47b) we make a change of variables, replacing p by p' , where for the first double integral in each case we let

$$p' = 2p - u \quad , \tag{48a}$$

and for the second double integral in each case we let

$$p' = 2p + u \quad , \tag{48b}$$

and in all cases replace q by q' , where

$$q' = 2q \tag{49}$$

then these three equations can be rewritten as

$$K_{\alpha}(u) = (16/\pi)^2 \left\{ \int_{-1}^{-u} dp \int_{-R}^{R} dq \, (p^2 + 2pu + q^2) + \int_{u}^{1} dp \int_{-R}^{R} dq \right.$$
$$\left. \times \, (p^2 - 2pu + q^2) \right\} \quad , \tag{50}$$

$$K_{\alpha_x}(\mu, u) = (16/\pi)^2 \left\{ \int_{-1}^{-u} dp \int_{-R}^{R} dq \, [(p^2 + 2pu)\cos^2\mu - 2(p+u)\, q \cos\mu \sin\mu \right.$$
$$+ q^2 \sin^2\mu]$$
$$+ \int_{u}^{1} dp \int_{-R}^{R} dq \, [(p^2 - 2pu)\cos^2\mu - 2(p-u)\, q \cos\mu \sin\mu$$
$$\left. + q^2 \sin^2\mu] \right\} \quad , \tag{51a}$$

$$K_{\alpha_y}(\mu, u) = (16/\pi)^2 \left\{ \int_{-1}^{-u} dp \int_{-R}^{R} dq \, [(p^2 + 2pu)\sin^2\mu + 2(p+u)\, q \cos\mu \sin\mu \right.$$
$$+ q^2 \cos^2\mu]$$
$$+ \int_{u}^{1} dp \int_{-R}^{R} dq \, [(p^2 - 2pu)\sin^2\mu + 2(p-u)\, q \cos\mu \sin\mu$$
$$\left. + q^2 \cos^2\mu] \right\} \quad , \tag{51b}$$

where for convenience, since it causes no ambiguity, we have dropped the primes from p' and q'. We have used the notation R in the limits of our q-integrations to denote

$$R = (1 - p^2)^{1/2} \quad . \tag{52}$$

If we perform the q-integrations in Eq.'s (50), (51a), and (51b), we get

$$K_\alpha(u) = 2\,(16/\pi)^2 \left\{ \int_{-1}^{-u} dp\, [p^2(1-p^2)^{1/2} + 2\,pu(1-p^2)^{1/2} + \tfrac{1}{3}\,(1-p^2)^{3/2}] \right.$$
$$\left. + \int_{u}^{1} dp\, [p^2(1-p^2)^{1/2} - 2\,pu\,(1-p^2)^{1/2} + \tfrac{1}{3}\,(1-p^2)^{3/2}] \right\} \quad , \tag{53}$$

$$K_{\alpha_x}(\mu, u) = 2\,(16/\pi)^2 \left\{ \int_{u}^{1} dp\, [p^2(1-p^2)^{1/2}\cos^2\mu + 2\,pu\,(1-p^2)^{1/2}\cos^2\mu \right.$$
$$+ \tfrac{1}{3}\,(1-p^2)^{3/2}\sin^2\mu]$$
$$+ \int_{u}^{1} dp\, [p^2(1-p^2)^{1/2}\cos^2\mu - 2\,pu\,(1-p^2)^{1/2}\cos^2\mu$$
$$\left. + \tfrac{1}{3}\,(1-p^2)^{3/2}\sin^2\mu] \right\} \quad , \tag{54a}$$

$$K_{\alpha_y}(\mu, u) = 2\,(16/\pi)^2 \left\{ \int_{-1}^{-u} dp\, [p^2(1-p^2)^{1/2}\sin^2\mu + 2\,pu\,(1-p^2)^{1/2}\sin^2\mu \right.$$
$$+ \tfrac{1}{3}\,(1-p^2)^{3/2}\cos^2\mu]$$
$$+ \int_{u}^{1} dp\, [p^2(1-p^2)^{1/2}\sin^2\mu - 2\,pu\,(1-p^2)^{1/2}\sin^2\mu$$
$$\left. + \tfrac{1}{3}\,(1-p^2)^{3/2}\cos^2\mu] \right\} \quad . \tag{54b}$$

The evaluation of these p-integrals is a straightforward matter making use of the following formulas taken from Dwight[7]:

$$\int dp\, p(1-p^2)^{1/2} = -\tfrac{1}{3}(1-p^2)^{3/2} \quad , \tag{55a}$$

$$\int dp\, p^2(1-p^2)^{1/2} = -\tfrac{1}{4}p(1-p^2)^{3/2} + \tfrac{1}{8}p(1-p^2)^{1/2} + \tfrac{1}{8}\sin^{-1}(p) \quad , \tag{55b}$$

$$\int dp\, (1-p^2)^{3/2} = \tfrac{1}{4}p(1-p^2)^{3/2} + \tfrac{3}{8}p(1-p^2)^{1/2} + \tfrac{3}{8}\sin^{-1}(p) \quad . \tag{55c}$$

Carrying out the necessary substitutions and simplifications, we get

$$K_\alpha(u) = (16/\pi)^2\left[\cos^{-1}(u) - u(1-u^2)^{1/2} - 2u(1-u^2)^{3/2}\right] \quad , \tag{56}$$

$$K_{\alpha_x}(\mu, u) = \tfrac{1}{4}(16/\pi)^2\left[\cos^{-1}(u) - u(1-u^2)^{1/2} - 2(\tfrac{1}{3} + \tfrac{4}{3}\cos^2\mu)u(1-u^2)^{3/2}\right], \tag{57a}$$

$$K_{\alpha_y}(\mu, u) = \tfrac{1}{4}(16/\pi)^2\left[\cos^{-1}(u) - u(1-u^2)^{1/2} - 2(\tfrac{1}{3} + \tfrac{4}{3}\sin^2\mu)u(1-u^2)^{3/2}\right], \tag{57b}$$

With Eq.'s (56), (57a) and (57b) in hand, we now turn our attention to the evaluation of $F_\alpha(\xi)$, $F_{\alpha_x}(\xi)$, and $F_{\alpha_y}(\xi)$, as given by Eq.'s (39), (41a), and (41b), respectively.

Because of the presence of the 5/6-powers in the integrals defining $F_\alpha(\xi)$, $F_{\alpha_x}(\xi)$, and $F_{\alpha_y}(\xi)$, it does not appear to be possible to evaluate these functions analytically. We have therefore had to make use of digital computer numerical techniques. It is, however, possible to obtain some insight into the asymptotic behavior of these three functions for very large and very small values of ξ by analytic methods. Before presenting the numerical results, we shall develop these asymptotic results.

We shall be concerned with the function

$$Q(\mu, u;\xi) = \tfrac{1}{2}\left[u^2 + 2u\xi\cos(\mu) + \xi^2\right]^{5/6} + \tfrac{1}{2}\left[u^2 - 2u\xi\cos(\mu) + \xi^2\right]^{5/6} - u^{5/3}, \tag{58}$$

which is common to the integrands defining $F_\alpha(\xi)$, $F_{\alpha_x}(\xi)$, and $F_{\alpha_y}(\xi)$

in Eq.'s (39), (41a), and (41b). We wish to develop the power series expansions for $Q(\mu, u;\xi)$ for $\xi << u$ and for $\xi >> u$. From these power series expansions, the nature of the asymptotic dependencies will become apparent.

We start with the case $\xi >> u$. In this case, we can write as the power series expansion

$$
\begin{aligned}
Q(\mu, u;\xi) = \xi^{5/3}\Big\{ & \tfrac{1}{2}\left[1 + 2(u/\xi)\cos(\mu) + (u/\xi)^2\right]^{5/6} \\
& + \tfrac{1}{2}\left[1-2(u/\xi)\cos(\mu) + (u/\xi)^2\right]^{5/6} - (u/\xi)^{5/3}\Big\} \\
\approx\ \xi^{5/3}\Big\{ & \tfrac{1}{2}\Big\{1+\left(\tfrac{5}{6}\right)\left[2(u/\xi)\cos(\mu) + (u/\xi)^2\right] \\
& + \frac{\left(\frac{5}{6}\right)\left(-\frac{1}{6}\right)}{2}\left[2(u/\xi)\cos(\mu) + (u/\xi)^2\right]^2 \\
& + \frac{\left(\frac{5}{6}\right)\left(-\frac{1}{6}\right)\left(-\frac{7}{6}\right)}{6}\left[2(u/\xi)\cos(\mu) + (u/\xi)^2\right]^3 \\
& + \frac{\left(\frac{5}{6}\right)\left(-\frac{1}{6}\right)\left(-\frac{7}{6}\right)\left(-\frac{13}{6}\right)}{24}\left[2(u/\xi)\cos(\mu) + (u/\xi)^2\right]^4 + \ldots\Big\} \\
& + \tfrac{1}{2}\Big\{\left[1 + \left(\tfrac{5}{6}\right)\left[-2(u/\xi)\cos(\mu) + (u/\xi)^2\right]\right. \\
& + \frac{\left(\frac{5}{6}\right)\left(-\frac{1}{6}\right)}{2}\left[-2(u/\xi)\cos(\mu) + (u/\xi)^2\right]^2 \\
& + \frac{\left(\frac{5}{6}\right)\left(-\frac{1}{6}\right)\left(-\frac{7}{6}\right)}{6}\left[-2(u/\xi)\cos(\mu) + (u/\xi)^2\right]^3 \\
& + \frac{\left(\frac{5}{6}\right)\left(-\frac{1}{6}\right)\left(-\frac{7}{6}\right)\left(-\frac{13}{6}\right)}{24}\left[-2(u/\xi)\cos(\mu) + (u/\xi)^2\right]^4 + \ldots\Big\} \\
& - (u/\xi)^{5/3}\Big\}
\end{aligned}
\tag{59}
$$

Now if we expand and retain terms only up to $(u/\xi)^4$, we get

$$Q(\mu,u;\xi) = \xi^{5/3}\Big\{ 1 + (\tfrac{5}{6})(u/\xi)^2 - (\tfrac{5}{6})(-\tfrac{1}{12})\,[4(u/\xi)^2\cos^2(\mu) + (u/\xi)^4]$$

$$+ (\tfrac{5}{6})(-\tfrac{1}{12})(-\tfrac{7}{18})\,[12\,(u/\xi)^4\cos^2(\mu)]$$

$$+ (\tfrac{5}{6})(-\tfrac{1}{12})(-\tfrac{7}{18})(-\tfrac{13}{24})\,[16\,(u/\xi)^4\cos^4(\mu)] - (u/\xi)^{5/3}\Big\} + \ldots$$

$$= -u^{5/3} + \xi^{5/3} + \tfrac{5}{6}\,u^2\,\xi^{-1/3}[1 - \tfrac{1}{3}\cos^2(\mu)]$$

$$- \tfrac{5}{72}\,u^4\,\xi^{-7/3}\,[1 - \tfrac{14}{3}\cos^2(\mu) + \tfrac{91}{27}\cos^4(\mu)] + \ldots \qquad (60)$$

In the case where $u >> \xi$, we can write

$$Q(\mu,u;\xi) = u^{5/3}\Big\{ \tfrac{1}{8}\,[1 + 2(\xi/u)\cos(\mu) + (\xi/u)^2]^{5/6}$$

$$+ \tfrac{1}{8}\,[1 - 2(\xi/u)\cos(\mu) + (\xi/u)^2]^{5/6} - 1\Big\} \quad . \qquad (61)$$

The expansion is essentially the same as that leading to Eq. (60), except that, of course, the roles of u and ξ are interchanged and the two leading terms, instead of being $u^{5/3}$ and $\xi^{5/3}$, as in Eq. (60), are both $u^{5/3}$, and so cancel. Thus the result is

$$Q(\mu,u;\xi) = \tfrac{5}{6}\,\xi^2\,u^{-1/3}[1 - \tfrac{1}{3}\cos^2(\mu)] - \tfrac{5}{72}\,\xi^4\,u^{-7/3}$$

$$\times\,[1 - \tfrac{14}{3}\cos^2(\mu) + \tfrac{91}{27}\cos^4(\mu)] + \ldots \qquad (62)$$

For very large values of ξ , i.e., values much greater than unity, we use Eq. (60) to establish the asymptotic dependence. We note first of all that if Q is replaced by a function independent of (μ,u) , then the three

integrals in Eq.'s (39), (41a), and (41b) will all vanish. This means that the $\xi^{5/3}$-term in Eq. (60) does not contribute to the value of $F_{\alpha}(\xi)$, $F_{\alpha_x}(\xi)$, or $F_{\alpha_y}(\xi)$. The $u^{5/3}$-term gives rise to a constant value (which can be associated with the angle-of-arrival variance), and then the leading term with a ξ-dependence has a $\xi^{-1/3}$-power dependence. Thus for values of ξ much larger than unity, $F_{\alpha}(\xi)$, $F_{\alpha_x}(\xi)$, and $F_{\alpha_y}(\xi)$ all approach a constant value with a deviation dependent on $\xi^{-1/3}$. For values of ξ much less than unity, we see from consideration of Eq. (62) that $F_{\alpha}(\xi)$, $F_{\alpha_x}(\xi)$, and $F_{\alpha_y}(\xi)$ all start with zero value at $\xi = 0$ and grow as ξ^2.

The numerical evaluation of the double integrals in Eq.'s (39), (41a), and (41b) is a straightforward matter. In the next section, we present the results of this numerical evaluation and sample data reduction for high altitude C_N^2. This will utilize solar limb measurements of angle-of-arrival isoplanatism made by A. Title.

Because of the similarity of the integrand for angle-of-arrival isoplanatism and for predetection compensation isoplanatism, we feel quite confident that instabilities in the inversion of the former integral, while they might (if present) affect the high altitude estimates of C_N^2, should have only minor influence on the calculated value of the latter integral. For this reason, we believe angle-of-arrival isoplanatism measurements will allow accurate calculation of the isoplanatic patch size for predetection compensation.

2.0 Isoplanatic Dependence of Predetection Compensation Imagery

2.1 Introduction

In the preceding sections, it is shown that we must be specific about the imaging process we have in mind if we are to be able to speak meaningfully about isoplanatism — that the isoplanatic dependence for predetection compensation imaging can be quite different from that for ordinary short-exposure imagery or for angle-of-arrival measurement, and at the same time developed an analytic formulation of the way angle-of-arrival isoplanatism depends on the distribution of the optical strength of turbulence, C_N^2 , along the propagation path. In earlier work,[3] we developed an expression which allowed the isoplanatic dependence of predetection compensation imagery to be calculated from knowledge of the distribution of C_N^2 along the propagation path.

Here we shall be concerned with the possibility that we can invert a set of measurements of the isoplanatic dependence of the angle-of-arrival to determine the distribution of C_N^2 along the propagation path, and then use those values of C_N^2 to allow us to calculate the isoplanatic dependence of predetection compensation. There is reason to hope that while the basic inversion process by which we calculate C_N^2 from the angle-of-arrival isoplanatism may be ill-conditioned and so yield a set of values of C_N^2 that have large errors, the errors in the individual values will be so correlated that if we use these values of C_N^2 to calculate the isoplanatic dependence of predetection compensation, the error contributions will be greatly reduced. We base this conjecture on the fact that although the two isoplanatism dependencies are not identical, there is a significant similarity in their nature, as we shall note shortly, in their dependence on the distribution of C_N^2 . As shall be seen, this conjecture is only partly borne out by results of numerical analysis of the transformation procedure.

In the next section, we shall briefly review the pertinent equations for the dependence of the two types of isoplanatism on the distribution of C_N^2 , and carry out appropriate numerical evaluation of certain functions involved in these equations. The section following that will treat the conversion of the basic problem to a form suitable for numerical analysis and will set up the inversion processes in a general form and carry out the generalized inversion. In the section after that, we shall consider the noise theory associated with the measurements and develop appropriate results for the resultant noise in the processed data. In the final section, we shall present results obtained by processing a set of measurements of the angle-of-arrival isoplanatism dependence generated by Dr. A. Title of the Lockheed Palo Alto Research Laboratory.

2.2 Relevant Formulas

It has been shown that in predetection compensated imaging using a point-source reference located an angular distance ϑ from the location of the region containing the source being imaged, the achieved modulation transfer function will be down from the diffraction-limited value for that aperture by a factor $\exp(-m)$, where m is a function of $\vec{\vartheta}$ and $\lambda\vec{f}$, $\vec{f}$ being the compensated image spatial frequency of interest (expressed in cycles/rad). It has been shown that the relationship between m and the distribution of C_N^2 along the propagation path is given by the expression

$$m(\vec{\vartheta}, \lambda\vec{f}) = 2.91\,(2\pi/\lambda)^2 \int_{\text{Path}} dz\, C_N^2\, (\lambda f)^{5/3} \left\{ 1 + \left(\frac{2\vartheta z}{\lambda f}\right)^{5/3} - \frac{1}{2}\left[1 + 2\left(\frac{2\vartheta z}{\lambda f}\right)\cos\phi + \left(\frac{2\vartheta z}{\lambda f}\right)^2\right]^{5/6} + \frac{1}{2}\left[1 - 2\left(\frac{2\vartheta z}{\lambda f}\right)\cos\phi + \left(\frac{2\vartheta z}{\lambda f}\right)^2\right]^{5/6} \right\} \quad . \tag{1}$$

where ϕ is the angle between the orientation of the vectors $\vec{\vartheta}$ and $\vec{f}$. If we know the distribution of C_N^2 along the propagation path, we could

calculate m directly, which is our basic objective — but here we shall be seeking other indirect methods of determining the value of m without explicit knowledge of the distribution of C_N^2 along the propagation path.

The mean square difference in the angle-of-arrival as seen by an aperture of diameter D viewing two sources with an angular separation ϑ, (less the square of the mean difference), is the so-called angle-of-arrival isoplanatism function. We denote this function by $B_{l,\alpha}(\vartheta)$. If we restrict the measurements to the components of difference parallel to or perpendicular to the orientation of the mean angular separation of the two sources, we obtain the two quantities $B_{l,\alpha_x}(\vartheta)$ and $B_{l,\alpha_y}(\vartheta)$, respectively. It has been shown that

$$B_{l,\alpha}(\vartheta) = D^{-1/3} \int_{\text{Path}} ds\, C_N^2\, F_\alpha(\vartheta s/D) \quad , \tag{2}$$

where

$$F_\alpha(\xi) = 2.91 \int_0^{2\pi} d\phi \int_0^1 u\, du\, K_\alpha(\phi, u)\, Q(\phi, u; \xi) \, , \tag{3}$$

$$K_\alpha(\phi, u) = \tfrac{1}{8} (16/\pi)^2 [\cos^{-1}(u) - u(1-u^2)^{1/2} - 2u(1-u^2)^{3/2}] \, , \tag{4}$$

$$Q(\phi, u; \xi) = \tfrac{1}{2} [u^2 + 2\, u\, \xi \cos\phi + \xi^2]^{5/6} + \tfrac{1}{2} [u^2 - 2\, u\, \xi \cos\phi + \xi^2]^{5/6} - u^{5/3} - \xi^{5/3} \, . \tag{5}$$*

Similarly,

$$B_{l,\alpha_x}(\vartheta) = D^{-1/3} \int_{\text{Path}} ds\, C_n^2\, F_{\alpha_x}(\vartheta s/D) \quad , \tag{6}$$

---

* It is to be noted that as developed earlier, the $\xi^{5/3}$-term is missing from the Q-formulation. However, since

$$\int_0^{2\pi} d\phi \int_0^1 u\, du\, K_\alpha(\phi, u) = 0 \quad ,$$

its presence or absence has no effect on F_α. The $\xi^{5/3}$-term is introduced to insure a small asymptotic value for Q with large ξ.

and

$$\mathcal{B}_{l,\alpha_y}(\vartheta) = D^{-1/3} \int_{\text{Path}} ds\, C_N^2\, F_{\alpha_y}(\vartheta s/D) \quad , \tag{7}$$

where

$$F_{\alpha_x}(\xi) = 2.91 \int_0^{2\pi} d\phi \int_0^1 u\, du\, K_{\alpha_x}(\phi,u)\, Q(\phi,u;\xi) \quad , \tag{8}$$

with

$$K_{\alpha_x}(\phi,u) = \tfrac{1}{2}(16/\pi)^2\left[\cos^{-1}(u) - u(1-u^2)^{1/2} - \tfrac{2}{3}(1+4\cos^2\phi)u(1-u^2)^{3/2}\right] , \tag{9}$$

and

$$F_{\alpha_y}(\xi) = 2.91 \int_0^{2\pi} d\phi \int_0^1 u\, du\, K_{\alpha_y}(\phi,u)\, Q(\phi,u;\xi) \quad , \tag{10}$$

with

$$K_{\alpha_y}(\phi,u) = \tfrac{1}{2}(16/\pi)^2\left[\cos^{-1}(u) - u(1-u^2)^{1/2} - \tfrac{2}{3}(1+4\sin^2\phi)u(1-u^2)^{3/2}\right] . \tag{11}$$

The relationship, via Q , between the expression for $\mathcal{B}_{l,\alpha}$ and the expression for $\mathcal{M}$ is apparent — but it is equally obvious that there is no reason to expect numerical results to be well correlated between the two quantities. We shall concentrate on development of a method of using $\mathcal{B}_{l,\alpha}$, $\mathcal{B}_{l,\alpha_x}$, or $\mathcal{B}_{l,\alpha_y}$ measurement data to indirectly calculate $\mathcal{M}$. We start this effort by noting that although $K_\alpha(\xi)$, $K_{\alpha_x}(\xi)$, and $K_{\alpha_y}(\xi)$ are defined by rather complicated expressions, they are definable by a set of numerical values, which we will now evaluate.

The calculation of the values of F_α , F_{α_x} , and F_{α_y} is a straightforward problem in multi-dimensional numerical analysis. The only potential problem is in loss of accuracy in the evaluation of $Q(\phi,u;\xi)$ when $u \gg \xi$ or $\xi \gg u$. We avoid this problem by making use of the asymptotic expressions

$$\underset{\xi \gg u}{Q(\phi,u;\xi)} = -u^{8/3} + \tfrac{8}{3}u^2\,\xi^{-1/3}\left[1 - \tfrac{1}{3}\cos^2\phi\right]$$

$$- \tfrac{8}{15}u^4\,\xi^{-7/3}\left[1 - \tfrac{14}{3}\cos^2\phi + \tfrac{21}{17}\cos^4\phi\right] , \tag{12}$$

and

$$Q(\phi, u;\xi) \underset{u>>\xi}{=} -\xi^{5/3} + \frac{5}{6}\xi^2 u^{-1/3}\left[1 - \frac{1}{3}\cos^2\phi\right] - \frac{5}{72}\xi^4 u^{-7/3}\left[1 - \frac{14}{3}\cos^2\phi + \frac{91}{27}\cos^4\phi\right] \quad . \qquad (13)$$

Making use of Eq.'s (3), (8), and (10) for F_α, F_{α_x}, and F_{α_y}, of Eq.'s (4), (9), and (11) for K_α, K_{α_x}, and K_{α_y}, and Eq.'s (5), (12), and (13) for Q, we have numerically evaluated $F_\alpha(\xi)$, $F_{\alpha_x}(\xi)$, and $F_{\alpha_y}(\xi)$ for ξ in the range 1×10^{-3} to 1×10^{5}. The results are listed in Table 1 and are plotted in Fig. 1. As can be seen, the F-functions have no very spectacular behavior. With the data in Table 1 and Eq.'s (2), (6), and (7) in hand, we are ready to start looking at how to go from the β_1-measurements to estimates of C_n^2. [By use of Eq. (1), it would then be an easy matter to get to evaluation of $\mathcal{M}$.] We take up the problem of getting C_n^2 values from the β_1-measurements in the next section, at least in a general sense.

2.3 Numerical Inversion

It would be convenient if we could analytically invert an expression such as Eq. (2) so that we could write

$$C_n^2 = \int d\vartheta\, \beta_{1,\alpha}(\vartheta)\, \Lambda(s,\vartheta) \quad . \qquad (14)$$

While it is obvious that the function Λ must exist, there does not appear to be any reasonable way to analytically determine this function. To get around this difficulty, we fall back on numerical techniques.

We start by converting the integral in Eq. (2) to a summation. As a practical matter, we shall restrict our attention to the astronomical problem of light propagating vertically down through the atmosphere. We shall replace the integral by a sum corresponding to ten uniformly spaced points in the altitude range from 0 to 20 km. (We imply by this the assumption that C_n^2 may be considered to be negligibly small above 20 km

altitude. We shall let h_i = (1,000 , 3000 , 5000 , . . . , 17000 , 19000 m) and $(C_N^2)_i$ denote the value of C_N^2 to be associated with the 2000 m interval centered at the altitude h_i . Then with Δh = 2000 m , we can write

$$\mathcal{B}_{I,\alpha}(\vartheta) = D^{-1/3} \sum_{i=1}^{10} \Delta h \, (C_N^2)_i \, F_\alpha (\vartheta \, h_i/D) \quad , \tag{15}$$

and similarly,

$$\mathcal{B}_{I,\alpha_x}(\vartheta) = D^{-1/3} \sum_{i=1}^{10} \Delta h \, (C_N^2)_i \, F_{\alpha_x} (\vartheta \, h_i/D) \quad , \tag{16}$$

and

$$\mathcal{B}_{I,\alpha_y}(\vartheta) = D^{-1/3} \sum_{i=1}^{10} \Delta h \, (C_N^2)_i \, F_{\alpha_y} (\vartheta \, h_i/D) \quad . \tag{17}$$

At this point, we shall restrict our attention to Eq. (17) for $\mathcal{B}_{I,\alpha_y}(\vartheta)$ (with the understanding that, although we shall not pursue it here, the same procedures could be applied to $\mathcal{B}_{I,\alpha}(\vartheta)$ and $\mathcal{B}_{I,\alpha_x}(\vartheta)$ data.) We consider a set of measurements of $\mathcal{B}_{I,\alpha_y}(\vartheta)$ made at various values of ϑ , which we denote by ϑ_j . This allows us to write

$$\mathcal{B}_j = \sum_{i=1}^{10} (C_N^2)_i \, F_{i,j} \quad , \tag{18}$$

where

$$\mathcal{B}_j \equiv \mathcal{B}_{I,\alpha_y}(\vartheta_j) \quad , \tag{19}$$

and

$$F_{i,j} = D^{-1/3} \, \Delta h \, F_{\alpha_y} (\vartheta_j \, h_i/D) \quad . \tag{20}$$

We note that Eq. (18) represents a set of simultaneous equations specifying the unknowns, $(C_N^2)_i$ in terms of the measured $\mathcal{B}_j$. According to the number of values of j that we consider, there will be fewer equations than unknowns, more equations than unknowns, or the same number. We have no simple recourse to determine the $(C_N^2)_i$ in the first case, and so must

insist that there be at least as many values of j as there are of i if we are to be able to meaningfully calculate $(C_N^2)_i$ from the β_j values. If there are more values of j than of i, then we can solve for the $(C_N^2)_i$ in a least-square sense. As a practical matter, however, it is most convenient to assume that all necessary data smoothing is done with a large set of β_j data in picking a set of values that smoothly interpolate the full set and that involve only as many final values of j as there are values of i. In this case, there are exactly as many simultaneous equations as there are unknowns, and F_{ij} is a square matrix. In particular, we will be dealing with a 10×10 F_{ij} matrix.

Making use of the data in Table 1, we have evaluated the F_{ij} matrix for the case $\vartheta_j = \{1 \text{ sec}, 3 \text{ sec}, 5 \text{ sec}, \ldots, 19 \text{ sec}\} \equiv \{4.85 \times 10^{-6} \text{ rad}, 14.54 \times 10^{-6} \text{ rad}, 24.24 \times 10^{-6} \text{ rad}, \ldots, 92.11 \times 10^{-6} \text{ rad}\}$. The values are listed in Table 2. This is a relatively modest size matrix, and it is a straightforward matter to obtain its inverse, $F_{i,j}^{-1}$ on a digital computer. In Table 3, we list the values of $F_{i,j}^{-1}$. It is now a straightforward matter to obtain from Eq. (18), by multiplying both sides by $F_{i',j}^{-1}$, summing over j, and where appropriate interchanging the order of i and j summation,

$$(C_N^2)_i = \sum_j F_{ij}^{-1} \beta_j \quad , \tag{21}$$

where we have replaced i' by i in writing this expression. This represents, in numerical form, the basic solution to the problem of calculating C_N^2 from measurements of $\beta_{l,\alpha_\gamma}(\vartheta)$, and is the equivalent of Eq. (14). In a sense, F_{ij}^{-1} represents $\Lambda(s,\vartheta)$.

Our interest, however, is in the calculation of m. To get a suitable expression for calculation of m from $\beta_{l,\alpha_\gamma}(\vartheta)$, we rewrite Eq. (1) with the integral approximated by a summation equivalent to that in Eq. (15). Thus we get

$$\mathcal{M}(\vec{\vartheta}, \lambda\vec{f}) = \sum_i G_i(\vec{\vartheta}, \lambda\vec{f})\,(C_N^2)_i \quad , \tag{22}$$

where

$$G_i(\vec{\vartheta}, \lambda\vec{f}) = 2.91\,(2\pi/\lambda)^2(\lambda f)^{5/3}\,\Delta h \left\{1 + \left(\frac{2\vartheta h_i}{\lambda f}\right)^{5/3} - \tfrac{1}{2}\left[1 + 2\left(\frac{2\vartheta h_i}{\lambda f}\right)\cos\phi + \left(\frac{2\vartheta h_i}{\lambda f}\right)^2\right]^{5/6} - \tfrac{1}{2}\left[1 - 2\left(\frac{2\vartheta h_i}{\lambda f}\right)\cos\phi + \left(\frac{2\vartheta h_i}{\lambda f}\right)^2\right]^{5/6}\right\} \quad . \tag{23}$$

If we now substitute Eq. (21) into Eq. (22), we get

$$\mathcal{M}(\vec{\vartheta}, \lambda\vec{f}) = \sum_{i,j} G_i(\vec{\vartheta}, \lambda\vec{f})\,F_{ij}^{-1}\,\mathcal{B}_j \quad , \tag{24}$$

which is the basic expression we have sought for calculation of the predetection compensation imaging isoplanatism dependence, $\mathcal{M}$, from measurements of the angle-of-arrival isoplanatism function, $\mathcal{B}$. In Table 4, we list calculated values of $\mathcal{A}_j(\vec{\vartheta}, \lambda\vec{f})$ where

$$\mathcal{A}_j(\vec{\vartheta}, \lambda\vec{f}) = \sum_i G_i(\vec{\vartheta}, \lambda\vec{f})\,F_{ij}^{-1} \quad , \tag{25}$$

and of course

$$\mathcal{M}(\vec{\vartheta}, \lambda\vec{f}) = \sum_j \mathcal{A}_j(\vec{\vartheta}, \lambda\vec{f})\,\mathcal{B}_j \quad . \tag{26}$$

With these results in hand, we are ready to start processing angle-of-arrival isoplanatism measurement data to calculate the predetection compensation isoplanatic dependence, $\mathcal{M}$. However, before actually carrying out such calculations, which we will take up in the last section, we shall first briefly consider the noise aspects of our data processing. We treat this in the next section.

2.4 Noise Considerations

The basic angle-of-arrival isoplanatic measurement is of the difference in the angle-of-arrival for two sources separated by an angular distance ϑ . We shall denote the difference that we measure by $x + n$, where x is the random value associated with atmospheric effects and n is the random value associated with noise in the angle-of-arrival sensor. (We may assume that the sensors are properly aligned so that x has a mean value of zero.) The quantities x and n are both gaussian random variables with zero mean. The data we wish to obtain from the sensor measurements is

$$\beta = \langle x^2 \rangle \quad . \tag{27}$$

To do this, we have to take advantage of the fact that the sensor noise can be determined separately*, yielding

$$\sigma^2 = \langle n^2 \rangle \quad . \tag{28}$$

The basic data processing procedure, starting with a set of N independent measurements, is to write

$$\Delta = \frac{1}{N} \sum_{k=1}^{N} (x_k + n_k)^2 \quad , \tag{29}$$

and the approximation

$$\beta \approx \Delta - \sigma^2 \quad . \tag{30}$$

---

* The sensor noise is determined by measuring $x+n$ in the case where the angular separation ϑ between the two sources is zero, i.e., there is only a single source. In this case, we know that $x = 0$ and measurements of $\langle n^2 \rangle$ can be obtained directly.

Because we can take a great deal of time, i.e., use very many samples, in our one-time measurement of σ^2 , we can expect this value to be quite accurate. On the other hand, our measurement of Δ , under the pressure of experimental considerations, will be determined with only a limited set of values of $x_k + n_k$. Inasmuch as x_k and n_k are both random variables, then Δ will also have some potentially significant random component. We wish to know how large this random component may be expected to be.

To calculate the variance of a measurement of β , we write

$$S = \langle (\beta - \langle \beta \rangle)^2 \rangle$$

$$= \left\langle \left(\frac{1}{N} \sum_{k=1}^{N} (x_k + n_k)^2 - \sigma^2 - \left\langle \frac{1}{N} \sum_{k=1}^{N} (x_k + n_k)^2 - \sigma^2 \right\rangle \right)^2 \right\rangle \quad , \tag{31}$$

in which we have made use of Eq.'s (29) and (30) to obtain this expression. Since σ^2 is not a random variable, it can be brought outside of the inner ensemble average, and so cancel the other σ^2 . This then yields

$$S = \left\langle \left(\frac{1}{N} \sum_{k=1}^{N} (x_k + n_k)^2 - \left\langle \frac{1}{N} \sum_{k=1}^{N} (x_k + n_k)^2 \right\rangle \right)^2 \right\rangle \tag{32}$$

This can be reduced to the form

$$S = \left\langle \left(\frac{1}{N} \sum_{k=1}^{N} (x_k + n_k)^2 \right)^2 \right\rangle - \left\langle \frac{1}{N} \sum_{k=1}^{N} (x_k + n_k) \right\rangle^2 \quad . \tag{33}$$

and writing the sum squared as a produce of sums, and that as a double sum, we get

$$S = \left\langle \frac{1}{N^2} \sum_{k,k'=1}^{N} (x_k^2 + 2x_k n_k + n_k^2)(x_{k'}^2 + 2x_{k'} + n_{k'} + n_{k'}^2) \right\rangle$$

$$- \left\langle \frac{1}{N} \sum_{k=1}^{N} (x_k^2 + 2x_k n_k + n_k^2) \right\rangle^2 \quad . \tag{34}$$

Now if we make use of the fact that each of the x_k's and n_k's are independent random variables, carrying out the multiplication in the double sum and dropping all terms whose ensemble average will vanish (noting that the ensemble average of $x_k n_k x_{k'} n_{k'}$ will vanish except when $k' = k$), we can rewrite Eq. (34) as

$$S = \Big\langle \frac{1}{N^2} \sum_{k=1}^{N} (x_k^4 + n_k^4) + \frac{1}{N^2} \sum_{\substack{k,k'=1 \\ k \neq k'}}^{N} (x_k^2 x_{k'}^2 + n_k^2 n_{k'}^2)$$

$$+ \frac{1}{N^2} \sum_{k,k'=1}^{N} (x_k^2 n_{k'}^2 + x_{k'}^2 n_k^2) + \frac{1}{N^2} \sum_{\substack{k=1 \\ k'=1}}^{N} 4\, x_k x_{k'} n_k n_{k'} \Big\rangle$$

$$- \Big\langle \frac{1}{N} \sum_{k=1}^{N} (x_k^2 + n_k^2) \Big\rangle^2$$

$$= \frac{1}{N} \Big[\langle x^4 \rangle + \langle n^4 \rangle \Big] + \frac{N-1}{N} \Big[\langle x^2 \rangle^2 + \langle n^2 \rangle^2 \Big]$$

$$+ 2 \langle x^2 \rangle \langle n^2 \rangle + \frac{4}{N} \langle x^2 \rangle \langle n^2 \rangle - (\langle x^2 \rangle + \langle n^2 \rangle)^2$$

$$= \frac{1}{N} \Big[\langle x^4 \rangle - \langle x^2 \rangle^2 + 4 \langle x^2 \rangle \langle n^2 \rangle - \langle n^2 \rangle^2 + \langle n^4 \rangle \Big]$$

$$+ \langle x^2 \rangle^2 + 2 \langle x^2 \rangle \langle n^2 \rangle + \langle n^2 \rangle - (\langle x^2 \rangle + \langle n^2 \rangle)^2 \quad . \qquad (35)$$

Subject to the assumption that x and n are both gaussian random variables, so that

$$\langle x^4 \rangle = 3 \langle x^2 \rangle^2 \quad , \qquad (36)$$

and

$$\langle n^4 \rangle = 3 \langle n^2 \rangle^2 \quad , \qquad (37)$$

we can recast Eq. (35) in the form

$$S = \frac{2}{N} \left(\langle x^2 \rangle + \langle n^2 \rangle \right)^2$$

$$= \frac{2}{N} \left(\beta + \sigma^2 \right)^2 \quad . \tag{38}$$

Eq. (38) represents the variance in our determination of the angle-of-arrival isoplanatism function, and makes it clear that to get acceptable answers we need to make enough measurements, i.e., N must be large.

To see how the variance in the measured values of the angle-of-arrival isoplanatism function goes over into variances in the computed values of the predetection compensation function, we refer back to Eq. (26). Recognizing that each of the $\dot{\beta}_j$ in that expression has its particular mean value $\langle \dot{\beta}_j \rangle$, and its own random component, $\delta\dot{\beta}_j$, with variance $\dot{S}_j$ (which variance may be different for the different values of j), and taking the variance of m as the sum over j of the variances of $\dot{\phi}_j \dot{\beta}_j$, we get

$$\sigma_m^2 = \sum_j [\dot{\phi}_j(\vec{\vartheta}, \lambda\vec{r})]^2 \, \dot{S}_j \quad . \tag{39}$$

Making use of Eq. (38), we can rewrite this as

$$\sigma_m^2 = \frac{2}{N} \sum_j [\dot{\phi}_j(\vec{\vartheta}, \lambda\vec{r})]^2 \, (\dot{\beta}_j + \sigma^2) \quad . \tag{40}$$

To proceed further, we see that we need to have values for σ^2 and for the $\dot{\beta}_j$'s. In the next section, we introduce this data and use it to calculate both σ_m^2 and m itself.

2.5 Measurement Data

A series of measurements of the image of the edge of the sun have been made by Dr. Allen Title, Lockheed Palo Alto Research Laboratory, from which he has been able to determine the angle-of-arrival isoplanatism function for a $D = 0.3$ m diameter aperture at a wavelength of $\lambda = 0.633 \times 10^{-6}$ m. The resultant measurement data is reproduced here as Table 5. These values correspond to the quantity $\Delta^{1/2}$ (in arc-seconds), as defined by Eq. (29), for various angular separations, ϑ. (The measurements are of the radial displacement of the image of the edge of the sun for angular separations circumferential along the edge of the sun — so that $\beta_{\alpha_y}(\vartheta)$ is the appropriate angle-of-arrival isoplanatism function.) Each entry in Table 5 represents an average over 128 readings, i.e., $N = 128$. Each of the columns refers to a different measurement run, some of them on different days. All measurements were taken with the line-of-sight close enough to the zenith that we believe that the zenith angle factor can be taken as unity for each measurement.

Because almost 20 minutes elapsed between the taking of the first and the last entries in each data set, it is doubtful that there is real consistency between the entries in a column, and so it is doubtful that an attempt to invert any simple data set by means of Eq. (26) would yield really sound results. However, by averaging all seven sets of data in Table 5, we can obtain a plausible estimate of β_j, from which we can then calculate m and σ_m. Due to the scatter in the β_j-data because of the 20-minute length of the measurement, we do not expect to achieve particularly accurate values for m. However, we expect that our estimates of σ_m should be quite sound, as they do not depend on the interrelationship of the various β_j, but rather on the general magnitude of each β_j value.

Table 6 lists values of β in radians-squared calculated using the average over the seven runs of the value of Δ at $\vartheta = 0$ as an estimate of

σ^2 . Using the average value of the β-values for each ϑ , we have prepared the plot shown in Fig. 2. The scatter in the data is, we believe, indicative of the variation in the turbulence conditions during the 20 minutes of each measurement run, reduced to some extent by the number of runs that have been averaged. We have fit this data with the expression

$$\hat{\beta}_{i,\alpha_y}(\vartheta) = \left[\left(\frac{1}{.5}\right)^2 + \left(\frac{1}{.02\vartheta^{1.5}}\right)^2 \right]^{-1/2} \times 10^{-12} \quad , \tag{41}$$

which we show plotted in Fig. 2 along with $1.15\,\hat{\beta}_{i,\alpha_y}$ and $0.85\,\hat{\beta}_{i,\alpha_y}$, representing what we think are approximately the $\pm$ 1-σ bounds for the data.

Using Eq. (41) to provide the data listed in Table 7, we have calculated $\hat{m}$ and $\frac{1}{2}N\hat{\sigma}_m^2$ using the equations

$$\hat{m} = \sum_j \phi_j(\vec{\vartheta}, \lambda\vec{f})\,\hat{\beta}_j \quad , \tag{42}$$

$$\tfrac{1}{2}\,N\,\hat{\sigma}_m^2 = \sum_j [\phi_j(\vec{\vartheta}, \lambda\vec{f})]^2\,(\beta_j + \sigma^2) \quad , \tag{43}$$

and have, in addition, calculated the quantity

$$\hat{\sigma}_{\hat{m}}^2 = (.15)^2 \sum_j [\phi_j(\vec{\vartheta}, \lambda\vec{f})]^2\,\hat{\beta}_j \quad . \tag{44}$$

These values are listed in Tables 8, 9, and 10, respectively.

The values of $\hat{m}$ are interesting and their meaning fairly obvious. It would seem that the isoplanatic patch size for predetection compensation imaging is only of the order of one to one-and-a-half arc-seconds if we wish to achieve an MTF within 10% of the diffraction-limited value for the higher spatial frequencies. However, when we consider the values of $\hat{\sigma}_{\hat{m}}^2$ in Table 10, it is apparent that very little confidence can be put in the values of m listed in Table , except perhaps for the smallest values of ϑ . This

is due to the large uncertainty in the measurement data caused by the apparent non-stationarity of the turbulence during the 20-minute measurement period.

If we consider the data in Table 9 for $\frac{1}{2} N \hat{\sigma}_m^2$, which represents the uncertainty in the calculated values of m that we could expect if we did not have the time spread problem, we could achieve an rms uncertainty of about ± 0.3 in the calculated value of m if we had about 4000 readings, i.e., if $N = 4 \times 10^3$. The ten required values of ϑ could be run 4096 times each, at 12.5 msec per measurement (as in Title's work) in a period of 512 sec, or just over 8 minutes. This would, however, require an automatic means for stepping the equipment through the various values of ϑ , which we expect is a straightforward equipment modification. To insure effective stationarity during the measurements, i.e., that the same turbulence profiles applied to data taken at each value of ϑ , it would be necessary to cycle through the values of ϑ several times (perhaps ten times) during a total data run. The data processing would be somewhat more complicated, but not really significantly so for the on-line computer system used by Dr. Title. With this arrangement, it would then be possible to determine the predetection compensation isoplanatism dependence with adequate accuracy, i.e., about $\pm 30\%$, using angle-of-arrival isoplanatism measurements.

2.6 Summary

We have shown how angle-of-arrival isoplanatism data can be used to calculate the isoplanatism dependence of predetection compensation imagery, and set up the necessary arithmetic for such a procedure. We have determined the expected nature of the uncertainty in the angle-of-arrival isoplanatism function values, and shown how these, in turn, determine the uncertainty in the calculated isoplanatic dependence of predetection compensation. We have examined a set of data on angle-of-arrival

isoplanatism dependence supplied to us by Dr. Allen Title, and have used it to calculate the expected values for the isoplanatism dependence of predetection compensation, and to calculate the expected uncertainty in those results. The results imply that the isoplanatic patch size for predetection compensation is 1 to 1.5 arc-seconds. However, it is noted that because of the non-stationarity of the turbulence during the measurement periods, the results have rather substantial uncertainties. We note that by certain modifications of the experiment, particularly of the data-taking procedure, measurements could be obtained that would yield values of the predetection compensation isoplanatism dependence that have only about 30% rms uncertainty. However, considering the large number of measurements required, implying an angle-of-arrival isoplanatism measurement uncertainty of about $(4096)^{-1/2} = 1.6\%$, we feel that we must conclude that measurement of angle-of-arrival isoplanatism (or probably of any other aspect of the isoplanatic dependence of short-exposure imagery) is not a straightforward approach to the measurement of the isoplanatic dependence of predetection compensation imagery.

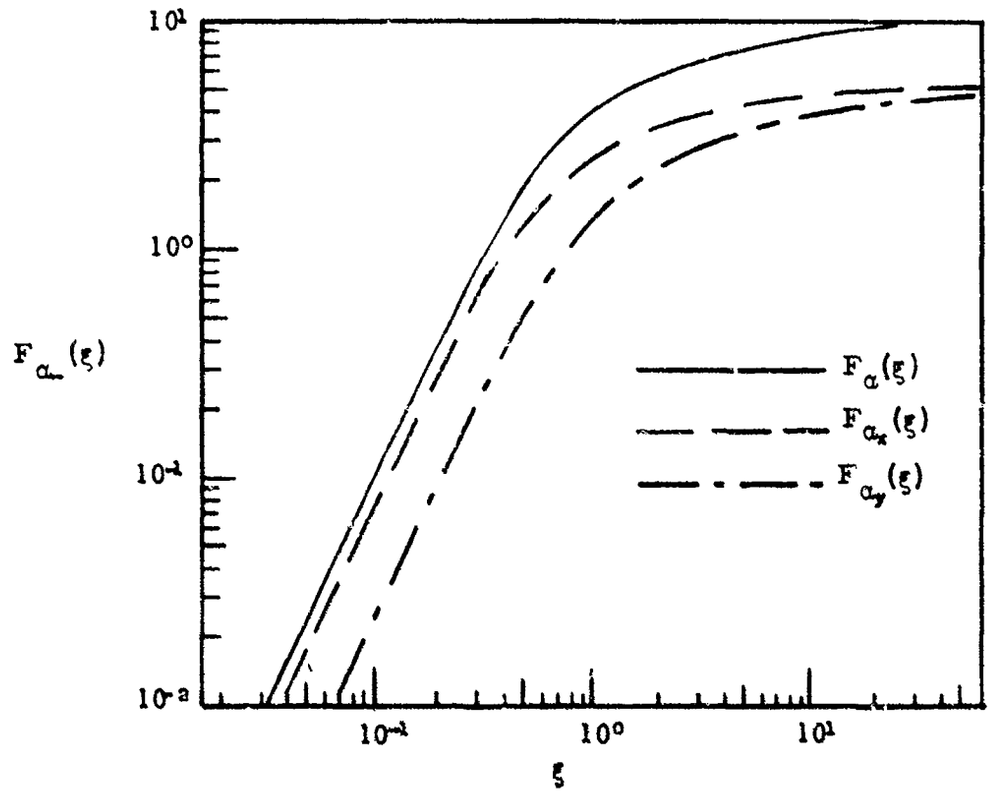

Figure 2.1. Dependence of $F_{\alpha_\infty}(\xi)$ on ξ.
The values plotted are taken from the data in Table 1.

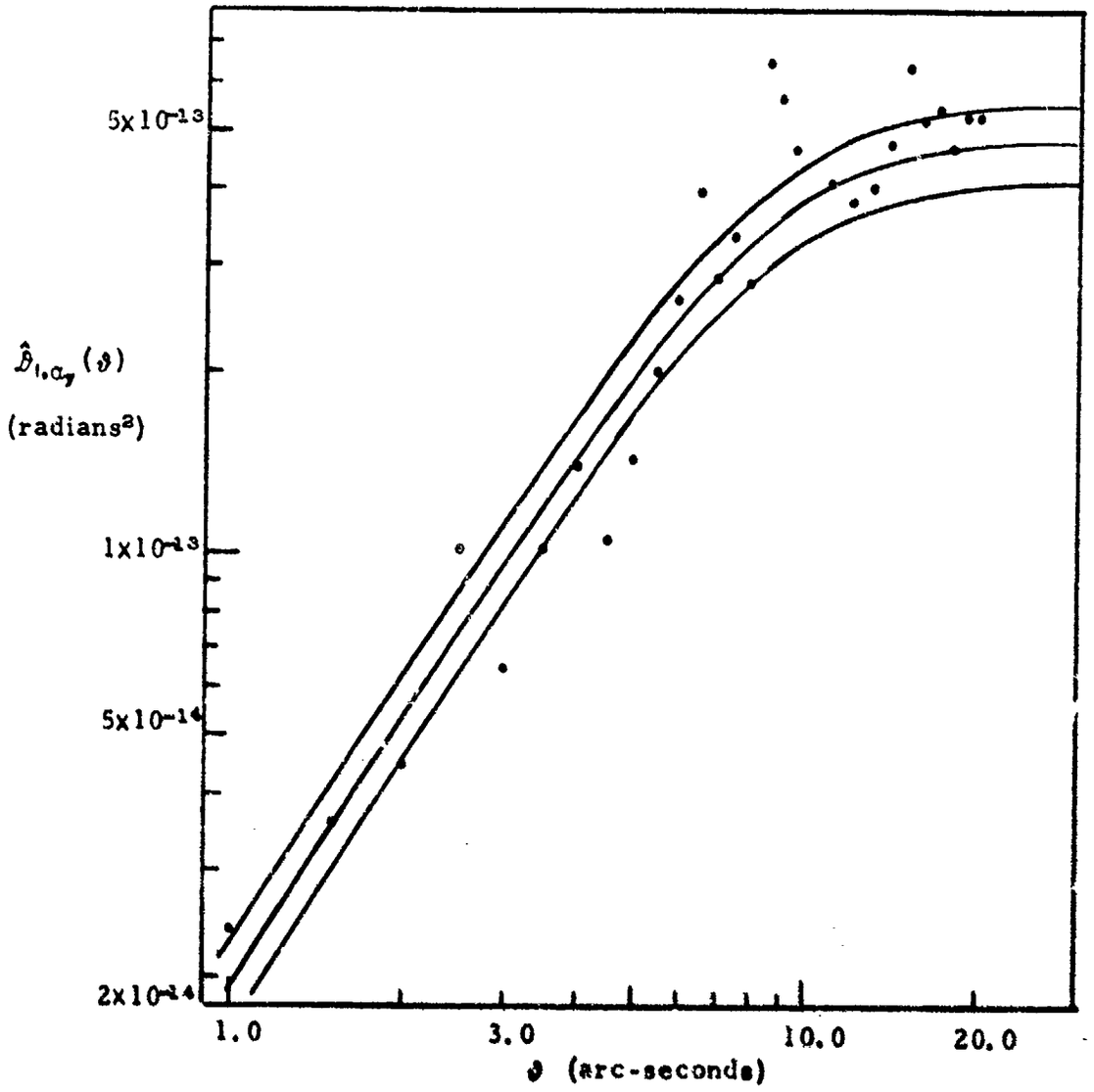

Figure 2.2. Measured Values of the Angle-of-Arrival Isoplanatism Dependence, and Interpolation Curve. The data points are taken from the average data column of Table 5. The curves represent the approximation function

$$\hat{\beta}_{1,\alpha_y}(\vartheta) = [(1/.5)^3 + (1/.02\,\vartheta^{1.5})^3]^{-1/3} \times 10^{-13} \quad (\text{rad}^2),$$

where ϑ is in arc-seconds, as well as $1.15\,\hat{\beta}_{1,\alpha_y}(\vartheta)$ and $0.85\,\hat{\beta}_{1,\alpha_y}(\vartheta)$.

Table 1

Calculated Values of $F_\alpha(\xi)$, $F_{\alpha_x}(\xi)$, and $F_{\alpha_y}(\xi)$

The values of ξ in the table are logarithmically uniformly spaced, four to a decade, (viz. $1.778 = 10^{1/4}$, $3.162 = 10^{2/4}$, $5.623 = 10^{3/4}$).

ξ	$F_\alpha(\xi)$	$F_{\alpha_x}(\xi)$	$F_{\alpha_y}(\xi)$
1.000×10^{-3}	1.069×10^{-6}	8.005×10^{-6}	2.676×10^{-6}
1.778	3.376	2.530×10^{-5}	8.443
3.162	1.067×10^{-4}	8.002	2.673×10^{-5}
5.623	3.376	2.530×10^{-4}	8.441
1.000×10^{-2}	1.067×10^{-3}	8.002	2.671×10^{-4}
1.778	3.377	2.530×10^{-3}	8.456
3.162	1.066×10^{-2}	7.990	2.670×10^{-3}
5.623	3.356	2.515×10^{-2}	8.416
1.000×10^{-1}	1.049×10^{-1}	7.850	2.639×10^{-2}
1.778	3.204	2.389×10^{-1}	8.147
3.162	9.205	6.794	2.411×10^{-1}
5.623	2.257×10^{0}	1.618×10^{0}	6.394
1.000×10^{0}	4.019	2.682	1.336×10^{0}
1.778	5.462	3.363	2.098
3.162	6.635	3.859	2.776
5.623	7.598	4.251	3.347
1.000×10^{1}	8.392	4.570	3.821
1.778	9.047	4.833	4.214
3.162	9.588	5.049	4.538
5.623	1.003×10^{1}	5.228	4.806
1.000×10^{2}	1.040	5.375	5.027
1.778	1.071	5.497	5.209
3.162	1.096	5.597	5.360
5.623	1.116	5.680	5.484
1.000×10^{3}	1.134	5.748	5.587
1.778	1.148	5.305	5.672
3.162	1.159	5.851	5.741
5.623	1.169	5.890	5.799
1.000×10^{4}	1.177	5.921	5.847
1.778	1.183	5.948	5.886
3.162	1.189	5.969	5.918
5.162	1.193	5.987	5.945
1.000×10^{5}	1.197	6.002	5.967

Table 2

10 x 10 Matrix of Values of F_{ij}

Values correspond to h_i = 1000 m , 3000 m , 5000 m , . . . and ϑ_j = 1 $\widehat{\text{sec}}$, 3 $\widehat{\text{sec}}$, 5 $\widehat{\text{sec}}$, . . . Because $F_{\alpha_{ij}}$ in Eq. (7) is a function of h (or s) times ϑ , the matrix is symmetric.

.00070	.00626	.01730	.03366	.05512	.08141	.11224	.14727	.18616	.22852
.00626	.05512	.14727	.27304	.42411	.58866	.75695	.92191	1.07930	1.22600
.01730	.14727	.37197	.64506	.92191	1.17842	1.40702	1.61462	1.79092	1.93553
.03366	.27304	.64506	1.02790	1.36196	1.65244	1.88140	2.05051	2.19649	2.33166
.05512	.42411	.92191	1.36196	1.72424	1.98489	2.17546	2.34943	2.49560	2.62243
.08141	.58866	1.17842	1.65244	1.98489	2.21705	2.41727	2.58188	2.72387	2.83906
.11224	.75695	1.40702	1.88140	2.17546	2.41727	2.60908	2.77159	2.89121	2.99270
.14727	.92191	1.61462	2.05051	2.34943	2.58188	2.77159	2.90772	3.02179	3.12660
.18616	1.07930	1.79092	2.19649	2.49560	2.72387	2.89121	3.02179	3.14034	3.25787
.22852	1.22600	1.93553	2.33166	2.62243	2.83906	2.99270	3.12660	3.25787	3.39361

Table 3

10 x 10 Matrix of Values of F_{ij}^{-1}

Values here correspond to the inverse of the matrix in Table 2.

-2462.91	1310.08	-843.17	22.85	376.36	-144.45	-39.00	331.65	-591.41	284.36
1310.08	-705.88	457.02	-11.07	-196.34	67.27	16.36	-145.66	256.98	-117.74
-843.17	457.02	-289.85	-3.31	135.79	-53.24	-19.50	104.85	-146.17	59.78
22.85	-11.07	-3.31	29.13	-57.46	46.87	39.27	-113.28	83.83	-21.22
376.36	-196.34	135.79	-57.46	47.95	-63.04	-62.98	220.23	-181.39	50.07
-144.45	67.27	-53.24	46.87	-63.04	72.32	67.68	-283.82	266.64	-82.38
-39.00	16.36	-19.50	39.27	-62.98	67.68	-20.83	-54.05	65.79	-22.09
331.65	-145.66	104.85	-113.28	220.23	-283.82	-54.05	568.85	-553.79	170.79
-591.41	256.98	-146.17	83.83	-181.39	266.64	65.79	-553.79	517.47	-154.72
284.36	-117.74	59.78	-21.22	50.07	-82.38	-22.09	170.79	-154.72	45.04

Table 4

Values of $\phi_j(\vec{\vartheta}, \lambda\vec{f})$

The ten values of ϕ_j are listed vertically for each value of image frequency, sorted in blocks according to the value of ϑ, with ϕ (the angle between the vectors $\vec{\vartheta}$ and $\vec{f}$) taking the two values of 0 and $\pi/2$.

PHI = 0

THETA = 2 MICRORADIANS

F = 4.E6	F = 2.E6	F = 1.E6	F = 0.5E6	F = 0.25E6
2.339E+12	1.295E+12	-2.803E+10	-1.742E+12	-4.176E+12
4.901E+12	4.985E+12	5.093E+12	5.242E+12	5.507E+12
-2.975E+12	-3.001E+12	-3.033E+12	-3.079E+12	-3.163E+12
9.351E+10	9.326E+10	9.295E+10	9.258E+10	9.267E+10
1.562E+12	1.558E+12	1.554E+12	1.547E+12	1.533E+12
-7.298E+11	-7.155E+11	-6.970E+11	-6.712E+11	-6.220E+11
-2.245E+11	-2.200E+11	-2.141E+11	-2.060E+11	-1.906E+11
1.749E+12	1.718E+12	1.682E+12	1.633E+12	1.538E+12
-2.787E+12	-2.767E+12	-2.740E+12	-2.702E+12	-2.629E+12
1.328E+12	1.323E+12	1.316E+12	1.307E+12	1.290E+12

PHI = 0

THETA = 4 MICRORADIANS

F = 4.E6	F = 2.E6	F = 1.E6	F = 0.5E6	F = 0.25E6
4.112E+12	-8.900E+10	-5.530E+12	-1.32EE+13	-3.539E+13
1.583E+13	1.617E+13	1.664E+13	1.748E+13	2.280E+13
-9.526E+12	-9.631E+12	-9.775E+12	-1.004E+13	-1.21EE+13
2.961E+11	2.951E+11	2.939E+11	2.942E+11	3.3E0E+11
4.948E+12	4.932E+12	4.911E+12	4.867E+12	4.082E+12
-2.272E+12	-2.213E+12	-2.131E+12	-1.975E+12	-2.171E+11
-6.983E+11	-6.799E+11	-6.541E+11	-6.051E+11	-5.438E+10
5.454E+12	5.341E+12	5.184E+12	4.882E+12	1.343E+12
-8.784E+12	-8.698E+12	-8.578E+12	-8.346E+12	-5.371E+12
4.200E+12	4.180E+12	4.151E+12	4.094E+12	3.289E+12

Table 4 (Continued)

PHI = 0

THETA = 6 MICRORADIANS

F = 4.0E6	F = 2.0E6	F = 1.0E6	F = 0.5E6	F = 0.25E6
3.499E+12	-6.063E+12	-1.891E+13	-4.117E+13	-9.524E+13
3.148E+13	3.228E+13	3.351E+13	3.691E+13	2.599E+13
-1.884E+13	-1.908E+13	-1.946E+13	-2.063E+13	-1.284E+13
5.809E+11	5.787E+11	5.768E+11	6.086E+11	6.023E+11
9.708E+12	9.672E+12	9.613E+12	9.367E+12	1.276E+13
-4.401E+12	-4.263E+12	-4.045E+12	-3.299E+12	-1.261E+13
-1.353E+12	-1.309E+12	-1.241E+12	-1.009E+12	-9.596E+12
1.060E+13	1.033E+13	9.912E+12	8.462E+12	3.160E+13
-1.717E+13	-1.697E+13	-1.665E+13	-1.549E+13	-3.471E+13
8.233E+12	8.185E+12	8.107E+12	7.815E+12	1.302E+13

PHI = 0

THETA = 8 MICRORADIANS

F = 4.0E6	F = 2.0E6	F = 1.0E6	F = 0.5E6	F = 0.25E6
-2.825E+11	-1.756E+13	-4.209E+13	-1.122E+14	-1.980E+13
5.133E+13	5.283E+13	5.551E+13	7.238E+13	5.435E+12
-3.059E+13	-3.103E+13	-3.188E+13	-3.460E+13	-3.753E+12
9.369E+11	9.332E+11	9.340E+11	1.685E+12	2.795E+12
1.566E+13	1.559E+13	1.545E+13	1.296E+13	6.308E+12
-7.025E+12	-6.765E+12	-6.269E+12	-4.894E+11	-2.385E+12
-2.158E+12	-2.077E+12	-1.921E+12	-2.679E+11	-2.319E+12
1.696E+13	1.646E+13	1.550E+13	4.262E+12	3.223E+12
-2.761E+13	-2.723E+13	-2.650E+13	-1.705E+13	-8.171E+12
1.327E+13	1.319E+13	1.300E+13	1.044E+13	5.775E+12

PHI = 0

THETA = 10 MICRORADIANS

F = 4.0E6	F = 2.0E6	F = 1.0E6	F = 0.5E6	F = 0.25E6
-7.736E+12	-3.931E+13	-7.778E+13	-2.521E+14	-8.090E+13
7.507E+13	7.758E+13	8.299E+13	1.259E+14	4.075E+13
-4.454E+13	-4.531E+13	-4.708E+13	-5.762E+13	-2.645E+13
1.357E+12	1.352E+12	1.371E+12	-1.170E+13	2.242E+11
2.269E+13	2.257E+13	2.225E+13	4.517E+13	2.004E+13
-1.006E+13	-9.646E+12	-8.572E+12	-3.011E+13	-7.454E+12
-3.998E+12	-2.960E+12	-2.624E+12	-6.047E+12	-4.568E+12
2.439E+13	2.355E+13	2.146E+13	6.811E+13	2.818E+13
-3.990E+13	-3.926E+13	-3.763E+13	-8.795E+13	-4.540E+13
1.921E+13	1.906E+13	1.865E+13	3.540E+13	2.147E+13

Table 4 (Continued)

PHI = 0

THETA = 12 MICRORADIANS

F = 4.E6	F = 2.E6	F = 1.E6	F = 0.5E6	F = 0.25E6
-1.929E+13	-6.307E+13	-1.307E+14	-1.754E+14	-2.738E+14
1.025E+14	1.064E+14	1.172E+14	8.250E+13	1.457E+14
-6.058E+13	-6.179E+13	-6.550E+13	-4.075E+13	-9.786E+13
1.837E+12	1.831E+12	1.932E+12	1.912E+12	6.801E+12
3.071E+13	3.052E+13	2.974E+13	4.053E+13	3.621E+13
-1.354E+13	-1.284E+13	-1.047E+13	-4.004E+13	-7.232E+12
-4.157E+12	-3.939E+12	-3.204E+12	-1.777E+13	1.669E+12
3.281E+13	3.147E+13	2.683E+13	1.003E+14	2.366E+13
-5.388E+13	-5.286E+13	-4.919E+13	-1.102E+14	-5.968E+13
2.549E+13	2.574E+13	2.481E+13	4.133E+13	3.140E+13

PHI = 0

THETA = 14 MICRORADIANS

F = 4.E6	F = 2.E6	F = 1.E6	F = 0.5E6	F = 0.25E6
-3.515E+13	-9.250E+13	-2.115E+14	-1.598E+14	-4.794E+14
1.334E+14	1.392E+14	1.616E+14	6.720E+13	2.569E+14
-7.861E+13	-8.044E+13	-8.857E+13	-4.168E+13	-1.680E+14
2.373E+12	2.369E+12	2.817E+12	2.523E+13	6.040E+12
3.966E+13	3.937E+13	3.723E+13	2.553E+12	6.747E+13
-1.734E+13	-1.629E+13	-1.058E+13	5.187E+12	-1.952E+13
-5.325E+12	-4.907E+12	-3.248E+12	7.152E+12	-2.226E+12
4.211E+13	4.004E+13	2.877E+13	-4.174E+13	4.708E+13
-6.943E+13	-6.787E+13	-5.871E+13	2.641E+13	-9.327E+13
3.354E+13	3.316E+13	3.078E+13	-6.685E+10	4.589E+13

PHI = 0

THETA = 16 MICRORADIANS

F = 4.E6	F = 2.E6	F = 1.E6	F = 0.5E6	F = 0.25E6
-6.574E+13	-1.336E+14	-3.563E+14	-6.287E+13	-6.127E+14
1.677E+14	1.752E+14	2.298E+14	1.725E+13	3.286E+14
-9.953E+13	-1.012E+14	-1.225E+14	-1.192E+13	-2.122E+14
2.963E+12	2.965E+12	5.350E+12	8.872E+12	4.076E+12
4.950E+13	4.905E+13	4.115E+13	2.003E+13	8.962E+13
-2.148E+13	-1.990E+13	-2.189E+12	-7.571E+12	-2.978E+13
-6.593E+12	-6.099E+12	-8.505E+11	-7.362E+12	-6.504E+12
5.225E+13	4.921E+13	1.353E+13	1.023E+13	6.682E+13
-8.646E+13	-8.412E+13	-5.414E+13	-2.594E+13	-1.176E+14
4.184E+13	4.127E+13	3.315E+13	1.834E+13	5.565E+13

Table 4 (Continued)

PHI = 0

THETA = 18 MICRORADIANS

F = 4.E6	F = 2.E6	F = 1.E6	F = 0.5E6	F = 0.25E6
-8.129E+13	-1.846E+14	-8.428E+14	-4.222E+13	-5.366E+14
2.054E+14	2.175E+14	4.339E+14	1.119E+13	2.866E+14
-1.203E+14	-1.242E+14	-2.221E+14	-9.066E+12	-1.838E+14
3.603E+12	3.624E+12	2.[illegible]4E+13	-9.685E+12	2.352E+12
6.017E+13	5.950E+13	2.260E+12	5.100E+13	7.911E+13
-2.591E+13	-2.359E+13	8.260E+13	-3.008E+13	-2.794E+13
-7.9[illegible]E+12	-7.226E+12	2.269E+13	-2.661E+13	-6.816E+12
6.315E+13	5.866E+13	-1.592E+14	1.013E+14	6.292E+13
-1.049E+14	-1.014E+14	8.998E+13	-1.251E+14	-1.073E+14
5.083E+13	4.998E+13	-4.166E+12	5.364E+13	5.172E+13

PHI = 0

THETA = 20 MICRORADIANS

F = 4.E6	F = 2.E6	F = 1.E6	F = 0.5E6	F = 0.25E6
-1.121E+14	-2.469E+14	-8.004E+14	-2.569E+14	-4.001E+14
2.463E+14	2.635E+14	3.998E+14	1.294E+14	2.117E+14
-1.438E+14	-1.495E+14	-1.829E+14	-9.032E+13	-1.345E+14
4.293E+12	4.354E+12	-3.714E+13	7.118E+11	6.615E+11
7.165E+13	7.063E+13	1.434E+14	6.363E+13	9.938E+13
-3.062E+13	-2.722E+13	-9.559E+13	-2.166E+13	-2.288E+13
-8.[illegible]97E+12	-8.331E+12	-1.920E+13	-1.450E+13	-6.146E+12
7.477E+13	6.815E+13	2.162E+14	8.947E+13	9.287E+13
-1.246E+14	-1.195E+14	-2.792E+14	-1.441E+14	-8.811E+13
6.059E+13	5.922E+13	1.124E+14	6.817E+13	4.386E+13

PHI = PI/2

THETA = 2 MICRORADIANS

F = 4.E6	F = 2.E6	F = 1.E6	F = 0.5E6	F = 0.25E6
3.[illegible]87E+11	-1.215E+12	-3.143E+12	-5.434E+12	-7.746E+12
5.068E+12	5.183E+12	5.331E+12	5.480E+12	5.527E+12
-3.024E+12	-3.061E+12	-3.105E+12	-3.149E+12	-3.162E+12
9.303E+10	9.265E+10	9.217E+10	9.169E+10	9.173E+10
1.555E+12	1.550E+12	1.543E+12	1.537E+12	1.535E+12
-7.02[illegible]E+11	-6.817E+11	-6.569E+11	-6.323E+11	-6.245E+11
-2.159E+11	-2.097E+11	-2.015E+11	-1.938E+11	-1.914E+11
1.69[illegible]E+12	1.653E+12	1.606E+12	1.559E+12	1.544E+12
-2.748E+12	-2.718E+12	-2.691E+12	-2.646E+12	-2.635E+12
1.318E+12	1.311E+12	1.303E+12	1.294E+12	1.292E+12

Table 4 (Continued)

PHI = PI/2

THETA = 4 MICRORADIANS

F = 4.E6	F = 2.E6	F = 1.E6	F = 0.5E6	F = 0.25E6
-3.952E+12	-5.070E+12	-1.725E+13	-2.459E+13	-2.912E+13
1.644E+13	1.692E+13	1.740E+13	1.755E+13	1.687E+13
-9.717E+12	-9.858E+12	-9.998E+12	-1.004E+13	-9.916E+12
2.941E+11	2.926E+11	2.908E+11	2.912E+11	3.092E+11
4.920E+12	4.900E+12	4.880E+12	4.873E+12	4.871E+12
-2.164E+12	-2.085E+12	-2.007E+12	-1.983E+12	-2.031E+12
-6.64EE+11	-6.308E+11	-6.154E+11	-6.077E+11	-6.213E+11
5.249E+12	5.097E+12	4.948E+12	4.901E+12	4.980E+12
-8.628E+12	-8.513E+12	-8.401E+12	-8.365E+12	-8.414E+12
4.167E+12	4.135E+12	4.109E+12	4.100E+12	4.109E+12

PHI = PI/2

THETA = 6 MICRORADIANS

F = 4.E6	F = 2.E6	F = 1.E6	F = 0.5E6	F = 0.25E6
-1.432E+13	-2.776E+13	-4.264E+13	-5.456E+13	-5.919E+13
3.287E+13	3.399E+13	3.452E+13	3.389E+13	3.226E+13
-1.926E+13	-1.954E+13	-1.974E+13	-1.960E+13	-1.959E+13
5.765E+11	5.731E+11	5.705E+11	5.864E+11	6.365E+11
9.648E+12	9.607E+12	9.579E+12	9.583E+12	9.541E+12
-4.16EE+12	-4.005E+12	-3.895E+12	-3.955E+12	-3.949E+12
-1.279E+12	-1.228E+12	-1.194E+12	-1.212E+12	-1.192E+12
1.01EE+13	9.879E+12	9.678E+12	9.735E+12	9.6E4E+12
-1.693E+13	-1.660E+13	-1.644E+13	-1.651E+13	-1.643E+13
8.151E+12	8.096E+12	8.059E+12	8.073E+12	8.044E+12

PHI = PI/2

THETA = 8 MICRORADIANS

F = 4.E6	F = 2.E6	F = 1.E6	F = 0.5E6	F = 0.25E6
-3.168E+13	-5.477E+13	-7.808E+13	-9.246E+13	-9.696E+13
5.373E+13	5.523E+13	5.570E+13	5.354E+13	5.176E+13
-3.130E+13	-3.174E+13	-3.187E+13	-3.148E+13	-3.212E+13
9.290E+11	9.233E+11	9.246E+11	9.818E+11	1.018E+12
1.55EE+13	1.549E+13	1.547E+13	1.547E+13	1.536E+13
-6.621E+12	-6.373E+12	-6.295E+12	-6.448E+12	-6.241E+12
-2.031E+12	-1.954E+12	-1.929E+12	-1.973E+12	-1.846E+12
1.619E+13	1.571E+13	1.556E+13	1.581E+13	1.527E+13
-2.707E+13	-2.667E+13	-2.656E+13	-2.671E+13	-2.627E+13
1.313E+13	1.304E+13	1.302E+13	1.304E+13	1.293E+13

Table 4 (Continued)

PHI = PI/2

THETA = 10 MICRORADIANS

F = 4.E6	F = 2.E6	F = 1.E6	F = 0.5E6	F = 0.25E6
-5.624E+13	-9.879E+13	-1.220E+14	-1.370E+14	-1.417E+14
7.867E+13	8.067E+13	8.022E+13	7.636E+13	7.506E+13
-4.561E+13	-4.619E+13	-4.609E+13	-4.568E+13	-4.716E+13
1.345E+12	1.337E+12	1.354E+12	1.468E+12	1.417E+12
2.253E+13	2.245E+13	2.245E+13	2.239E+13	2.220E+13
-9.481E+12	-9.163E+12	-9.193E+12	-9.334E+12	-8.910E+12
-2.998E+12	-2.908E+12	-2.819E+12	-2.841E+12	-2.586E+12
2.324E+13	2.263E+13	2.268E+13	2.285E+13	2.176E+13
-3.993E+13	-3.857E+13	-3.860E+13	-3.866E+13	-3.781E+13
1.900E+13	1.849E+13	1.890E+13	1.889E+13	1.867E+13

PHI = PI/2

THETA = 12 MICRORADIANS

F = 4.E6	F = 2.E6	F = 1.E6	F = 0.5E6	F = 0.25E6
-9.413E+13	-1.354E+14	-1.732E+14	-1.879E+14	-1.927E+14
1.074E+14	1.096E+14	1.076E+14	1.024E+14	1.017E+14
-6.205E+13	-6.269E+13	-6.271E+13	-6.221E+13	-6.433E+13
1.919E+12	1.811E+12	1.862E+12	2.021E+12	1.823E+12
3.050E+13	3.041E+13	3.042E+13	3.029E+13	2.997E+13
-1.272E+13	-1.236E+13	-1.256E+13	-1.254E+13	-1.197E+13
-3.899E+12	-3.785E+12	-3.849E+12	-3.784E+12	-3.430E+12
3.124E+13	3.057E+13	3.091E+13	3.068E+13	2.914E+13
-5.269E+13	-5.219E+13	-5.242E+13	-5.216E+13	-5.091E+13
2.570E+13	2.559E+13	2.563E+13	2.554E+13	2.521E+13

PHI = PI/2

THETA = 14 MICRORADIANS

F = 4.E6	F = 2.E6	F = 1.E6	F = 0.5E6	F = 0.25E6
-1.274E+14	-1.879E+14	-2.306E+14	-2.449E+14	-2.493E+14
1.397E+14	1.418E+14	1.375E+14	1.318E+14	1.314E+14
-8.047E+13	-8.106E+13	-8.017E+13	-8.102E+13	-8.342E+13
2.349E+12	2.344E+12	2.450E+12	2.616E+12	2.245E+12
3.940E+13	3.932E+13	3.933E+13	3.910E+13	3.859E+13
-1.630E+13	-1.597E+13	-1.633E+13	-1.603E+13	-1.543E+13
-4.998E+12	-4.895E+12	-5.004E+12	-4.791E+12	-4.390E+12
4.013E+13	3.950E+13	4.012E+13	3.923E+13	3.742E+13
-6.793E+13	-6.746E+13	-6.787E+13	-6.710E+13	-6.557E+13
3.319E+13	3.308E+13	3.319E+13	3.293E+13	3.252E+13

Table 4 (Continued)

PHI = PI/2

THETA = 16 MICRORADIANS

F = 4.E6	F = 2.E6	F = 1.E6	F = 0.5E6	F = 0.25E6
-1.739E+14	-2.479E+14	-2.936E+14	-3.078E+14	-3.114E+14
1.754E+14	1.768E+14	1.700E+14	1.643E+14	1.641E+14
-1.008E+14	-1.012E+14	-9.995E+13	-1.020E+14	-1.043E+14
2.831E+12	2.935E+12	3.117E+12	3.233E+12	2.692E+12
4.919E+13	4.912E+13	4.910E+13	4.877E+13	4.807E+13
-2.023E+13	-1.998E+13	-2.047E+13	-1.981E+13	-1.928E+13
-6.202E+12	-6.125E+12	-6.262E+12	-5.859E+12	-5.469E+12
4.987E+13	4.939E+13	5.020E+13	4.848E+13	4.657E+13
-8.467E+13	-8.431E+13	-8.481E+13	-8.341E+13	-8.176E+13
4.141E+13	4.133E+13	4.141E+13	4.104E+13	4.059E+13

PHI = PI/2

THETA = 18 MICRORADIANS

F = 4.E6	F = 2.E6	F = 1.E6	F = 0.5E6	F = 0.25E6
-2.276E+14	-3.146E+14	-3.618E+14	-3.762E+14	-3.789E+14
2.142E+14	2.146E+14	2.049E+14	1.999E+14	1.996E+14
-1.229E+14	-1.230E+14	-1.216E+14	-1.249E+14	-1.271E+14
3.564E+12	3.547E+12	3.857E+12	3.862E+12	3.174E+12
5.983E+13	5.978E+13	5.970E+13	5.925E+13	5.839E+13
-2.450E+13	-2.439E+13	-2.492E+13	-2.390E+13	-2.351E+13
-7.509E+12	-7.477E+12	-7.606E+12	-7.997E+12	-8.669E+12
6.045E+13	6.024E+13	6.103E+13	5.843E+13	5.660E+13
-1.029E+14	-1.027E+14	-1.031E+14	-1.011E+14	-9.947E+13
5.039E+13	5.031E+13	5.036E+13	4.983E+13	4.939E+13

PHI = PI/2

THETA = 20 MICRORADIANS

F = 4.E6	F = 2.E6	F = 1.E6	F = 0.5E6	F = 0.25E6
-2.992E+14	-3.875E+14	-4.351E+14	-4.499E+14	-4.518E+14
2.560E+14	2.547E+14	2.424E+14	2.383E+14	2.379E+14
-1.466E+14	-1.463E+14	-1.450E+14	-1.497E+14	-1.516E+14
4.245E+12	4.239E+12	4.660E+12	4.497E+12	3.700E+12
7.128E+13	7.127E+13	7.110E+13	7.049E+13	6.956E+13
-2.909E+13	-2.919E+13	-2.963E+13	-2.829E+13	-2.811E+13
-8.916E+12	-8.947E+12	-9.019E+12	-8.210E+12	-7.974E+12
7.185E+13	7.201E+13	7.255E+13	6.909E+13	6.748E+13
-1.224E+14	-1.225E+14	-1.227E+14	-1.200E+14	-1.166E+14
5.994E+13	6.000E+13	5.998E+13	5.927E+13	5.891E+13

Table 5

Measured RMS Angle-of-Arrival Variation, $\Delta^{1/2}$

Measurement Separation, ϑ (arc-sec)	RMS Angle-of-Arrival Variation $\Delta^{1/2}$ (arc-seconds)						
	Run #7	Run #13	Run #14	Run #15	Run #18	Run #20	Run #21
0.0	0.053	0.049	0.047	0.036	0.038	0.103	0.037
0.5	0.036	0.039	0.048				
1.0	0.083	0.059	0.048	0.035	0.050	0.098	0.054
1.5	0.071	0.072	0.052				
2.0	0.075	0.075	0.064	0.049	0.054	0.087	0.072
2.5	0.068	0.091	0.093				
3.0	0.058	0.112	0.058	0.056	0.041	0.121	0.073
3.5	0.080	0.119	0.054				
4.0	0.095	0.118	0.057	0.070	0.082	0.134	0.098
4.5	0.092	0.101	0.063				
5.0	0.093	0.136	0.065	0.065	0.074	0.137	0.090
5.5	0.111	0.137	0.171				
6.0	0.151	0.162	0.074	0.085	0.091	0.133	0.128
6.5	0.157	0.170	0.094				
7.0	0.114	0.193	0.090	0.073	0.096	0.135	0.152
7.5	0.115	0.191	0.084				
8.0	0.120	0.200	0.087	0.080	0.081	0.152	0.130
8.5	0.211	0.226	0.076				
9.0	0.153	0.291	0.107	0.114	0.117	0.221	0.148
9.5	0.132	0.229	0.088				
10.	0.163	0.193	0.103	0.086	0.094	0.155	0.134
11				0.101	0.113	0.152	0.185
12				0.092	0.106	0.214	0.138

Table 5 (Continued) - Measured Angle-of-Arrival Variation, $\Delta^{1/2}$

Measurement Separation, ϑ (arc-sec)	RMS Angle-of-Arrival Variation $\Delta^{1/2}$ (arc-seconds)						
	Run #7	Run #13	Run #14	Run #15	Run #18	Run #20	Run #21
13				0.096	0.117	0.151	0.198
14				0.114	0.106	0.217	0.170
15				0.114	0.096	0.219	0.262
16				0.084	0.101	0.220	0.226
17				0.075	0.099	0.232	0.239
18				0.129	0.099	0.197	0.177
19				0.128	0.104	0.158	0.244
20				0.111	0.099	0.228	0.198

Table 6

Estimated Values of $B_{l,a_y}(\vartheta)$

These values are developed from the average values of the data in Table 5, using the $\vartheta = 0$ values to estimate σ^2 .

ϑ (arc-seconds)	$B_{l,a_y}(\vartheta)$ (radians-squared)
1.0	2.41×10^{-14}
1.5	3.57×10^{-14}
2.0	4.51×10^{-14}
2.5	1.022×10^{-13}
3.0	6.51×10^{-14}
3.5	1.022×10^{-13}
4.0	1.397×10^{-13}
4.5	1.062×10^{-13}
5.0	1.441×10^{-13}
5.5	2.005×10^{-13}
6.0	2.637×10^{-13}
6.5	3.971×10^{-13}
7.0	2.862×10^{-13}
7.5	3.336×10^{-13}
8.0	2.805×10^{-13}
8.5	6.480×10^{-13}
9.0	5.686×10^{-13}
9.5	4.651×10^{-13}
10.	3.522×10^{-13}
11.	4.170×10^{-13}
12.	3.840×10^{-13}
13.	4.037×10^{-13}
14.	4.794×10^{-13}
15.	6.399×10^{-13}
16.	5.232×10^{-13}
17.	5.457×10^{-13}
18.	4.723×10^{-13}
19.	5.306×10^{-13}
20.	5.306×10^{-13}

Table 7

Nominal Values of B_j

Values are calculated from Eq. (41)

j	ϑ_j (sec)	B_j (rad^2)
1	1	2.000×10^{-14}
2	3	1.067×10^{-13}
3	5	2.041×10^{-13}
4	7	2.976×10^{-13}
5	9	3.669×10^{-13}
6	11	4.125×10^{-13}
7	13	4.412×10^{-13}
8	15	4.593×10^{-13}
9	17	4.709×10^{-13}
10	19	4.787×10^{-13}

Table 8

Calculated Predetection Compensation Isoplanatism Factor, $\hat{m}$

	ϕ (μrad)	$\hat{m}$ f=4X10^6 (cycles/rad)	f=2X10^6 (cycles/rad)	f=1X10^6 (cycles/rad)	f=0.5X10^6 (cycles/rad)	f=0.25X10^6 (cycles/rad)
For $\phi = 0$	2	0.26	0.25	0.23	0.20	0.17
	4	0.78	0.72	0.64	0.53	0.32
	6	1.47	1.32	1.13	0.86	0.51
	8	2.28	2.02	1.67	1.02	0.93
	10	3.20	2.79	2.22	0.82	0.89
	12	4.20	3.60	2.73	1.62	0.23
	14	5.28	4.45	3.13	2.11	-0.55
	16	6.42	5.31	3.24	2.94	-1.08
	18	7.61	6.18	1.66	3.43	-0.80
	20	8.85	7.04	2.60	2.84	-0.29
For $\phi = \pi/2$	2	0.23	0.21	0.18	0.14	0.10
	4	0.66	0.56	0.44	0.31	0.17
	6	1.19	0.98	0.72	0.44	0.19
	8	1.79	1.41	0.97	0.53	0.15
	10	2.43	1.85	1.20	0.58	0.06
	12	3.10	2.28	1.40	0.59	-0.07
	14	3.79	2.70	1.56	0.55	-0.24
	16	4.48	3.09	1.70	0.47	-0.45
	18	5.18	3.47	1.79	0.35	-0.68
	20	5.88	3.82	1.86	0.19	-0.95

Table 9

Estimated Variance-Factor, $\frac{1}{2} N \hat{\sigma}_{\eta}^{2}$, for Calculated Value of η

This quantity is defined by Eq. (43) and applies to data taken with no significant statistical non-stationarity.

	ϑ (μrad)	$\frac{1}{2} N \hat{\sigma}_{\eta}^{2}$				
		f=4X10^{8} (cycles/rad)	f=2X10^{8} (cycles/rad)	f=1X10^{8} (cycles/rad)	f=0.5X10^{8} (cycles/rad)	f=0.25X10^{8} (cycles/rad)
For $\phi = 0$	2	5.5	5.4	5.4	5.3	5.3
	4	54.7	54.1	53.7	53.5	48.6
	6	209.8	207.9	207.0	204.7	792.9
	8	545.2	541.1	539.6	489.7	47.3
	10	1143.7	1137.0	1132.7	5573.1	1183.1
	12	2095.9	2086.4	2063.0	7991.9	3512.3
	14	3498.5	3486.4	3363.7	1205.2	10078.9
	16	5454.1	5438.7	4935.5	477.1	16591.6
	18	8070.5	8047.7	24659.0	9026.9	13188.4
	20	11459.9	11416.5	56173.2	11924.5	7969.8
For $\phi = \pi/2$	2	5.4	5.3	5.3	5.4	5.6
	4	53.8	53.9	54.8	56.8	58.2
	6	207.8	209.6	215.7	223.6	222.9
	8	543.0	552.0	572.1	586.3	576.5
	10	1146.1	1172.8	1218.3	1229.9	1205.1
	12	2113.1	2174.1	2254.2	2247.0	2200.7
	14	3548.3	3666.3	3782.6	3738.5	3662.8
	16	5564.1	5766.3	5909.1	5811.1	5701.8
	18	8279.9	8595.8	8742.4	8575.9	8438.4
	20	11821.4	12279.5	12396.4	12146.8	12001.0

Table 10

Estimated Variance, $\hat{\sigma}_{\hat{m}}^2$, for Calculated Values of $\hat{m}$

This quantity is defined by Eq. (44) based on the apparent spread in the measurement data, and apparently encompasses the non-stationarity of the phenomena.

	ϑ (μrad)	$\hat{\sigma}_{\hat{m}}^2$				
		f=4X10^8 (cycles/rad)	f=2X10^8 (cycles/rad)	f=1X10^8 (cycles/rad)	f=0.5X10^8 (cycles/rad)	f=0.25X10^8 (cycles/rad)
For $\phi = 0$	2	0.086	0.086	0.084	0.083	0.080
	4	0.857	0.846	0.831	0.803	0.530
	6	3.285	3.234	3.150	2.895	13.203
	8	8.520	8.369	8.091	5.345	0.759
	10	17.835	17.471	16.596	84.531	19.155
	12	32.601	31.830	29.184	133.080	44.378
	14	54.269	52.761	44.531	16.272	124.001
	16	84.353	81.558	53.868	7.655	204.921
	18	124.425	119.412	286.962	156.417	165.605
	20	176.097	167.285	852.015	193.070	103.596
For $\phi = \pi/2$	2	0.084	0.083	0.081	0.081	0.081
	4	0.837	0.824	0.812	0.810	0.813
	6	3.201	3.152	3.125	3.146	3.099
	8	8.297	8.180	8.165	8.201	7.968
	10	17.366	17.166	17.228	17.150	16.580
	12	31.764	31.499	31.701	31.242	30.188
	14	52.943	52.677	53.021	51.822	50.169
	16	82.448	82.299	82.652	80.321	78.051
	18	121.907	122.042	122.084	118.232	115.499
	20	173.028	173.639	172.859	167.108	164.271

References for Part II

1. E. H. Linfoot and E. Wolf, Proc. Phys. Soc. 66B, 145 (1953).

2. R. E. Hufnagel and N. R. Stanley, "Modulation Transfer Function Associated with Image Transmission Through Turbulent Media," J. Opt. Soc. Am. 54, 52 (1964)

3. D. L. Fried, "Theoretical Study of Non-Standard Imaging Concepts," Rome Air Development Center Technical Reports, RADC-TR-74-185 (May 1974) and RADC-TR-74-267 (Oct. 1974). (783 276) & (A002 160)

4. op cit, RADC-TR-74-185, Eq. (40).

5. D. L Fried, "Differential Angle-of-Arrival: Theory, Evaluation, and Measurement Feasibility," Radio Sci. 10, 71 (1975); Eq. (5)

6. R. F. Lutomirski and R. G. Buser, "Mutual Coherence Function of a Finite Optical Beam and Application to Coherent Detection," Appl. Opt. 12, 2153 (1973). To obtain Eq. (19), we need to suppress the inner and outer scale of turbulence effects and perform the spatial frequency integration.

7. H. B. Dwight, "Tables of Integrals and Other Mathematical Data," 3rd Ed. MacMillan Co., New York 1957; Eq.'s (350.3), (351.01), and (352.01)

8. D. L. Fried, "Optical Resolution Through a Randomly Inhomogeneous Medium for Very Long and Very Short Exposures," J. Opt. Soc. Am. 56, 1372 (1966)

9. D. Korff, "Analysis of a Method for Obtaining Near-Diffraction-Limited Information in the Presence of Atmospheric Turbulence," J. Opt. Soc. Am. 63, 971 (1973).

Appendix A

Short-Exposure Imagery Isoplanatism Theory

As a matter of completeness, we shall present here the details of a theory of isoplanatic dependence for post-detection compensated short-exposure imagery. It will be our objective here to show that this theory does not result in the simple linear relationship between isoplanatic dependence and the distribution of the strength of turbulence over the propagation path, and that, in fact, the relationship is highly nonlinear.

The focal plane electromagnetic field function $u_j(\vec{x})$ associated with the j^{th} point source, at location $\vec{x}$, with $\vec{x}$ referenced to the nominal center of the image of the j^{th} source can be written as[8]

$$u_j(\vec{x}) = \int d\vec{r}\, W(\vec{r};D) \exp[i\phi_j(\vec{r})] \exp(ik\vec{x}\cdot\vec{r}/F) \quad , \tag{A1}$$

where $\vec{r}$ denotes coordinates in the aperture plane, $\phi_j(\vec{r})$ is the wavefront distortion (taken to be entirely real) for the j^{th} source relative to the undistorted wavefront for the j^{th} source, and F is the focal length. We have deliberately suppressed a constant of proportionality in the equation. The image intensity is

$$\begin{aligned} I_j(\vec{x}) &= [u_j(\vec{x})]^* u_j(\vec{x}) \\ &= \iint d\vec{r}\, d\vec{r}'\, W(\vec{r})\, W(\vec{r}') \exp\{i[\phi_j(\vec{r}) - \phi_j(\vec{r}')]\} \\ &\quad \times \exp[ik\vec{x}\cdot(\vec{r} - \vec{r}')/F] \quad . \end{aligned} \tag{A2}$$

Since the source is a point source, its Fourier transform corresponds to the optical transfer function for imaging within the isoplanatic patch

around that source. For the j^{th} point source, the optical transfer function at spatial frequency $\vec{f}$ can be written as

$$\tau_j(\vec{f}) = A \int d\vec{x} \exp(i\vec{f} \cdot \vec{x})\, I_j(\vec{x}) \quad , \tag{A3}$$

where A is a constant of proportionality chosen to make the optical transfer function have unity value at zero frequency. If we substitute Eq. (A2) into Eq. (A3) and rearrange the order of integrations, we get

$$\tau_j(\vec{f}) = A \iint d\vec{r}\, d\vec{r}'\, W(\vec{r})\, W(\vec{r}') \exp\{i[\phi_j(\vec{r}) - \phi_j(\vec{r}')]\}$$
$$\times \int d\vec{x} \exp\{i[(k/F)(\vec{r} - \vec{r}') + \vec{f}] \cdot \vec{x}\} \quad . \tag{A4}$$

In Eq. (A4), the $\vec{x}$-integration can be performed, yielding a delta-function -- which then makes it a trivial matter to perform the $\vec{r}'$-integration. Taking advantage of this possibility, we can reduce Eq. (A4) to the form

$$\tau_j(\vec{f}) = A \int d\vec{r}\, W(\vec{r})\, W(\vec{r} + \vec{f}\, F/k) \exp\{i[\phi_j(\vec{r}) - \phi_j(\vec{r} + \vec{f}\, F/k)]\} \quad . \tag{A5}$$

We note that inasmuch as ϕ_j is a random function, then so is τ_j. [It is appropriate to note that the coefficient A, however, is not a random variable since it is defined by $\tau_j(\vec{f})$ for $\vec{f} \equiv 0$, in which case the ϕ_j-dependence disappears from Eq. (A5).]

We take as our measure of the isoplanatic dependence of post-detection compensation of short-exposure imagery the correlation between the optical transfer function at frequency $\vec{f}$ for two point sources at $\vec{\theta}_1$ and $\vec{\theta}_2$. We write this as

$$C_{12}(\vec{f}) = \langle \tau_1(\vec{f})\, \tau_2^*(\vec{f}) \rangle \,/\, [\langle \tau_1(\vec{f}) \rangle \langle \tau_2(\vec{f}) \rangle^*] \quad . \tag{A6}$$

Obviously, the entire isoplanatic dependence is contained in the numerator, $\langle \tau_1(\vec{f})\, \tau_2^*(\vec{f}) \rangle$, and in this appendix, we shall be concerned with development of a formulation for this quantity.

Making use of Eq. (A5) and appropriately simplifying, we can write

$$\langle \tau_1(\vec{f})\, \tau_2^*(\vec{f}) \rangle = \iint d\vec{r}\, d\vec{r}\,' \, W(\vec{r})\, W(\vec{r}+\vec{f}\,F/k)\, W(\vec{r}\,')\, W(\vec{r}\,'+\vec{f}\,F/k)$$

$$\times \langle \exp\{ i[\phi_1(\vec{r}) - \phi_1(\vec{r}+\vec{f}\,F/k) - \phi_2(\vec{r}\,') + \phi_2(\vec{r}\,'+\vec{f}\,F/k)] \} \rangle . \quad \text{(A7)}$$

Taking advantage of the fact that the argument of the exponential in Eq. (A7) is a gaussian random variable with zero mean, we can cast the ensemble average in the form

$$\langle \exp\{ i[\phi_1(\vec{r}) - \phi_1(\vec{r}+\vec{f}\,F/k) - \phi_2(\vec{r}\,') + \phi_2(\vec{r}\,'+\vec{f}\,F/k)] \} \rangle$$

$$= \exp\{ -\tfrac{1}{2} \langle [\phi_1(\vec{r}) - \phi_1(\vec{r}+\vec{f}\,F/k) - \phi_2(\vec{r}\,') + \phi_2(\vec{r}\,'+\vec{f}\,F/k)]^2 \rangle \} . \quad \text{(A8)}$$

We note that the ensemble average on the right-hand-side of Eq. (A8) can be cast in the form of isoplanatic phase structure functions. We write

$$\langle [\phi_1(\vec{r}) - \phi_1(\vec{r}+\vec{f}\,F/k) - \phi_2(\vec{r}\,') + \phi_2(\vec{r}\,'+\vec{f}\,F/k)]^2 \rangle$$

$$= \langle [\phi_1(\vec{r}) - \phi_1(\vec{r}+\vec{f}\,F/k)]^2 \rangle - \langle [\phi_1(\vec{r}) - \phi_2(\vec{r}\,'+\vec{f}\,F/k)]^2 \rangle$$

$$+ \langle [\phi_1(\vec{r}) - \phi_2(\vec{r}\,')]^2 \rangle + \langle [\phi_1(\vec{r}+\vec{f}\,F/k) - \phi_2(\vec{r}\,'+\vec{f}\,F/k)]^2 \rangle$$

$$- \langle [\phi_1(\vec{r}+\vec{f}\,F/k) - \phi_2(\vec{r}\,')]^2 \rangle + \langle [\phi_2(\vec{r}\,'+\vec{f}\,F/k) - \phi_2(\vec{r}\,')]^2 \rangle$$

$$= \mathcal{D}_{1,\phi}(\vec{f}\,F/k;0) - \mathcal{D}_{1,\phi}(\vec{r}-\vec{r}\,'-\vec{f}\,F/k;\vec{\vartheta}) + \mathcal{D}_{1,\phi}(\vec{r}-\vec{r}\,';\vec{\vartheta})$$

$$+ \mathcal{D}_{1,\phi}(\vec{r}-\vec{r}\,';\vec{\vartheta}) - \mathcal{D}_{1,\phi}(\vec{r}-\vec{r}\,'+\vec{f}\,F/k;\vec{\vartheta}) + \mathcal{D}_{1,\phi}(\vec{f}\,F/k;0)$$

$$= 2\,\mathcal{D}_{1,\phi}(\vec{f}\,F/k;0) + 2\,D_{1,\phi}(\vec{r}-\vec{r}\,';\vec{\vartheta}) - \mathcal{D}_{1,\phi}(\vec{r}-\vec{r}\,'+\vec{f}\,F/k;\vec{\vartheta})$$

$$- \mathcal{D}_{1,\phi}(\vec{r}-\vec{r}\,'-\vec{f}\,F/k;\vec{\vartheta}) \quad . \quad \text{(A9)}$$

If we substitute Eq. (A9) into Eq. (A8), and then substitute the result into Eq. (A7) and change the variables of integration from $\vec{r}$, $\vec{r}'$ to $\vec{u}$, $\vec{v}$, where

$$\vec{u} = \vec{r} - \vec{r}' \tag{A10}$$

$$\vec{v} = \tfrac{1}{2}(\vec{r} + \vec{r}') \quad , \tag{A11}$$

then we get a result which can be cast in the form

$$\langle \tau_1(\vec{f})\, \tau_2{}^*(\vec{f}) \rangle = \exp\{\mathcal{B}_{1,\phi}(\vec{f}\ F/k;0)\} \int d\vec{u}\ \tilde{K}(\vec{u}\ ,\ \vec{f}\ F/k)$$

$$\times \exp\{-\mathcal{B}_{1,\phi}(\vec{u};\vec{\vartheta}) + \tfrac{1}{2}\mathcal{B}_{1,\phi}(\vec{u}+\vec{f}\ F/k;\vec{\vartheta}) + \tfrac{1}{2}\mathcal{B}_{1,\phi}(\vec{u}-\vec{f}\ F/k;\vec{\vartheta})\} \ . \tag{A12}$$

Here we have used the function $\tilde{K}$ to denote the area of overlap of four circles, defined by the equation

$$\tilde{K}(\vec{u}\ ,\vec{\Delta}) = \int d\vec{v}\ W(\vec{v}+\tfrac{1}{2}\vec{u})\ W(\vec{v}+\tfrac{1}{2}\vec{u}+\vec{\Delta})\ W(\vec{v}-\tfrac{1}{2}\vec{u})\ W(\vec{v}-\tfrac{1}{2}\vec{u}+\vec{\Delta}) \ . \tag{A13}$$

The function $\tilde{K}$ has been evaluated by Korff[9] and we need not repeat the rather complicated results here.

If we now make use of Eq. (1-20) of the main text to introduce propagation theory results, we can cast Eq. (A12) in the form

$$\langle \tau_1(\vec{f})\, \tau_2{}^*(\vec{f}) \rangle = a(\vec{f}) \int d\vec{u}\ \tilde{K}(\vec{u},\vec{f}\ F/k) \exp\left\{2.91\, k^2 \int_{\text{Path}} ds\ C_N{}^2 \left[-|\vec{u}+\vec{\vartheta}s|^{5/3} \right.\right.$$

$$\left.\left. + \tfrac{1}{2}\,|\vec{u}+\vec{\vartheta}s + \vec{f}\ F/k|^{5/3} + \tfrac{1}{2}\,|\vec{u}+\vec{\vartheta}s - \vec{f}\ F/k|^{5/3} \right\} \right] \ , \tag{A14}$$

where

$$a(\vec{f}) = \exp\{-\mathcal{B}_{1,\phi}(\vec{f}\ F/k)\}$$

$$= \exp\left\{-2.91\, k^2\, (\vec{f}\ F/k)^{5/3} \int_{\text{Path}} ds\ C_N{}^2\right\} \ . \tag{A15}$$

The significant thing to be noted about Eq. (A14) is that the path-integration appears in the exponent so that we can not interchange order of integration between it and the $\vec{u}$-integration. This then prevents us from performing the $\vec{u}$-integration independently in a manner that is independent of the C_N^2-distribution. As a consequence, we would have to invert a multiple integral to obtain C_N^2-data from short-exposure post-detection compensation measurements, i. e., from measurements of $\langle \tau_1(\vec{f})\, \tau_2^*(\vec{f}) \rangle$. It is for this reason that we attach so much significance to the angle-of-arrival isoplanatism measurements, since such data is easily inverted to give high altitude C_N^2 estimates.

☆U.S. GOVERNMENT PRINTING OFFICE: 1976-614-357/150

MISSION
of
Rome Air Development Center

RADC is the principal AFSC organization charged with planning and executing the USAF exploratory and advanced development programs for information sciences, intelligence, command, control and communications technology, products and services oriented to the needs of the USAF. Primary RADC mission areas are communications, electromagnetic guidance and control, surveillance of ground and aerospace objects, intelligence data collection and handling, information system technology, and electronic reliability, maintainability and compatibility. RADC has mission responsibility as assigned by AFSC for demonstration and acquisition of selected subsystems and systems in the intelligence, mapping, charting, command, control and communications areas.